LEADING EDGE FLUTTER OF A SUPERCAVITATING HYDROFOIL

Thesis by

Kiam Thian Oey

In Partial Fulfillment of the Requirements

for the degree of

Doctor of Philosophy

California Institute of Technology

Pasadena, California

1979

(Submitted April 30, 1979)

ABSTRACT

Leading edge flutter is a problem that is unique to a super-cavitating hydrofoil. At high speed, the leading edge portion has been observed to oscillate while the trailing edge remains motionless.

In this study, several flat plate hydrofoils were tested. The experimental results indicate that the phenomenon is a complex function of speed, angle of attack, cavitation number and mass ratio. Leading edge flutter was also observed to cause cavity pinching. A theoretical study was also conducted. Two mathematical models are presented here. The first one models the flexible chord foil as a rigid chord foil hinged at the trailing edge; the second model treats the fluid-structure interaction problem of a flexible chord foil cantilevered at the trailing edge. Both models resemble leading edge flutter near zero cavitation number in some respects. At short and moderate cavity lengths, leading edge flutter phenomenon is influenced by the cavity closure condition.

DEDICATION

This work is dedicated to my parents.

ACKNOWLEDGMENTS

On this little corner of the page, I would like to express my sincere gratitude to the following persons without whom this work would have been impossible to complete:

to my advisers, Professors Charles D. Babcock and Christopher Brennen whose wisdom and insight have guided me through the dark alleys of science.

to members of the examining committee, Professors Leveret Davis, Hans W. Liepmann, and Theodore Wu.

to Sandy Wise and Marlys Ricards for their excellent typing, and to Betty Wood for the fine drawings.

to members of the GALCIT technical staff, Herb Gaebler, Harry Hamaguchi, Clarence Hemphill, Jack Kingan, Vince Sodha, Gerald Turner and Milton Wood.

Finally, and certainly not the least, I would like to thank the people at David Taylor Naval Ship Research and Development Center for their financial support since the beginning of this project.

TABLE OF CONTENTS

CHAPTER	TITLE	PAGE
	Dedication	ii
	Acknowledgments	iii
	Abstract	iv
	Table of Contents	v
	Nomenclature	
I	Introduction	1
II	Discussions of Parameters	4
III	Experimental Program	10
	III-1 Experimental setups and procedures in the Free Surface Water Tunnel	11
	III-2 Experimental setups and procedures in the High Speed Water Tunnel	14
	III-3 Results and Discussions	19
	a. General observations on the flutter behavior	19
	b. Flutter speeds at $\sigma = 0$ and parameter study	22
	c. Flutter boundaries at finite cavity length and at various angles of attack	25
	d. Flutter boundaries as a function of cavitation number	29
	e. Effects of different leading edge shapes	30
	f. Oscillating load and displacement	30
	g. Cavity pressure	32
	h. Observations of the flow pattern	34
	i. The effect of gravity on the flutter boundary	41

TABLE OF CONTENTS (continued)

CHAPTER	TITLE	PAGE
	j. Non-cavitating wake flow	42
	k. Miscellaneous observations	44
IV	Analysis of Leading Edge Flutter	46
	IV-1 Single Degree of Freedom Flutter Model	46
	IV-2 Cantilevered Foil Model	54
	IV-3 Improvement of the Models	58
V	Future Experiments	60
VI	Summary and Conclusions	61
TABLES		63
FIGURES		69
APPENDICES		
A	The ratio of the radiated energy to the kinetic energy of the foil	126
B	A semi-empirical formula for the natural frequency of the foil in a cavitating flow at $\sigma = 0$	127
C	Divergence	129
D	Estimation of the pressure created by the collapse of the bybbly coulds	135
E	Nonsteady hydrodynamics of a rigid foil in pitching oscillation	137
REFERENCES		139

NOMENCLATURE

Roman Alphabet

$AR = S/b$ aspect ratio

a = flexible chord length

b = overall chord length

c = speed of sound in water

$C_L = L/\frac{1}{2}\rho_w U^2 b$ coefficient of lift per unit span

$C_{L,\alpha} = \partial C_L/\partial\alpha$ lift curve slope

$C_M = M/\frac{1}{2}\rho_w U^2 b^2$ coefficient of moment per unit span

$C_{M,\alpha} = C_{MR,\alpha} + jC_{MI,\alpha}$ derivative of C_M with respect to α

$C_{P_a} = P_a/\frac{1}{2}\rho_w U$ Coefficient of atmospheric pressure

d = depth of submergence

$D = d/b$ dimensionless depth of submergence

E = Young's modulus

$\hat{E} = \frac{5}{2}\frac{\rho_w \omega b}{\rho_s c}$, the ratio of the radiated acoustical energy of the kinetic energy of the foil.

$F = U/\sqrt{bg}$ Froude number

g = gravity

h = amplitude of the free surface wave

$i = \sqrt{-1}$ in spatial variable

$j = \sqrt{-1}$ in time variable

$k = \frac{\omega b}{U}$ the reduced frequency

ℓ = cavity length measured from the leading edge

$\bar{\ell}$ = wavelength of the free surface wave

L = lift

NOMENCLATURE (continued)

M = hydrodynamic moment, positive nose up

$\overline{M}$ = U/c mach number

P_a = atmospheric pressure

P_c = cavity pressure

P_∞ = free stream static pressure

Re = Ub/ν Reynolds number

S = span

t = thickness of the foil

t_o = thickness at the base

U = free stream velocity

W = $\frac{1}{2}\rho_w U^2 b/\gamma$ Weber number

$W(k)$ = frequency response function for heaving motion

z = location of the axis of pitching oscillation in terms of the fraction of chord length measured from the leading edge

Greek Alphabet

α = angle of attack, positive leading edge up

β = shape factor of the thickness distribution as in $t = t_o\, x^{\beta}$

γ = surface tension

ζ = $U_{flutter}/U_{divergence}$ the ratio of flutter to divergence speeds

$\overline{\eta}$ = h/b dimensionless amplitude of free surface wave

η = U/U_{Div} the ratio of the velocity to the divergence speed.

λ = ℓ/b dimensionless free surface wave length

NOMENCLATURE (continued)

$\mu = \rho_s t/\rho_w b$ mass ratio

ν = kinematic viscosity

$\hat{\nu}$ = Poisson's ratio

ρ_s = density of the foil

ρ_w = density of the water

$\sigma = (P_\infty - P_c)/\frac{1}{2}\rho_w U^2$ cavitation number

ω = circular frequency of the foil

$\hat{\omega} = \omega/\sqrt{\frac{E}{\rho_s}}\,\frac{l}{b}\,\frac{t}{b}$ frequency ratio

$\Omega(k)$ = frequency response function for pitching motion

INTRODUCTION

In all commercial transportation, progress means comfort and speed. Over the water hydrofoils are the only vehicles that can achieve both goals. The typical speed of a passenger carrying hydrofoil is about 50 knots, with even higher speeds capable in military craft (Ref. 1). Within this speed range, most of these hydrofoils operate in the subcavitating regime. Preventing these foils from becoming ventilating or cavitating above this speed is a difficult task.

It is expected that in the future this speed limit will increase. Foils for such high speed boats will have to operate in the supercavitating regime since the only means left to supress cavitation is by increasing the depth of submergence of the foil. This becomes impractical from the viewpoint of structural rigidity and stability of the craft. Hydrofoils are not the only ones that operate in the cavitating regime. Examples of other machinery designed to operate in the cavitating flow regimes are supercavitating propellers and pumps. Supercavitating propellers are used for high speed boats and supercavitating pumps are used where size, weight, and high rate of flow are prime requirements (such as those used for rocket engines).

With increasing operating speeds, dynamic and static instability of these foils or blades becomes more and more likely. These various instabilities will be briefly reviewed in the following paragraphs.

The first type of instability is torsion-bending flutter. This dynamic instability is a self-excited oscillation involving spanwise torsion and bending modes of a foil. The foil oscillates at a single flutter frequency with bending and torsional modes, in such

a way that the foil extracts energy from the free stream to sustain or increase the oscillation. Literature on torsion-bending flutter is abundant and designers have been successful in avoiding this problem. Most of the work has been done on hydrofoil wing and strut flutter and very little on the supercavitating propellers and pumps. This is partly due to the complexity of the flow around this machinery and in part due to the fact that the blades are relatively rigid in the bending and torsion mode. This type of flutter, therefore, is not a serious problem.

Another problem that occurs when the foils or blades operate in the cavitating regime is forced vibration. This forced vibration is due to the unsteadiness of flows with short cavities (less than 1 ½ chords) or partial cavitation. As stated above, this is not a dynamic interaction between fluid and structure, but rather an instability of the flow itself. The unsteadiness is present regardless of whether the foil is rigid or flexible. The resulting vibration of the foil is random in nature although the flexibility of the foil itself may alter the randomness.

The third instability is leading edge flutter which is the topic of this study. A typical cross section of a supercavitating foil is shown in Fig. 1. The leading edge is relatively flexible in comparison to the trailing edge. At high speeds it has been observed that the foil oscillated with the first bending mode (as shown). The oscillation involves only a single chordwise deformation mode and not rigid body motion. The first reported observation of this so called, leading edge flutter was made by Waid & Linberg (Ref. 2) at the California Institute

of Technology Hydrodynamic Laboratory in 1957 and, more recently, by P.K. Spangler (Ref. 3). Figures 2, 3, and 4 show modes of leading edge flutter taken from these references; some of these modes show spanwise phase variation.

Besides the obvious detrimental effect of fatigue of the material, the resulting oscillation could prevent this machinery from operating properly. One should be especially concerned about the occurence of this flutter with low aspect ratio foils such as propellers, pumps and the canard wing of a hydrofoil. The reason for concern is that the frequency of the vibrational modes involving chordwise deformation could be lower or comparable to the torsion or bending frequency in these cases. As a rule of thumb, the lower the natural frequency, the lower the flutter speed. Table I shows the modes of vibration of a California Institute of Technology Hydrodynamic Lab model 35-435 (actual model shown in Fig. 5) in the order of increasing frequency. This model serves to illustrate the point discussed above.

Although the reported cases of leading edge flutter have been confined to laboratory observations, leading edge flutter has been known to occur in a supercavitating propeller (Ref. 4). It has also been postulated as being the cause of fatigue of the leading edges of some supercavitating impellers.

Another type of instability of a supercavitating foil is leading edge divergence. This occurs when the static deflection of the chord due to the steady hydrodynamic load becomes unbounded at a certain critical speed. This instability may be viewed as a special case of leading edge flutter at zero frequency. This problem will also be discussed in this study.

II. DISCUSSION OF PARAMETERS

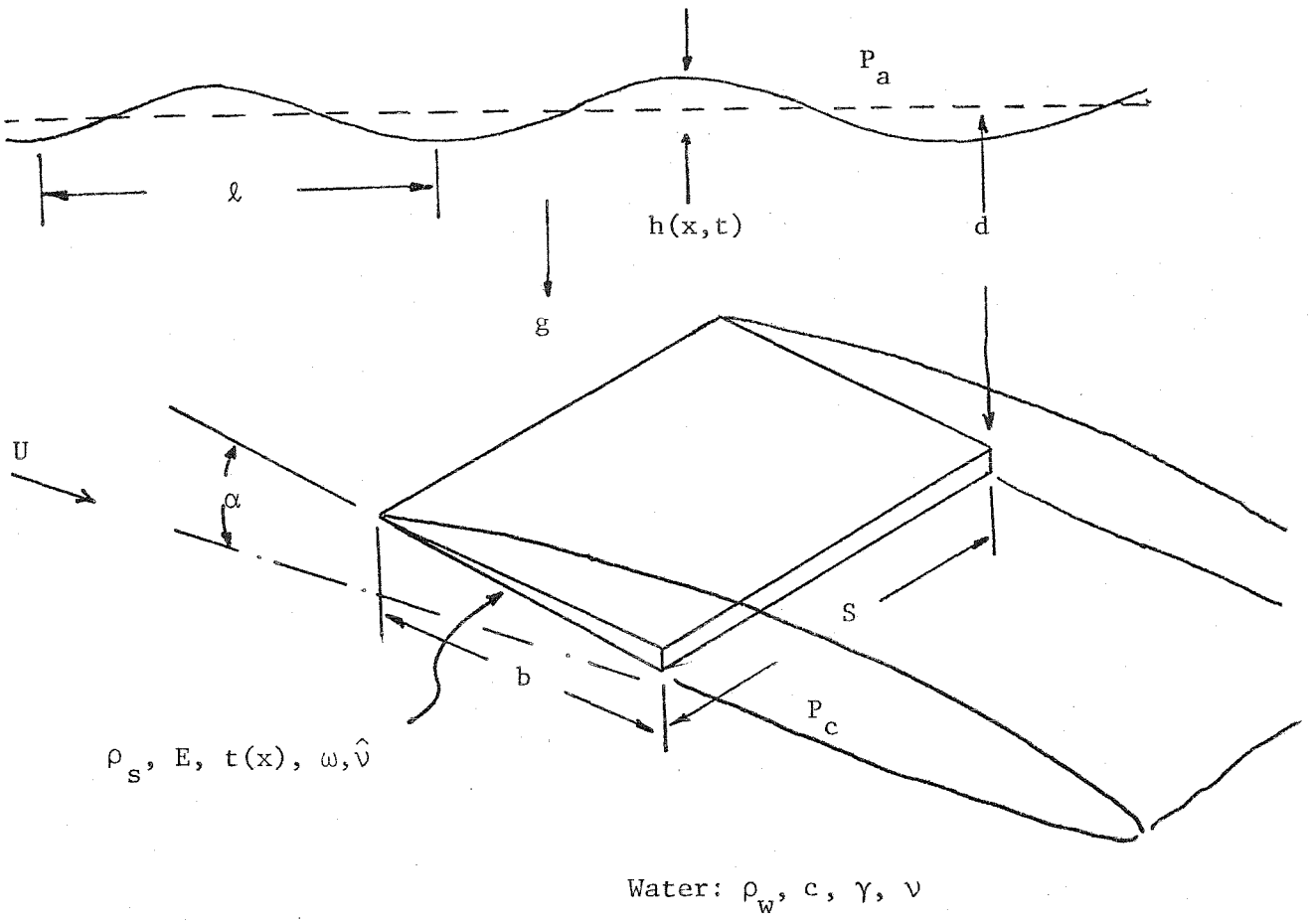

In this section the various physical parameters that determine the leading edge flutter conditions of a supercavitating hydrofoil are discussed. The above figure shows all parameters to be considered. The parameters such as atmospheric pressure P_a, free surface wave length ℓ, amplitude of surface wave h and depth d represent the effects of the free surface. In this discussion, the cavity pressure P_c has been chosen as a parameter. Actually the cavity pressure is a determined quantity when all the other parameters such as water temperature, thermal conductivity of water and air content are given. However, the determination of cavity pressure from basic parameters for a real flow is not

feasible and most hydrodynamic calculations are performed by introducing an experimentally determined cavity pressure. In some cases when dealing with the mathematical treatment of the hydrodynamics, it might be desirable to use the length of the cavity as a parameter instead of the cavity pressure or cavitation number.

In general the parameters may be categorized as follows:

STRUCTURAL:	ρ_s	:	Density of foil
	E	:	Young's modulus
	ν	:	Poisson ratio
	S	:	Span
	b	:	Chord length
FLUID:	P_a	:	Atmospheric pressure impressed on the free surface
	$\bar{\ell}$	:	Wave length of free surface wave
	$h(x,t) = h_o\tilde{h}(x,t)$	:	Amplitude of surface wave where $\tilde{h}(x,t) = O(1)$
	U	:	Free stream velocity
	ρ_w	:	Density of water
	c	:	Speed of sound in water
	P_c	:	Cavity pressure
	γ	:	Surface tension
	ν	:	Kinematic viscosity
	d	:	Average depth of submergence of foil
	g	:	Gravity

COMMON TO BOTH STRUCTURE AND FLUID:

	α	:	Angle of attack of the foil
	$t(x) = t_o\tilde{t}(x)$	;	Thickness distribution where $\tilde{t}(x) = O(1)$ and t_o is the thickness at the base
	ω	:	Frequency of oscillation of foil

The functional relation for determination of flutter boundaries may be written in terms of the above 19 parameters as follows:

$$f(\rho_s, E, \hat{\nu}, S, b, P_a, \ell, h(x,t). U, \rho_w, c, P_c, \gamma, \nu, d, \alpha, t(x), g, \omega) = 0$$

The above is a functional relation between 19 parameters or between 16 dimensionless parameters.

The 16 dimensionless parameters may be obtained by using Buckingham π theorem, but simple inspection will reveal that many commonly known dimensionless numbers may be formed readily from these 19 parameters. The rest may be constructed from physical argument.

COMMONLY KNOWN DIMENSIONLESS PARAMETERS ARE:

$R_e = \frac{Ub}{\nu}$: Reynolds number

$F = \frac{U}{\sqrt{bg}}$: Froude number

$W = \frac{\frac{1}{2}\rho_w U^2 b}{\gamma}$: Weber number

$\lambda = \frac{\bar{\ell}}{b}$: Dimensionless free surface wave length

$\bar{\eta} = \frac{h_o}{b}$: Dimensionless amplitude of free surface wave

$D = \frac{d}{b}$: Dimensionless depth

α : Angle of attack

$k = \frac{\omega b}{U}$: Reduced frequency

$\mu = \frac{\rho_s tbS}{\rho_w b^2 S}$: The ratio of mass of the foil to the apparent mass of water

$AR = \frac{S}{b}$: Span/chord, aspect ratio

$\hat{\nu}$: Poisson ratio

$$\hat{\omega} = \frac{\omega}{\sqrt{\frac{E}{\rho_s}}\frac{1}{b}\frac{t}{b}}$$ Frequency ratio, the ratio of frequency to the natural frequency of the foil.

The other parameters are:

$$\sigma = \frac{P_\infty - P_c}{\frac{1}{2}\rho_w U^2}$$ Cavitation number, where P_∞ = free stream static pressure, $P_\infty = P_a + \rho_w gd$

$$C_{P_a} = \frac{P_a}{\frac{1}{2}\rho_w U^2}$$ Coefficient of atmospheric pressure

$$\bar{M} = U/c$$ Mach number

$$\hat{E} = \frac{5}{2}\frac{\rho_w}{\rho_s}\frac{\omega b}{c}$$ Ratio of radiated acoustical energy to the kinetic energy of the foil in vibration (see appendix A for derivation of this quantity). It is a counterpart to the percent critical damping.

The functional relationship for flutter condition can be written in terms of dimensionless parameters as:

$$f(R_e, F, W, \lambda, \bar{\eta}, D, \alpha, k, \mu, AR, \hat{\nu}, \hat{\omega}, \sigma, C_{P_a}, \bar{M}, \hat{E}) = 0$$

The above functional relation is a very general one and not amenable to mathematical formulation. Several simplifying assumptions can be made if they are true for practical purposes or justifiable. The following dimensionless parameters may be neglected if the stated conditions are fulfilled.

R_e For high Reynolds number flow the boundary layer is so thin that it does not affect the pressure distribution on a supercavitating foil. Also the boundary layer separation which could remarkably alter the pressure distribution on the foil cannot occur in a supercavitating foil in view of favorable pressure gradient on the lower surface of the foil. Furthermore, the variation of Reynolds number encountered in the application does not significantly change the flow pattern of the flow.

AR and $\hat{\nu}$	For a one-dimensional structure (only chordwise deformation is considered) and 2-D fluid mechanics, these parameters may be neglected. The Poisson ratio $\hat{\nu}$ many be included in the modulus E to take account the suppression of anticlastic curvature in the spanwise direction.
$\bar{M}$	For practical application $M \ll 1$ since the speed of sound in water is very high (4500 ft/sec).
$\hat{E} = \frac{5}{2}\frac{\rho_w b}{\rho_s c}$	For low frequencies (say below 200 cps) the acoustic energy radiated may be neglected and leading edge flutter problem may be treated strictly as a hydroelastic problem.

Thus for an inviscid, incompressible and low-frequency system, the functional relation is given by

$$f(F, W, \lambda, \bar{\eta}, D, \alpha, k, \mu, AR, \hat{\nu}, \hat{\omega}, \sigma, C_{P_a}) = 0$$

If further we assume that the foil is deeply submerged then the effects of free surface, such as free surface wave and influence of free surface on the hydrodynamic loading, may be neglected. The following parameters may be taken out of the relationship: F : λ: $\bar{\eta}$ and D. Hence, for inviscid, incompressible, low-frequency and deep-sea conditions, the relation is:

$$f(W, \alpha, k, \mu, AR, \hat{\nu}, \hat{\omega}, \sigma, C_{P_a}) = 0$$

For one-dimensional structure (considering chordwise deformation only), AR and $\hat{\nu}$ drop out of the function. Hence:

$$f(W, \alpha, k, \mu, \hat{\omega}, \sigma, C_{P_a}) = 0$$

For fluid with low surface tension, such as water, the Weber number is only important when considering disturbance of small wave length on the cavity wall, and hence may be neglected.

In summary, for inviscid, incompressible, low-frequency, deep-sea, chordwise deformation only and no surface tension, the relation becomes simply:

$$f(\alpha, k, \mu, \hat{\omega}, \sigma) = 0$$

Note that the coefficient of atmospheric pressure C_{P_a} has been taken out of the relationship since it affects only the parameter σ and σ is an experimentally determined quantity.

In the above discussion it was assumed that the frequency of the vibrating foil could be characterized by the chord length b. In the experiments to be described, and in applications to hydrofoils and cavitating pump impellers, only a portion of the chord actually vibrates. This portion is designated as "a" and it is necessary to introduce a new parameter, a/b, into the above expression. This represents the ratio of the flexible part of the foil to the complete chord. This ratio is well defined in the experimental work where the chord stiffness abruptly changes, but may be less well defined in applications with continuous changes in foil thicknesses. Nevertheless, it is important to make the distinctions since the flexible part of the foil may represent only a small part of the complete foil yet the hydrodynamic forces may be influenced by the complete foil. The non-dimensional relation now becomes

$$f(\alpha, k, \mu, \hat{\omega}, \sigma, a/b) = 0$$

The characteristic length used to define the non-dimensional parameters may now be chosen to be either a or b depending on which seems most appropriate.

III. EXPERIMENTAL PROGRAM

Before these experiments were undertaken, leading edge flutter had only been observed accidentally while testing foils for their performance characteristics. This study is the first attempt to observe leading edge flutter in a controlled environment. The objectives of this experiment may be summarized as the following:

1.) to investigate the various parameters that are relevant to leading edge flutter

2.) to learn more about the mechanism of flutter

3.) to obtain a set of criteria for the onset of flutter

To achieve these goals, two sets of experiments were conducted in the water tunnels at the C.I.T. Hydrodynamic Laboratory. The first experiment was conducted in the Free Surface Water Tunnel (FSWT) and the second was in the High Speed Water Tunnel (HSWT). The High Speed Water Tunnel is a closed circuit tunnel with variable pressure in the test section.

The models used in these two experiments are shown in figure 6. They are basically flat plates with a portion of the trailing edge fixed or clamped to a rigid mounting bar, thus leaving the leading edge portion flexible. This configuration structurally simulates a typical supercavitating foil and the 30° wedge at the leading edge ensures a fixed separation point for the cavity. The overall chord length of these foils is 6 inches. Foils tested in the FSWT have a span of 14 inches and foils tested in the 2-dimensional test section of the HSWT have a span of 6 inches. These flat foils were made of aluminum alloy and various thicknesses were tested.

III-1 Experimental set-ups and procedures in the Free Surface Water Tunnel

The Free Surface Water Tunnel (FSWT) is an open channel tunnel with the test section opened to the atmosphere and has a maximum velocity of 25 fps. The experimental set-up in this tunnel is shown in figure 7. The foil was mounted to the strut as shown and the height of the strut in relation to the water surface could be varied. This effectively varied the free stream static pressure and, hence, the cavitation number to a limited extent. The drag links shown were used to take the drag of the foil and to vary the angle of attack by sliding them back and forth.

Since the speed of the tunnel was not high enough to create natural cavitation, air was injected to the suction side of the foil to create artificial ventilation. Figure 7 shows the tubes used for air injection. The lowest velocity at which a cavity could be formed with air injection was 4 fps. Air injection was necessary to sustain the cavity up to 16 fps. Above this speed, the foil ventilated through the struts and air injection was no longer necessary.

The basic measurements taken in this experiment were the frequency responses of the foil for various velocities, angles of attack, depths of submergence, and rates of air injection. The frequency response was oftained by applying a constant amplitude oscillating force to the leading edge of the foil and plotting the response of the strain gages on the foil as a function of frequency. The frequency response curve

is an indicator of the amount of damping of the foil and may be used to indicate the onset of flutter. The excitation force for the frequency response measurement was provided by an electromagnetic shaker as shown in figure 7. The shaker was connected to the leading edge of the foil by a thin music wire and a weak spring was placed in series to isolate the shaker system from the foil itself. A load cell, as shown in the figure, was used to monitor the magnitude of the oscillating force applied to the foil.

To insure a constant amplitude force for the frequency response measurements, a servomonitor system was used. This system is schematically shown in figure 8,and figure 9 shows the photograph of this equipment at the test site. In the following paragraphs, the operation of this system will be described in order to point out some subtle characteristics it exhibited when used to measure the response of the foil in a flow.

The heart of the system is the servomonitor. It ensures that the oscillating force across the load cell is constant, regardless of the frequency. This is essential in order to obtain a meaningful frequency response measurement. The signal from the load cell is amplified by the oscilloscope and then filtered by the tracking filter. The output of the tracking filter is fed into the servomonitor. The servomonitor maintains a constant RMS value of this signal by adjusting the power to the shaker accordingly. It is therefore important to filter the noise out of the load cell signal so that the RMS value maintained by the servomonitor may be interpreted as the peak to peak value of the load across the load cell.

The signal from the strain gage on the foil is also amplified by the oscilloscope and then filtered. The filtered signal is passed through

the RMS meter and plotted against the frequency by the recorder. The resulting frequency response curve indicates the amount of damping present in the system. The wider the bandwidth the more damping is present in the system. The bandwidth and the Q-factor are defined below.

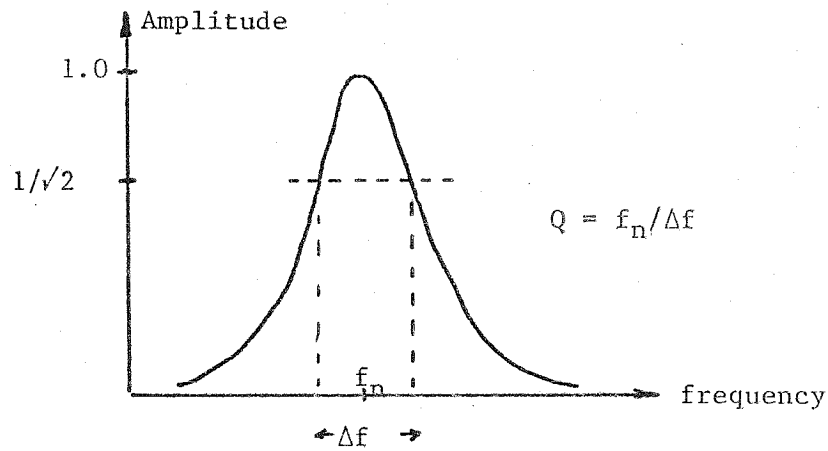

For linear or viscous damping, the Q-factor is simply related to the percent critical damping by $\xi = 1/(2Q)$.

When the foil is fluttering, a certain level of force will appear across the load cell due to the compression and extension of the isolating spring. If the level of this load is less than the level preset at the servo, then the servo will add power to the shaker to bring the load up to the preset value. If the level of oscillating force on the load cell due to flutter is equal to or more than the preset value, then the servo-monitor will turn off the shaker. Hence, the frequency response obtained when the foil flutters does not correspond to a constant applied force. Nevertheless, such observations during flutter still have some qualitative value. It must be pointed out that under this condition, the resulting Q-factor is lower than the actual one.

A total of four foils of different thicknesses were tested in the FSWT. Table 2 lists these foils and their natural frequencies in air and under water. Both theoretical and experimental values are presented.

III-2 Experimental set-ups and procedures in the High Speed Water Tunnel

This experiment was conducted in the California Institute of Technology Hydrodynamic Laboratory using the 2-D section of the High Speed Water Tunnel (HSWT). Figure 10 shows the general view of the tunnel. The flow is from the right to the left. This tunnel is a closed circuit water tunnel with variable pressure in the test section and capable of speeds up to 60 fps. The combination of speed and variable pressure in the test section makes this tunnel an ideal tool for investigating cavitating flow because the velocity and the cavitation number (or cavity length) may be varied more or less independently.

The model tested in the HSWT is shown in figure 11 and a photograph of this model on its mounting base is included as figure 12. The model is a flat aluminum plate with a 30° wedge machined at the leading edge to insure a fixed separation point for the cavity. It has a full chord length of 6" and a span of 6". The model was attached to the mounting bar with flat head screws as shown. The whole assembly of the foil, the mounting bar and the base was bolted to the mechanism for changing the angle of attack. A fairing plate was also installed and adjusted to make it flush with the tunnel wall. A clearance of 0.025" was maintained between the foil and both side walls of the tunnel.

The instrumentation consisted of three semiconductor strain gages on the foil, one strain gage on the mounting bar and a piezoelectric pressure transducer. The strain gages on the foil were used to monitor the ampli-

tude frequency and mode of oscillation (by comparing the phases between the gages). The strain gage on the mounting bar was calibrated and its output is a measure of the load normal to the foil. The piezoelectric pressure transducer was fixed to the mounting bar and used to monitor the pressure fluctuations inside the cavity. All the electrical signals were taken out of the tunnel through a cavity pressure probe on the lucite window and then through a waterproof junction box; they were displayed on oscilloscopes and recorded using an FM tape recorder. The recorded signals were processed by a digital signal processor for their spectra and cross correlations.

A mercury manometer was used to read the difference between the cavity pressure and the free stream static pressure. One leg of the manometer was connected to the junction box which was open to the cavity and the other to the static pressure tap in the test section ahead of the model (see the location in fig. 10). This reading was used to evaluate the cavitation number, σ.

During the preliminary tests, it was found that the flutter amplitude was most severe when the cavity was relatively short. Hence, an emergency valve was installed. When this valve was pushed, air was dumped into the cavity, creating a larger cavity and reducing the flutter amplitude. This same set-up was also used to supply a steady flow of air to the cavity at low speeds (below 20 fps). With air injection a cavity may be formed at speeds as low as 16 fps, thus extending the operating range of the tunnel.

In addition to the above instrumentation, a HYCAM high speed, 16mm motion picture camera was used to study the flow pattern. Motion pictures

of the flow were taken at a rate of 600 frames per second on High Speed Ektachrome color film and black and white film. Color film was primarily used because of its better gradation. Movies were made of the flow around the leading edge of the foil and of the flow around the rear end of the cavity, in addition to an overall view of the tunnel during flutter. Close-up motion pictures were also taken of the collapse and rebound of the bubbly clouds shed by the cavity during flutter. A motion picture frame analyzer machine was used to determine the rate of collapse and rebound of the bubbly region and to make sketches of the flow pattern.

Models tested in the HSWT

A total of six flat plate hydrofoils was tested. All foils have a 30° wedge at the leading edge and are made of 6061 T-6 anadoized aluminum plates. Table 3 shows the numbering system, relevant dimensions and natural frequencies of these foils. Foils 2, 3A, and 3 are the same as those tested in the FSWT except that the span has been reduced to 6". The thicker foil 4 was added to the list because of the higher operating speed of the HSWT.

Foils 5 and 6 were designed to test whether the flutter speed is dependent solely on the natural frequency of the foil in a cavitating flow. The test was designed to keep the overall chord length and the natural frequency in a cavitating flow the same as foil 3 and to vary the length of the flexible chord or the parameter a/b. If the flutter speed is solely dependent on the natural frequency, i.e. the reduced speed $U/\omega b$ is always a constant, then foils with longer or shorter flexible chord would have the same flutter speed.

To maintain the same natural frequency as foil 3 in a cavitating

flow, it was necessary to adjust the thickness of the foil according to the length of the flexible chord as outlined in appendix B. Unfortunately, changing the thickness also changes the mass ratio parameter μ which cannot be compensated for without resorting to a more elaborate sandwich type construction.

Foil 5 has a shorter flexible chord length (2.5" instead of 3.5" as for foil 3) and a thickness of 0.050". The flexible chord was reduced by moving the mounting holes forward. However, this leaves another flexible portion at the rear of the foil. Since the rigidity of a cantilevered plate is proportional to the cube of the length of the flexible part, the rear part of the foil may be considered rigid in comparison to the forward cantilevered part. Foil 6 has a longer flexible chord (4.23") and a thickness of 0.125". An adaptor plate was necessary to maintain the same chord length as foil 3. Figure 13 shows how these foils were attached to the mounting bar.

Experimental Procedure

The search for the flutter boundary was initiated by running the foil at a low velocity with the lowest possible pressure in the test section in order to generate the longest possible cavity. While maintaining the velocity, the pressure in the test section was gradually increased to shorten the cavity. This was continued until flutter was encountered.

When the cavity length was less than 1½ chords, the flow became unstable as pointed out in the introduction. The foil oscillated randomly due to forced excitation. The search for flutter was continued through this unsteady region until the cavity length was approximately one chord, and if at that point the oscillation remained random, then the

search at this velocity was terminated. The search at a higher velocity (usually in 2 fps increments) was then carried out in the same manner.

When flutter was encountered, readings of the cavity pressure, cavity length and velocity were taken and signals from the strain gages and pressure transducers were recorded on tape . This procedure was repeated for angles of attack of 7°, 10°, and 13°. The lowest angle of attack that a cavity could be formed and still clear the mounting bar was 7°.

In an unbounded fluid, the cavity length has a unique relationship to the cavitation number in such a way that the zero cavitation number corresponds to an infinitely long cavity. However, due to the wall effect in the water tunnel, there is a positive limit on the minimum cavitation number that can be achieved; this lower limit is called the choking cavitation number.

This limit stems from the definition of the cavitation number itself i.e. $\sigma = (P_\infty - P_c)/\frac{1}{2}\rho_w U^2$ where P_∞ is the free stream static pressure ahead of the foil, P_c is the cavity pressure and the denominator is the dynamic head of the flow. When the cavity becomes "infinitely long" in the test section, its upper and lower walls will be parallel to the tunnel wall and the cavity pressure will be equal to the static pressure of the fluid above and below the cavity. However, the static pressure of the fluid surrounding the foil differs from the static pressure ahead of the foil due to blockage; hence the cavity pressure will never be equal to P_∞ and this limits the cavitation number. Fig. 14 shows the choking cavitation number as a function of blockage ratio taken from ref. 5.

III-3 Results and Discussion

The order of presentation of the results has been arranged so that the reader will first obtain a more or less complete picture of the flutter boundaries while other observations are left to the later sections.

III-3·a General observations on the flutter behavior

Before presenting the results, it would be appropriate to discuss the test conditions in the FSWT since most of the results presented in this section were obtained using this facility. The test in the FSWT was conducted with forced ventilation up to 16 fps. Above this speed, the foil ventilated through the struts. The cavity length varied from about 3½ chords at 16 fps to about 5½ chords at 18 fps and extended well into the diffusor at higher speeds. Therefore the test above 16 fps corresponded to a near zero cavitation number condition. Figure 15 shows the foil with ventilation through the struts and a relatively long cavity.

The results of the experiments in the FSWT indicated that a cavitating foil lost its damping of the first bending mode with increasing speed. This point is illustrated in fig. 16 where the Q-factor of the first bending mode is plotted as a function of velocity at various levels of excitation force. The curves show a general increase of the Q-factor or decreasing damping with increasing velocity. This loss of damping is accompanied by increasing amplitude of both forced and self oscillation cases as shown in figure 17. The no force curve shows a rapid increase of the amplitude of self oscillation at around 22 fps. The response of the foil below this speed is minimal and mainly due to the turbulence of the flow. Above this speed the oscillation is a self-excited oscillation.

Notice that the variation in the Q-factor of figure 15 does not

show a similar rapid increase as the self-oscillation curve in figure 17. This discrepancy is due to the fact that when the foil becomes self-excited, the Q-factor obtained from the measurement is lower than the actual value; a fact pointed out earlier in section 1.

Besides the velocity, the frequency response curve is also affected by other parameters; among these is the angle of attack. In the FSWT experiment, the angle of attack was not a parameter that could be independently varied. Changing the angle of attack also changed the cavity length or the cavitation number. Since the test section was open to the atmosphere, pressure cannot be adjusted to keep a constant cavity length. However, as pointed out earlier, the cavity length above 16 fps was relatively long and any variation in the cavity length due to the change in angle of attack did not alter the near zero cavitation number condition.

The effect of angle of attack is shown in figure 18 for $\alpha = 8^\circ$, $9\frac{1}{2}^\circ$, and 13°. The case for $\alpha = 11^\circ$ was shown in the previous figure. The two figures clearly show the dependency on the angle of attack. By comparing the case for 0.2 Lbf p - p excitation force, one can see that the case for $\alpha = 11^\circ$ has the highest response of all. The other foils tested, (foil 3A in the FSWT and all foils tested in the HSWT), showed a similar behavior. This case will be discussed further in the next section.

The rate of air injection was another parameter that was found to affect the frequency response. Increasing the rate of air injection increases the cavity length or decreases the cavitation number. Figure 19 shows the effect of air injection on the response of the foil.

The dashed lines show the case of forced excitation before the foil became ventilated through the struts. The curves show that the response to forced excitation increases with increasing rate of air injection. The solid lines represent the self oscillation case after the foil became ventilated to the atmosphere. It shows that level of self-oscillation increases with increasing air injection; however, for low rates (300-400 SCFH) the effect is minimal.

One of the physical parameters that determines the flutter boundary of a foil is its stiffness. This quantity manifests itself in the form of the natural frequency which was used in the dimensional analysis for normalizing the flutter velocity and the flutter frequency. Figure 20 shows the variation of the natural frequency as a function of velocity for both forced and self-oscillation cases. The decrease in the natural frequency with increasing velocity is an expected phenomenon resulting from the existence of an effective negative hydrodynamic spring which decreases the overall stiffness of the foil. This negative hydrodynamic spring is the result of the steady state hydrodynamic load where an upward deflection of the foil results in an increase of the load and hence acts as a spring whose "resisting force" is in the same direction as the displacement.

The natural frequency also varied with the level of the applied force, but these variations were rather ill-defined. If the damping was non-linear (which was certainly true in this case since the damping was mainly due to the hydrodynamic loads) and viscous damping was negligible, then one might expect a natural frequency which decreases with amplitude, but, if anything, the reverse appears to occur. However, non-linearity in damping is not the only factor that can cause a shift in the natural

frequency with increasing amplitude; another factor is the non-linearity in the stiffness which, in this case, would also be of hydrodynamic origin.

From the same figure it can also be observed that the frequency of self-oscillation is close to the natural frequency of the foil itself prior to the onset of self-oscillation. This was true for all the foils tested. One may conclude that the dimensionless parameter $\omega = \omega_f/\omega_n$ is always constant and may be removed from the consideration of flutter boundaries.

The experiment in the FSWT essentially indicated that the following parameters are relevant to leading edge flutter: α, angle of attack, velocity, and cavitation number or cavity length. The effect of the mass ratio parameter was not investigated in the FSWT experiment; however the experiment in the HSWT demonstrated the effect. This effect will be described in the next section.

So far in this presentation, the term flutter velocity has been avoided because the onset of flutter was not well defined in the FSWT experiment. Experiments in the HSWT showed otherwise. The flutter speed was distinct; when the conditions were right, the onset of flutter may be described as a switching process. Flutter started and ceased at the same conditions; no hysteresis with respect to the cavity length was observed. The reason for the more gradual process in the FSWT experiments will be discussed in the next section.

III-3·b <u>Flutter speeds at $\sigma = 0$ and parametric study</u>

The main purpose of this section is to correlate the data of the flutter boundaries with the parametric study in Chapter II. In order to facilitate this correlation, asymptotic values of flutter speeds at zero cavitation number or infinite cavity length will be presented along with

other relevant parameters . The Reynolds number at which the flutter data were taken varied from 10^6 to 3×10^6. This small variation in Reynolds number is unlikely to cause radical changes in the flow pattern, and hence, it will be assumed that this parameter does not influence the flutter boundary.

It was concluded in Chapter II that the flutter boundary would be of the form:

$$f(\alpha, U/\omega b, \mu, \hat{\omega}, \sigma, a/b) = 0$$

The results of the experiment in the FSWT indicate that the ratio of the flutter frequency to the natural frequency of the foil in a cavitating flow before the onset of flutter is more or less unity. Therefore the frequency ratio parameter $\hat{\omega}$ may be neglected. The parametric dependency of the flutter boundary simply becomes:

$$f(\alpha, U/\omega b, \mu, \sigma, a/b) = 0$$

The dependency of the flutter boundary on the angle of attack α and the cavitation number σ was demonstrated in the FSWT. Results from the HSWT experiment also showed the dependence on these two parameters, and this subject will be discussed further in the next section.

The effects of the mass ratio, μ , and the ratio of the flexible chord to the overall chord, a/b, may be seen in Table 4. The table shows the values of the reduced speeds, the mass ratio, and the ratio of the flexible chord to the overall chord. The values of the reduced flutter speeds at infinitely long cavity are taken from figures 23 through 25. These values are tablulated in table 5 for all angles of attack. Extrapolated values are used whenever data are not available. For comparison purposes, the values of all parameters are based on the values

of foil 3 at an angle of attack of 7°. Since the dependence on the angle of attack is similar for all foils, the choice of the angle of attack does not make any difference in the table. Two sets of values are shown; they are based on the overall chord length b as a characteristic length and the flexible chord length a.

From Table 4, the following may be concluded:

(i) Comparison between foils 3 and 4 indicates that the increase in flutter speed of foil 4 is solely due to an increase in the mass ratio parameter μ. For a 40% increase in the mass ratio, the reduced flutter speed increases by 0.05 when based on the overall chord (or 0.09 when based on the flexible chord a. Theoretical calculation (Ch. 4) indicates that the reduced flutter speed is insensitive to the mass ratio parameters. This will be discussed later in Chapter IV.

(ii) The trend of decreasing ratio of a/b is to increase the reduced velocity and vice versa. This trend can be seen by comparing foils 3 and 5. If one assumes the parameter a/b is immaterial, then using the quantitative value of the effect of μ as in (i) above, the expected values of the reduced velocity of foil 5 are $U/\omega b = 0.15$ and $U/\omega a = 0.29$; however, the experimental values are $U/\omega b = 0.18$ and $U/\omega a = 0.43$. This fact indicates that the decrease of the ratio a/b of foil 5 has an effect of increasing the value of the reduced velocity. The effect is less pronounced when the reduced velocity is based on the overall chord length b. The reversed effect, i.e. decreasing reduced velocity with increasing a/b, can also be demonstrated by comparing foils 4 and 6.

(iii) It was postulated before that the flutter speed might be dependent solely on the frequency of the foil, i.e. $U/\omega b$ is always a constant. Comparison between foils 3 and 6 which have the same natural frequency in a cavitating flow proves otherwise.

From the above discussion one may conclude that the reduced flutter velocity at $\sigma = 0$ is a function of the mass ratio parameter μ and the ratio of the flexible to the overall chord. Increasing mass ratio parameter increases the reduced flutter velocity and increasing a/b decreases the reduced flutter velocity. The dependency of the reduced flutter velocity on the angle of attack and the cavitation number will be discussed in the next section.

Although the detail of the dependence of the flutter boundary on the various parameters is of basic interest, a designer needs only to know, at least for a preliminary design, the range of the reduced velocity when flutter will occur. From figs. 23 to 25 one may conclude that flutter would likely occur when $U/\omega b$ is between 0.15 and 0.25. These values increase with increasing mass ratio or heavier foil. Also for a cavitating flow, one needs not be concerned with leading edge divergence since flutter will occur first. Appendix C discusses the divergence problem.

III-3·c Flutter boundaries at finite cavity length and at various angles of attack

As pointed out in the previous section, the flutter boundary is a function of the angle of attack α and the cavitation number σ or the cavity length. This dependency is best illustrated by foil 3.

Figure 21 shows the flutter boundary for foil 3 at an angle of attack of $+7^{\circ}$. It is plotted as a function of the reduced velocity $U/\omega b$ on the vertical axis and the nondimensionalized cavity length ℓ/b on the horizontal axis. The domain may be divided into three different regions as shown. Region A is the flutter free region. In this region, the foil exhibited only a static deflection due to the steady load and

there was no visible or measurable oscillation. Above this region is the flutter region B. In this region, the foil fluttered with a relatively steady harmonic motion in the first bending mode. More discussion on this region follows later. Region C is the region where the foil experienced vibration due to the unsteadiness of flow with short or partial cavitation. This region is characterized by hammering actions that result from the violent changes in the size of the cavity and by random oscillations.

The amplitude of flutter increased with decreasing cavity length. (This also suggests an explanation for the gradual onset observed in the earlier FSWT tests. As the speed was increased, the cavity length also increased and hence the flutter boundary was approached in a "grazing" manner.) In the cross-hatched region shown in fig. 21, there were resonances of the flutter amplitude at certain cavity lengths. This is sketched in fig. 22. Notice that flutter may or may not cease between these "resonance lengths" and there is a general trend of increasing amplitude with decreasing cavity length. The points in the cross hatched region of fig. 21 indicate the cavity lengths at which these resonances peak, and there are more distinct resonance lengths at higher velocities as can be seen in the figure. The mechanism of this resonance phenomenon is apparently connected to the phenomenon of cavity pinching which will be described in Chapter III-3·h.

The variation of flutter boundary with angle of attack is shown in figure 23 for $\alpha = 10^\circ$ and 13° together with $\alpha = 7^\circ$ for comparison purposes. Unlike the case for $\alpha = 7^\circ$, the flutter boundary at $\alpha = 10^\circ$ shows only a small variation in the flutter speed with cavity length. The test at $\alpha = 13^\circ$ was not carried out to a shorter cavity length because of the

increasingly severe flutter amplitude; however, judging from the results of other foils (for example, foil 6 in fig. 24), it is believed that the flutter boundary at $\alpha = 13^\circ$ will also show only a small variation with the cavity length. No resonances, with respect to the cavity length were observed for $\alpha = 10^\circ$ and 13°.

Because of the experimental limitations, complete flutter boundaries for all the foils were not obtained. Two foils, 3A and 5, were destroyed because their flutter speeds were lower than the minimum speed at which a cavity could be formed. When the cavity was formed, these foils found themselves well above the flutter speed and the high flutter amplitude destroyed the foils. From the available results it may be concluded that all the foils tested would exhibit the similar flutter boundary. The only difference among them then is a shift in the vertical axis, i.e. the reduced speed, $U/\omega b$, due to the variation in the means ratio parameter μ. Fig. 24, for foil 6 illustrates this point. By comparing this figure with that of foil 3 in fig. 23, one can see the similarity in the shape of the flutter boundaries. Notice that the flutter boundary at $\alpha = 7^\circ$ could not be obtained for foil 6 because the use of the adaptor plate, which was necessary in order to mount this foil, raised the height of the mounting bar which then interfered with the cavity. The difference in the flutter speed, which amounted to a shift in the vertical axis, was caused by the difference in the mass ratio parameter, as pointed out earlier.

The effect of the mass ratio can also be seen by comparing the flutter boundaries of foil 4, as shown in fig. 25, to those of foils 3 and 6 in the previous figures. Foil 4 has the same mass ratio as foil

6 and hence the same flutter boundaries. The flutter speed of this foil is higher than foil 3 since it has a higher mass ratio.

It is interesting to notice a feature that is common to all the flutter boundaries presented so far; at a relatively long cavity length or near zero cavitation number, the flutter speed is minimum at $\alpha = 10^\circ$. This is not a mere coincidence. It was also pointed out in the first section of this chapter that the damping of the foils tested in the FSWT was minimum at $\alpha = 11^\circ$ and consequently, so was the flutter velocity. It must be pointed out that tests in the FSWT were done with cavity lengths that were always greater than three chords, and hence, comparison with the asymptotic values of the foils tested in the HSWT is justified.

It is difficult to judge the significance of the angle of attack around $\alpha = 10^\circ$ to 11° without any experimental data on the unsteady hydrodynamics itself. The available unsteady hydrodynamic data are for rigid foils executing heaving or torsional oscillation around one angle of attack only, thus making any correlation inconclusive. Measurements of the steady load on the foil taken in the FSWT indicate that the load remains linear up to $\alpha = 20^\circ$ and there was no sign of stalling around 10° to 11°.

One important conclusion that can be drawn from this fact is that leading edge flutters observed in the FSWT and HSWT tunnels are indeed the same phenomenon despite differences of the flows in the two tunnels. This conclusion was taken for granted in the previous discussion.

III-3·d Flutter boundaries as a function of cavitation number

For a fixed angle of attack in a steady flow, the cavitation number has a unique one to one relationship with the cavity length; the longer the cavity, the smaller is the cavitation number. Figure 26 shows this relationship for various angles of attack when the foil was fluttering. As can be seen, the cavity length becomes very long near the choking cavitation number.

During flutter, it was observed that the rear part of the cavity became periodically pinched off from the main cavity. This phenomenon will be described in the next chapter. The pinched off part of the cavity carried with it a considerable volume of gases. Depending on the cavity volume or length, this process can affect the relationship between the cavitation number and the cavity length to the extent that this relationship may no longer be unique. This has been known to be true for a ventilated cavity at a certain rate of air injection (ref. 7). However, figure 26 suggests that such non-uniqueness does not occur to any significant degree in the present tests. Therefore one may replot the flutter boundary in terms of the cavitation number. Fig. 27 shows the flutter boundaries of foil 4 as a function of the reduced velocity and cavitation number.

If one assumes that the reduction in flutter speed for short cavity flow from its asymptotic value at $\ell/b \simeq \infty$ is caused by unsteadiness due to short cavity or high cavitation number σ, then fig. 27 shows that the case for $\alpha = 7^\circ$ is affected more than the higher angles of attack. This notion agrees with the fact that flow with a short cavity or high σ at a lower angle of attack is inherently less stable than its counterpart at a higher angle of attack. If it had been possible to go

to a higher σ, at $\alpha = 10^\circ$ or 13°, a reduction of flutter speed similar to the $\alpha = 7^\circ$ case might have been observed.

III-3·e Effects of different leading edge shapes

At the beginning of this experiment, the effect of the shape of the leading edge on flutter was of concern. One of the driving forces of the flutter was postulated as being the oscillating lift resulting from the oscillation of the separation point of the cavity at the leading edge.

Four different leading edge shapes were tested on foil 3A in the FSWT. These are shown in figure 28. In all of these cases the foil fluttered at the same speed even though high speed movies taken during flutter revealed local differences in the behavior of the separation point near each of these different leading edges. The separation point for the 30° wedge remained fixed to the tip of the leading edge throughout the entire oscillation cycle while other leading edge shapes show an occasional movement of the separation point.

From these observations, one may conclude that the oscillation of the separation point of the cavity is not central to the existence of leading edge flutter and has little effect on the flutter behavior.

III-3·f Oscillating load and displacement

Although flutter should be avoided in the first place, knowledge of the magnitude of the oscillating lift would help the design engineers to build structures that would minimize the damage if flutter did occur. Data on the oscillating load that is normal to the foil will be presented in this section. This load was measured by the strain gage on the mounting bar of the foil in the HSWT experiments.

Fig. 29 shows the magnitude of this load as a function of the cavity length at $\alpha = 10^\circ$. The data were taken at a more or less constant velocity, in this case 27½ to 32 fps. The curve shows increasing magnitude of the load with decreasing cavity length. This behavior agrees with the fact that for a steady flow, the lift coefficient increases with shorter cavity. Data at a lower angle of attack were taken at a wide range of velocities since the flutter boundary shows a wide variation of flutter speed with cavity length (see fig. 23). Fig. 30 shows that these data are best when plotted against the velocity. At lower velocities the oscillating load is more or less proportional to the velocity squared instead of being dependent on the cavity length as the $\alpha = 10^\circ$ case. The magnitude of the oscillating lift during flutter has the same order of magnitude as the steady lift. Note that the steady lift was not measured during the experiment; however the calculated lift at, say, $\alpha = 7^\circ$ and 35 fps is about 120 Lbf. This is of the same order of half the peak to peak lift during flutter.

Figs. 31 and 32 show the displacement of the foil during flutter. The displacement shows the same behavior as the oscillating load. As a matter of fact, the traces of the displacement and load signals are in phase, i.e. an upward displacement with increasing load. It was pointed out before that the flutter frequency was the natural frequency of the foil in a cavitating flow. This seems to contradict the experimental result since at the natural frequency the load and displacement should be 90° out of phase. However one must remember that the foil itself, excluding the surrounding water, has a much higher natural frequency. At flutter it is being driven well below its natural frequency. Hence

the load should be in phase with the displacement and the experimental results indicate that this is the case.

III-3·g Cavity pressure

It is well known that for a forced ventilated flow, the cavity pressure oscillates when a certain critical rate of air injection is reached (ref. 7). The oscillation in cavity pressure results in an oscillation of the hydrodynamic load which could be the driving force of leading edge flutter. However the foils tested in the FSWT fluttered when the cavity was opened freely to the atmosphere. Because the pressure inside the cavity was more or less constant, one may conclude that the oscillation of the cavity pressure is not central to the existence of leading edge flutter. Experiments in the HSWT with natural cavitation further confirmed this conclusion. This will become clear in the following discussion on the cavity pressure oscillation in the HSWT.

The oscillating cavity pressure was obtained from a pressure transducer located inside the cavity. Fig. 33 shows a typical trace of the pressure inside the cavity. The trace is basically sinusoidal with with the same frequency as the flutter frequency. To obtain the amplitude of the cavity pressure at the flutter frequency, the cavity pressure signal was Fast Fourier Transformed using a digital signal processor. The cavity pressure that will be presented here is the Fourier component at the flutter frequency in terms of peak to peak pressure in lbf/in^2.

Fig. 34 shows the cavity pressure as a function of leading edge displacement for both foils 3 and 4. Data were plotted regardless of the cavity length. If the cavity pressure were the driving force of flutter,

then it should increase with increasing flutter amplitude. The reverse seems to be true and indicates that the oscillation in the cavity pressure is the result of flutter. When the same data are plotted against the cavity length as done in fig. 35, they show increasing pressure with shorter cavity. This is because of the fact that a shorter cavity has a smaller volume and hence its pressure is affected more by the oscillation of the foil which acts as a piston.

The phase relationship between the cavity pressure and the foil displacement is shown in fig. 36. The data were obtained by taking the cross-correlation functions between the pressure and displacement signals using the digital signal processor. Positive phase means that the increase in pressure leads the upward displacement. Data are scattered but mostly on the negative phase, i.e., the pressure lags the upward displacement of the foil. If the foil truly acts as a piston then the pressure should be in phase with the displacement. However, the matter is complicated by the fact that increasing the displacement increases the angle of attack which causes the cavity to increase in size and hence tends to reduce the pressure. Also the waves on the upper cavity change the volume of the cavity. Furthermore the matter may be complicated by the thermodynamic effect. At low cavity pressure, the pressure tends to remain constant as the cavity volume changes since the heat necessary to vaporize the water is readily available at the interface. This might not be true, however, if the oscillations are of "high" frequency. In view of the complex dependency of the cavity pressure on the various parameters, it is not surprising that the data are scattered.

Summarizing, one finds:

a. Cavity pressure oscillation decreases with increasing amplitude of oscillation.

b. The cavity pressure oscillation ranges from 0.05 to 0.5 psi p-p; this is about an order of magnitude lower than the pressure required to generate the observed oscillating load (typically 1.5 to 7.5 psi p-p). The above summary reinforces the conclusion drawn from the FSWT experiment that the oscillation of the cavity pressure is not central to the existence of leading edge flutter.

III-3·h Observation of the Flow Pattern

When the foil was fluttering in the HSWT, it was observed that the rear end of the cavity was periodically pinched off from the main cavity. The pinched-off cavity collapsed and rebounded in synchronization with the oscillation of the foil. The collapse and rebound process created pressure pulses which might have an effect upon flutter itself. In this section, investigation of this periodic cavity pinching and its role in the flutter phenomena will be discussed. The investigations involved taking high speed movies and monitoring pressure fluctuations around the foil.

The flow pattern when the foil was fluttering was radically different from the steady case. Figures 37 and 38 show the photographs of the cavities when the foil was fluttering and in a steady flow . The

first figure shows the flow with a relatively short cavity and the second figure shows the flow pattern when the cavity is relatively long. In the steady case, the cavity surfaces are free from waves. By contrast in the fluttering case, waves of high amplitude can be seen on the upper cavity surface. These waves are created by the oscillation of the leading edge of the foil and propagate to the rear end of the cavity. As the waves travel along the upper cavity surface, they grow in amplitude and become distorted as they reach the rear end of the cavity. The actual shape of the cavity surface was difficult to photograph because of the presence of small bubbles which masked the view. Figure 39 is a sketch of the cavity wall of fig. 38. Waves are also present on the lower cavity surface, but their amplitude is small compared to the upper ones as can be seen in the photographs. When the waves on the upper and lower cavity surfaces meet at the rear end of the cavity, they cause a portion of the cavity to become pinched off from the main cavity forming a separate bubble. This is clearly shown in fig. 37 and the process will be described later in detail. A similar flow pattern was also observed when the foil was put at a negative angle of attack. Figure 40 shows the flow pattern when the foil was inverted. Both photographs show the cavities at the leading edge collapsing due to the severity of the flutter amplitude. It must be pointed out that at a lower flutter amplitude, the cavity remained attached to the leading edge as described in section III-3·e.

The flow pattern in the FSWT experiment was somewhat different. Although the waves on the upper cavity surface due to the leading edge oscillation were present, they did not cause cavity pinching.

This was apparently due to the fact that the waves in the FSWT did not become so distorted as in the HSWT. One may conclude from the experiment in the FSWT that the cavity pinching process is not central to the existence of leading edge flutter; however its influence cannot be neglected. The effects of cavity pinching will be described later.

The phenomenon of cavity pinching for a forced ventilated flow rather than a cavitating flow has been reported previously in literature (refs. 7 and 8). However cavity pinching has not been reported before for a vaporous cavitation. Although the two phenomena are similar in appearance, their mechanisms are entirely different. In the forced ventilated case, the instability is caused by the oscillation of the cavity pressure at the natural frequency of the volume of the cavity. In the vaporous cavity case, the pinching is caused by the oscillation of the leading edge and has not been reported for a rigid foil. In the forced ventilated case, the cavity pressure oscillation is the driving force of the phenomenon while in the vaporous case, the cavity pressure is a consequence of the volumetric changes of the cavity during flutter. Furthermore, in the forced ventilated case, the frequency of the oscillation depends on the cavity size and the rate of air injection, while in the vaporous cavitation case, the frequency locks to the natural frequency of the foil in a cavitating flow. The wave length of the waves in the forced ventilated case is an integer fraction of the overall cavity length and the length of the cavity that is pinched off is any integer multiple of the wave length. By contrast in the vaporous case, the wave length is more or less equal to U_c/f where U_c is the particle velocity on the cavity surface and f is the flutter frequency. The length of the pinched-off cavity is less than ¼ wave length. The detail of the cavity pinching in the

HSWT experiment will be described next.

As pointed out earlier, the waves created by the oscillation of the leading edge grow in amplitude. The growth of these waves is linear with the distance near the leading edge. The amplification factor, based on the amplitude of leading edge oscillation, is presented in figure 41. As can be seen, over a distance of only 3" (½ chord), the amplitude grows five times. Apparently the amplification becomes non-linear beyond this distance. By the time a wave reaches the closure region, it has become so distorted that it looks like a train of spikes. When one of these spikes gets to the end of the cavity, it causes the cavity to become pinched and literally cuts loose the end of the cavity. This process is repeated when the next spike arrives.

Figure 42, taken from a high speed movie of the cavity when the foil was fluttering, shows the step by step process of the pinching. The time interval between each frame is 1/600 sec., corresponding to the 600 frames per second at which the movie was taken. Because of the very intense unsteadiness of the flow at the rear end of the cavity, the pinched off cavity soon becomes more like a bubbly cloud rather than a single bubble. This bubbly cloud grows in size, collapses and then rebounds. The collapse and rebound process continues with ever weakening intensity as the bubbly cloud is swept downstream by the flow. The shape of this so-called bubbly cloud is shown below.

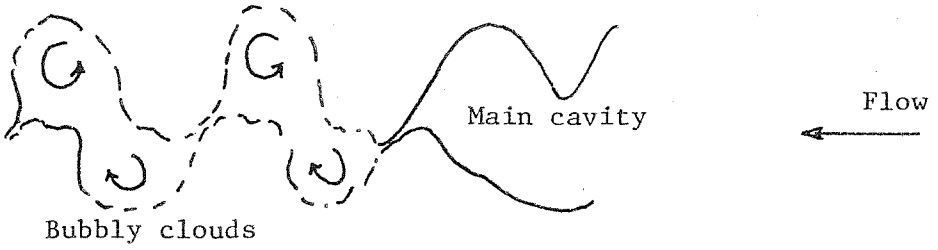

The upper and lower cores are actually a pair of vortices rotating in the opposite directions, as shown. Each bubbly cloud is connected to the next one with what appears from the side view to be an "umbilical cord." This is clearly shown in fig. 37. The upper vortex rotates in the counter-clockwise direction and the lower one in the clockwise direction. This vortex street is of course a manifestation of the oscillating lift on the foil. From the high speed motion picture it is clear that the upper vortices rotate at a faster rate than the lower ones. Approximate rates of rotation of the upper and lower vortices are about 40 and 30 revolutions per minute, respectively (at about 30 fps). This pair of vortices is similar to the Karman vortex street behind a blunt body except the cores are bubbly and the bubbly vortices collapse and rebound in synchronization with the oscillation of the foil. Similar vortex streets have been observed for foils with short cavities and high angle of attack but without the collapse and rebound of the bubbly cloud (ref. 9). The two-dimensionality of the flow disappears at about 15 inches behind the rear end of the cavity. Using strobe lights one can see the surface of this bubbly cloud covered with small bubbles with an average radius of approximately ¼". It is not known whether there are larger bub-

bles inside this bubbly region.

Three different time intervals were observed between pinching-off and the first collapse. They are:

Case 1. Immediately after the bubble becomes separated from the main cavity. This occured with foil 3 at 31½ fps, $\alpha = -7^\circ$ and a cavity length of 2 chords.

Case 2. One period of oscillation after the separation. This occured with foil 3 at 33 fps, $\alpha = 7$, $\ell/b = 2$.

Case 3. One and one-half periods of oscillation after the separation. This case was observed for foil 3 at 36½ fps, $\alpha = 7^\circ$, $\ell/b \simeq 4$.

For cases 1 and 2, the phase relationship between foil displacement, pinch-off and collapse are illustrated below. The phase relationship with the displacement of the foil is unknown for case 3. It must be emphasized that the cases stated above are three isolated cases and the conditions for which those cases occur may not be unique. It is conceivable that other periods also exist.

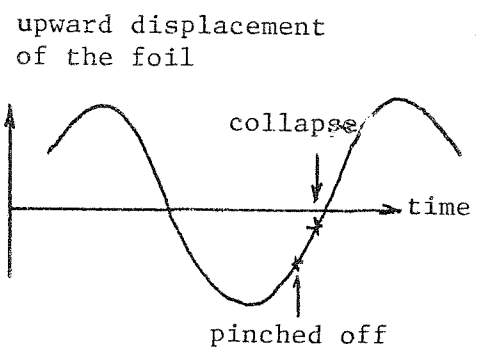

CASE 1

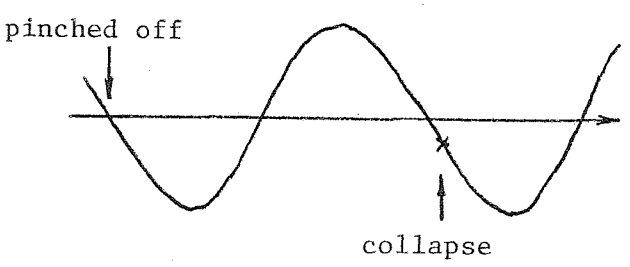

CASE 2

Figure 43 shows the growth and collapse of the bubbly cloud as a function of time for case 3. This graph was obtained from analyzing the high speed motion picture of the region near the end of the cavity taken at 600 frames per second. The horizontal axis is the frame number and the time interval between the frames is 1/600 sec. The vertical axis is the average radius of the bubbly area as projected on the tunnel's window. The collapse and rebound of the bubbly cloud create pressure pulses whose magnitude is proportional to the rate of the change of the volume of the bubble. The typical shape of this pressure pulse is shown in fig. 44. The sharp positive spikes are caused by the rebounds of the bubbly clouds. Also shown is the spectrum of the pressure pulses which contain odd and even harmonics of the flutter frequency. During flutter one can hear a very loud buzzing noise coming from the rear end of the cavity.

It was pointed out earlier that the pressure pulses generated by the collapse and rebound of the bubbly clouds might have an effect upon flutter itself. To understand the interaction between the bubbly cloud and the foil, one must examine the magnitude of the pressure pulse and its phase relationship with the oscillation of the foil.

For the purpose of estimating the order of magnitude of the pressure pulses acting on the wetted side of the foil, the following will assumed:

1. The bubbly cloud is a single spherical bubble.
2. The bubble collapses and rebounds at a constant rate.

   The term $\ddot{R}$ of eqn (1) in appendix D is neglected.

For the case in fig. 43, the pressure acting on the foil during the

collapse cycle is 0.9 psi and during the rebound cycle the pressure is 0.2 psi (please see appendix D for details of the calculation). These figures are in the same order of magnitude of the observed pressure pulses. Fig.45 shows the component of the pressure pulse at the flutter as a function of the distance from the rear end of the cavity. The pressure is in the same order of magnitude as the pressure required to generate the observed oscillating lift ($\pm$ 3 psi) and certainly will have an influence on the flutter amplitude. It is expected that the effects of the collapse and rebound of the bubbly cloud will not diminish as they would in an unbounded fluid because of the presence of the tunnel wall. After a certain distance from its source (say one or two tunnel heights), pressure pulses will be transmitted as in a tube. Furthermore, as the cavity becomes longer, the collapse and rebound of the bubbly region become more severe since the static pressure increases in the diffuser.

The effects of the pressure pulses generated by the collapse and rebound of the bubbly cloud are best understood if one examines the phase relationship with the displacement of the foil. Cross-correlation between the pressure pulse and displacement revealed that they could be either exactly in or out of phase with each other. (See also case 1 and 2 discussed previously.) Since these pressure pulses are transmitted to the foil with almost no delay at all, they could either reinforce the unsteady hydrodynamic load that causes flutter or subdue it. This was apparently the reason why in the cross-hatched region of fig. 21 the flutter amplitude resonated with respect to the cavity length as shown in fig. 22. Flutter amplitude is reinforced when the pressure pulses are in phase with the upward deflection of the foil and vice versa.

III-3·i <u>The Effect of Gravity on the Flutter Boundary.</u>

It could be suggested that gravity might have an effect upon the

upper cavity surface and hence upon the flutter boundary. The effect of gravity was tested by turning the foils upside down so as to put them at a negative angle of attack. The resulting flutter boundary for $\alpha = -7^\circ$ was exactly the same as that for positive angle of attack. No other test was carried out. However, there is no reason why this should not be true for other foils or angles of attack in the same velocity range. The ratio of the centrifugal force due to the curvature of the cavity wall to the gravity force may be approximated as U^2/Rg where U is the free stream velocity, R is the average radius of the cavity wall, and g is the gravity acceleration. In this test, the typical operating speed was 30 fps and the radius of curvature at the leading edge was about 0.5 ft., giving a ratio of about 55. In view of this ratio, it is not surprising at all that the gravity does not affect the flutter boundary.

III-3·j <u>Non-Cavitating Wake Flow</u>

Since a non-cavitating wake flow over a foil is in some respects similar to the supercavitating flow as shown below, the question arises as to whether leading edge flutter can also occur for a single phase flow.

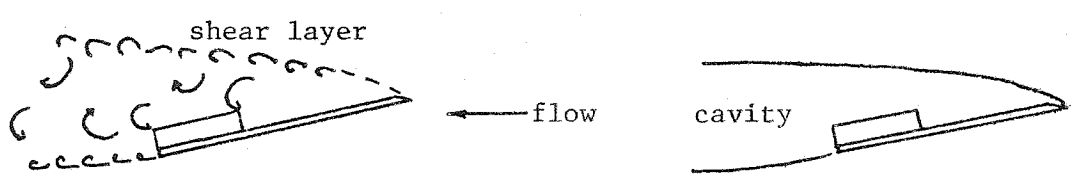

WAKE FLOW CAVITY FLOW

Frequency response measurements were made in the FSWT for the wake flow case. The result did not indicate any change in the amount of damping

with increasing velocity. However, the test was not carried very far above the flutter speed because the formation of a ventilated cavity could not be prevented. In the HSWT, foil 3 which had a minimum flutter speed of 21 fps at $\alpha = 7^{\circ}$ was tested all the way up to 35 fps with a non-cavitating wake. The formation of the cavity was suppressed by increasing the pressure in the test section up to 8 psi. No indication of flutter was observed and the foil remained stable. A similar test was also performed on foil 3A with the same result.

Fig. 46a presents a typical trace of fluctuating pressure in the wake behind foil 3A at 18 fps and $\alpha = 7^{\circ}$. Fig. 46b shows its corresponding power spectrum. The vertical scale of the spectrum is the square of the magnitude of pressure. The upper trace is the spectrum of the pressure and the lower trace is that of the displacement of the foil. The natural frequency of this foil in a cavitating flow is 44 cps; it is lower in the wake flow (about 36 cps) due to the higher apparent mass. Even though the spectrum of the pressure fluctuation has components around the natural frequency of the foil in a wake flow, the response of the foil is minimal.

With regard to the question posed at the beginning of this section, one may conclude that leading edge flutter in a non-cavitating wake flow is unlikely. Leading edge divergence is probably the primary hydroelastic interaction for a flexible chord foil with a non-cavitating wake (please see appendix C for a discussion on divergence).

Flutter is a phenomenon that is highly dependent on the unsteady hydrodynamics. Even though in a steady flow the cavitating and non-cavitating wake flows are similar, the unsteady loads for the two cases are

different for the following reasons. The first is the contribution of the apparent mass. The apparent mass of the non-cavitating wake flow is approximately twice that of the cavitating flow. The second factor comes from the difference between the dynamics of the shear layer and the cavity surface. In the shear layer case, the disturbance created by the leading edge oscillation is damped by the viscosity, while in the cavity flow, the leading edge oscillations create waves on the cavity surface. These waves are amplified as they propagate to the rear end of the cavity. The differences in the flow geometry for the two cases could conceivably make a difference in the unsteady hydrodynamic load. This difference together with the contribution of the apparent mass may explain the differences in the hydro-elastic response of cavitating and non-cavitating foils.

III-3·k Miscellaneous Observations

In this section miscellaneous observations are reported. The relationships of these observations to the leading edge flutter phenomenon are not clear at this time.

During the experiment with foil 5 in the HSWT, it was observed that the foil fluttered with the flow configurations as shown in fig. 47. The first case was a flow with a bubbly partial cavitation which extended to the middle of the chord (fig. 47a). The foil fluttered at 17 fps and $\alpha = 7^{\circ}$ with a steady frequency of 53 cps. When the speed of the tunnel was increased, the bubbly partial cavitation disappeared and a cavity was formed on the mounting bar. This caused a high pressure to be imposed on the upper surface and with further increases in velocity, another cavity was formed on the lower surface. The final flow configuration is shown in fig. 47b and the foil fluttered between 17-20 fps at $\alpha = 7^{\circ}$.

The first case points out the connection between the unsteadiness associated with a partial cavitation flow and leading edge flutter. It demonstrates that the randomness of the flow could be altered by the flexibility of the foil. In this case the randomness "locked" to the natural frequency of the foil. The second case illustrates that leading edge flutter is also possible for a flow configuration that is radically different from that of a hydrofoil.

A flutter mode other than the first bending mode was also observed during the experiment in the FSWT. Foil 2 fluttered with the first bending mode as soon as a cavity could be formed at 4.3 fps and with a frequency of 12 Hz. When the tunnel speed was increased to 7.2 fps, the mode of flutter could change to the first torsion mode with a frequency of 20.5 cps (please see table 2). This mode is actually the same as the first bending mode except for the phase variation in the spanwise direction. Notice that the reduced flutter speeds are the same for both modes, i.e., $U/\omega b = 0.11$. One may make a conjecture that higher order modes can also be excited at the same reduced speed. Higher order modes of flutter are reported in refs. 2 and 3.

IV. ANALYSIS OF LEADING EDGE FLUTTER

It was concluded in the last chapter that the leading edge flutter boundary depended on the various parameters such as the angle of attack, the cavity length and the mass ratio parameter. Because of the complex dependency of the flutter boundary on these parameters, it is not likely that a single mathematical model can describe the whole aspect of leading edge flutter. However, if one limits the scope to the case of zero cavitation number or infinite cavity length then the problem is greatly simplified. Two mathematical models for the case of zero cavitation number are presented in this chapter. The first is a Single Degree of Freedom Model. In this case, leading edge flutter oscillation is modelled as an oscillation of a rigid foil hinged at the trailing edge. The second model treats the fluid-structure interaction of a flexible chord foil cantilevered at the trailing edge. Finally at the end of this chapter, attempts will be made to explain why the non-cavitating wake does not flutter.

IV-1 Single Degree of Freedom Flutter Model

The effect of the deformation of the chord during flutter is to change the effective angle of attack of the foil. The oscillation of the angle of attack may be simulated by an oscillation of a rigid flat foil hinged at the trailing edge as shown below.

This model falls under the classification of single degree of freedom flutter which is generally believed to be impossible except under very special circumstances. It will be shown here that for the case of a supercavitating foil hinged at the trailing edge, flutter is always possible. However before the analysis is outlined, a brief historical sketch of single degree of freedom flutter will be presented in order to put the leading edge flutter problem in proper perspective.

The early analysis of flutter was done using quasi steady aerodynamic derivatives. Within the context of this analysis, a single degree of freedom oscillation, i.e., heaving or pitching oscillation with the axis of rotation located on the foil itself, is stable at all speeds. In 1934 Theodorsen developed the linearized non-stationary airfoil theory. Using this theory, in 1949 B. Smilg (ref.10) showed that single degree pitching oscillation flutter is possible when the axis of rotation is located between the quarter chord point and the leading edge. However an additional condition exists; the foil must be unreasonably heavy. As an example, a 15% thick airfoil hinged at the leading edge will flutter only if it is made of solid steel! The notion that single degree of freedom flutter was impossible persists. In the mid 50's the unsteady hydrodynamic theory for heaving oscillation was developed by Parkin (ref. 11) and Wu (ref. 12) . However the solution for pitching oscillation was not available until 1962 when Martin (ref. 13) and Parkin (ref. 14) solved this flow. Prior to this, supercavitating flutter analysis was done using the unsteady aerodynamic theory for an airfoil fitted with a spoiler. This theory was developed by L.C. Woods (ref. 15) who did notice that a single degree of freedom flutter was possible for a fully

stalled airfoil with the axis of rotation located at the midchord. With the availability of solutions for heaving and pitching motions, it is theoretically possible to investigate the stability of pitching oscillation about any axis on the foil by superposition of these two cases. The possibility of a single degree of freedom in pitching oscillation was apparently overlooked by researchers in this field.

Analysis

Consider a rigid foil as shown below.

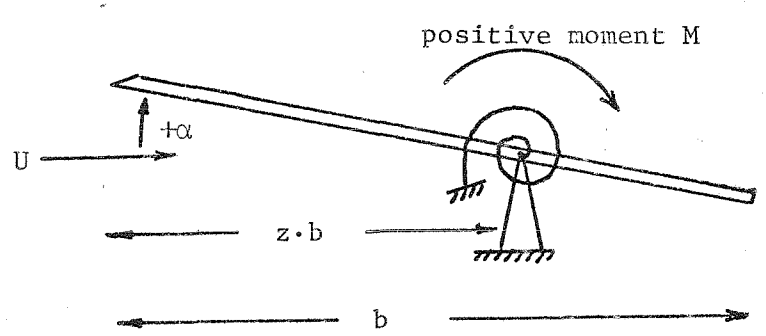

$I = I_o \rho_s t\, b^3$, moment of inertia about the hinge point.

The foil hinged at a distance zb away from the leading edge. All positive quantities are defined above. The equation of motion may be written directly as:

$$I\ddot{\alpha} + K\alpha = M$$

For a harmonic motion, one may write:

$$\alpha = \alpha_o e^{j\omega t} \quad \text{where} \quad \omega = \omega_R + j\,\omega_I$$

and $M = (M_R + j\,M_I)\, e^{j\omega t}$

Substituting into the equation of motion and separating the real and imaginary parts, one obtains :

real part: $I(\omega_R^2 - \omega_I^2) - K = -M_R/\alpha_o$ (I)

imaginary part: $2I\omega_R\omega_I = -M_I/\alpha_o$ (II)

The oscillatory angle of attack α grows in amplitude when $\omega_I < 0$. Since I and ω_R are positive quantities, equation II implies that the condition for instability is $M_I > 0$. The polar plots of the complex coefficient of moment derivative $C_{M,\alpha}$ are presented in fig. 48 as a function of the reduced frequency for various locations of the hinge point. The detailed calculations of these quantities are left to appendix E. The region above the horizontal axis, i.e. $M_I > 0$, is the instability region. In this region, the oscillation of the foil will cause the foil to extract energy from the flow and hence cause the oscillation to diverge. The figure shows that when the foil is hinged at a point located between approximately 0.6 chord and the trailing edge, there is a range of values of k where the oscillation is unstable.

When the free stream velocity is relatively low, the value of the reduced frequency $k = \omega b/U$ is relatively large. With increasing velocity, this value decreases and when it reaches the critical value as shown in fig. 48, the foil will theoretically become unstable. The question of whether the foil will or will not flutter can only be answered by examining the variation of k with increasing velocity. If the value of k can reach the critical value of k then the foil will flutter, otherwise it will remain stable. The natural frequency may be obtained by artificially forcing the foil to oscillate at a constant amplitude or setting $\omega_I = 0$ in equation I. The frequency equation simply becomes:

$$\omega_R^2 = \frac{K - M_R/\alpha_o}{I} = \frac{K - C_{MR,\alpha}\ \frac{1}{2}\rho_w\ U^2 b^2}{I} \qquad \text{(III)}$$

Where $C_{MR,\alpha}$ is the real part of coefficient of moment derivative. The static divergence speed is reached when $\omega_R \to 0$ or $K - C_{MR,\alpha} \frac{1}{2}\rho_w U^2 b^2 = 0$. Therefore the divergence speed is given by

$$U^2_{div} = \frac{2K}{C_{MR,\alpha}(0)\ \rho_w b^2}$$

Equation III may be non-dimensionalized by the divergence speed. If one defines the following quantities as:

$U = \eta U_{div}$ velocity

$I = I_o \rho_s t b^3$ moment of inertia, and

$\mu = \frac{\rho_s t}{\rho_w b}$ mass ratio parameter

then equation III may be written in dimensionless form as:

$$\frac{1}{\eta^2} = \frac{2I_o\mu}{C_{MR,\alpha}(0)}\ k^2 + \frac{C_{MR,\alpha}(k)}{C_{MR,\alpha}(0)}$$

The value of $C_{MR,\alpha}(k)\ /C_{MR,\alpha}(0)$ is available from appendix E or from fig. 48; thus the variation of k with η may be calculated.

Fig. 49 shows the variation of the reduced natural frequency with velocity for various values of the parameter $C_{MR,\alpha}(0)\ /(2I_o\mu)$. It shows that the reduced frequency decreases monotonically from a large value at low velocity to zero at the divergence speed. However, before the divergence speed is reached, the foil will flutter when the reduced frequency equals the critical value. In contrast to the super-cavitating hydrofoil case, an airfoil hinged at the leading edge possesses a limit on the value of k that can be achieved. This is shown in fig. 50. The limit of k decreases with increasing mass ratio and vice versa. Depending on the value of μ and I_o, this limit may or may not reach the critical value of the reduced frequency of $k = 0.36$. This is the reason why a very heavy foil can flutter and a very light one

cannot flutter.

Several conclusions may be immediately drawn from fig. 49, they are:

1.) The flutter boundary at $\sigma = 0$ is dependent only on the parameter k and U/U_{div} or ω/ω_n.

2.) Flutter always occurs before divergence since the value of $\eta = U/U_{div}$ is always less than unity.

3.) The thinner the foil (i.e. the smaller μ) the closer the flutter speed is to the divergence speed.

The agreements and discrepancies between theory and experiment are immediately apparent from the above list. First of all, the experiment confirmed item 2; flutter always occurs before divergence. Item 3, of course, cannot be proven experimentally since the foil will be damaged by flutter before the divergence speed can be reached. However, very thin foils are not of practical interest since they diverge before a cavity could be formed. The highest practical value of the parameter $C_{MR,\alpha}(0)/(2I_o\mu)$ is approximately 30 (corresponding to foil 3AA with μ based on the flexible chord length).

The theory predicts that there is only one reduced flutter velocity for all of the foils tested. For the case of a foil hinged at the trailing edge, this value is $1/k = 1/7$ or 0.143. The experimental results show that at $\sigma = 0$, the value of the reduced flutter speed is dependent also on the angle of attack and the mass ratio parameter. The experimental values of the reduced velocity range from 0.15 to 0.25 for all values of the angle of attack and mass ratio. Although the theoretical value is in good agreement with the lower end of the experimental value, there is a serious disagreement as far as the parametric dependency

is concerned. The dependency on the angle of attack obviously indicates that the unsteady hydrodynamics is a function of the angle of attack itself. This dependence is beyond the scope of the linear theory used here. The effect of varying the thickness of the foil and thus the mass ratio parameter is to vary the natural frequency of the foil and its mode of oscillation. Since the single degree of freedom model fixes the mode of oscillation, the critical value of the reduced frequency is determined immediately from the hydrodynamics. The variation of the critical reduced frequency with mass ratio is again beyond the scope of this simple model. Further discussion on the mass ratio parameter will be delayed until the next section when the eigenvalue model is discussed.

The above paragraph discusses the correlation between the theoretical and experimental reduced velocity. A more urgent question that needs to be answered from a designer's point of view is "how well does this theory preduct the flutter speed and frequency?" If one knows the value of the parameter $C_{M,\alpha}(0)/(2I_o\mu)$ in fig. 49 then the ratio of the flutter speed to the divergence speed is determined. The calculation of the divergence speed is outlined in Appendix C. The value of $C_{M,\alpha}(0)$ is available from Appendix E and its value is $(1 - 5/16)\,\pi/2$. The value of μ may be calculated from the known parameters of the foil and $I_o = 1/3$ for uniform thickness foil that is hinged at the trailing edge. Knowing all these parameters, the theoretical flutter speed may be calculated. The theoretical flutter frequency is calculated from the definition of the critical reduced velocity, i.e., $U/\omega b = 0.143$. Two cases are considered. The first is the case where the divergence speed is calculated by taking into account the presence of the rigid portion of the trailing edge. The second case neglects this portion and the foil

is assumed to have an overall chord length equal to the flexible chord length. The tables below list the experimental and theoretical values for these two cases.

CASE I:

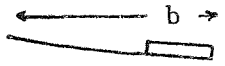

	VELOCITY, fps		FREQUENCY, cps		$U/\omega b$	
FOIL #	EXP AT 10°	THEORY	EXP	THEORY	EXP AT 10°	THEORY
3	28	16.0	60.6	35.0	0.15	0.143
4	52	26.7	83.3	57.9	0.20	0.143
6	36	21.2	60.0	47.3	0.19	0.143

CASE II:

	VELOCITY, fps		FREQUENCY, cps		$U/\omega a$	
					EXP AT 10°	THEORY
3	28	18.8	60.6	71.8	0.26	0.143
4	52	31.4	83.3	119.7	0.34	0.143
6	36	23.6	60.0	74.6	0.27	0.143

The theory consistently predicts lower values of the flutter velocities. In case I it underestimates the flutter velocity by an average of 44% and in case II by 36%. The agreement between the theoretical and experimental frequencies seems to be better. The theory underestimates the frequency by an average of 31% for case I and overestimates by an average of 28% for case II. Overall, case II seems a better model for calculating the flutter velocity and frequency.

It is difficult to pinpoint the exact cause of the discrepancies between the experiment and theory; however its sources may be identified by the following:

1.) Experiments on the unsteady loads of a supercavitating foil (for example, ref. 16) indicate that there are discrepancies between theory and experiment. This is especially true for the phase angle between the displacement and load which is the determining factor in the instability.

2.) Experimental conditions are different from the idealized conditions of the linearized theory. For example, in the water tunnel, a truly zero-cavitation number condition cannot be achieved.

3.) Since the cavity length in the experiment is finite, complicated flow phenomena such as the pinching of the cavity and the collapse and rebound of the bubbly coulds may influence the flutter boundary.

One would be tempted to list the general inadequacies of a single degree of freedom model as a cause of the discrepancies between the experiment and theory. However, a more sophisticated treatment of a cantilevered foil which will be presented seems to produce larger discrepancies between theory and experiment. The tunnel wall effect for 2-D unsteady choked supercavitating flow has been studied theoretically by J. H. Kim (ref. 23). His result indicates that if the tunnel wall is taken into consideration, the reduced flutter frequency would increase and therefore increase the discrepancies between theory and experiment.

IV-2 Cantilevered Foil Model (ref. 6)

Consider a supercavitating foil cantilevered at the trailing edge as shown below.

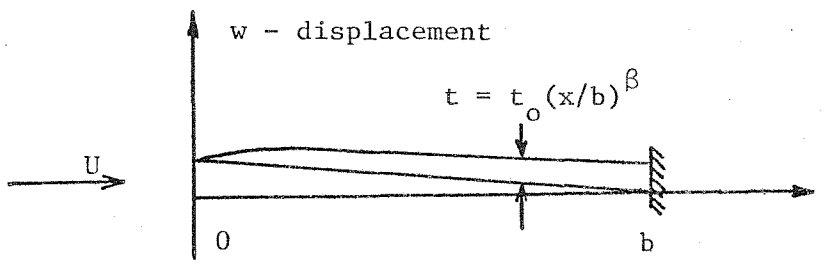

If one considers only the chordwise deformation, then the equation of motion of the foil may be written as a beam equation:

$$\frac{\partial^2}{\partial x^2}\left(D\,\frac{\partial^2 w}{\partial x^2}\right) + \rho_s t\,\frac{\partial^2 w}{\partial t^2} = p(x,t)$$

where

$$D = \frac{Et^3}{12(1-\nu^2)}$$

and $p(x,t)$ = the hydrodynamic loading.

The unsteady part of the motion may be separated from the steady state part and assuming a harmonic motion, one may write the equation of motion as:

$$\frac{d^2}{dx^2}\left(D\,\frac{d^2\tilde{w}}{dx^2}\right) - \rho_s t\omega^2\tilde{w} = \tilde{p}(x)$$

The boundary conditions are:

At the root $x = b$:

No displacement $\tilde{w} = 0$

Zero slope $\frac{d\tilde{w}}{dx} = 0$

At the tip $x = 0$

No moment $\quad D \dfrac{d^2\tilde{w}}{dx^2} = 0$

No shear $\quad \dfrac{d}{dx} D \dfrac{d^2\tilde{w}}{dx^2} = 0$

The above equation is an eigenvalue problem since the hydrodynamic loading $\tilde{p}(x)$ is a function of the deformation $\tilde{w}(x)$ itself. This problem has been solved by H. Murai (ref. 6) and S. Shimizu (ref. 17) for the case of a foil with thickness distribution of the form:

$$t(x) = t_o (x/b)^{\beta}$$

where β ranges from 0.5 to 1. The case of $\beta = 1$ corresponds to a wedge and $\beta = 0$ corresponds to a flat plate. The result at $\beta = 0$ presented here is an extrapolation of their calculation . Fig. 51 shows the critical value of the reduced frequency k as a function of the shape factor β. For a flat plate, the critical value of k is 11.5. The flutter velocity is given by:

$$\frac{Et_o^3}{12(1-\nu^2)\rho_w U_f^2 b^3} = 5.37 + 10.67\mu$$

The table below lists the theoretical and experimental values of flutter velocity and frequency. The theoretical values are obtained by neglecting the rigid rear portions of the foils and using the flexible chord length as the overall chord.

	VELOCITY, fps		FREQUENCY, cps		$U/\omega a$	
FOIL #	EXP AT 10°	THEORY	EXP	THEORY	EXP	THEORY
3	28	13.9	60.6	87.2	0.15	0.09
4	52	23.1	83.3	145.0	0.20	0.09
6	36	17.4	60.0	90.4	0.19	0.09

Compared to the single degree of freedom model, this model results in a larger discrepancy between the experiment and theory. Explanations of the discrepancies given previously are also generally applicable to this model.

The mode of oscillation of the foil during flutter is an eigenvector of the equation of motion and it is of course affected by the parameter $\rho_s t(x)$ in the equation of motion. Once the mode of oscillation is known, the critical value of k is a determined quantity. The parameter $\rho_s t$ is directly related to the mass ratio parameter $\mu = \rho_s t/\rho_w b$ and its effect on the critical value of k is shown in fig. 51. The curves show that the critical value of k is not sensitive to the mass ratio. According to the theory, two foils with identical geometry but different thicknesses, i.e. foils 3 and 4, should have the same reduced flutter frequency. Experiments show otherwise, however. If one assumes that the theory is correct then the discrepancy can only be explained if the unsteady hydrodynamics is not solely a function of the reduced frequency k. This implies that other parameters such as the Reynolds number and Weber number might be important in the experiment.

IV-3 Improvement of the Models

The two models discussed in the preceeding sections assume that the foil is either hinged or cantilevered at the trailing edge. In reality, a super-cavitating hydrofoil has a considerable rigid chord at the trailing edge. It was demonstrated in III-3.b that the rigid portion of the chord at the trailing edge has an influence on the flutter velocity.

The first step toward understanding the effect of the rigid trailing edge portion is to include it in the Single Degree of Freedom Model. The new model is shown below.

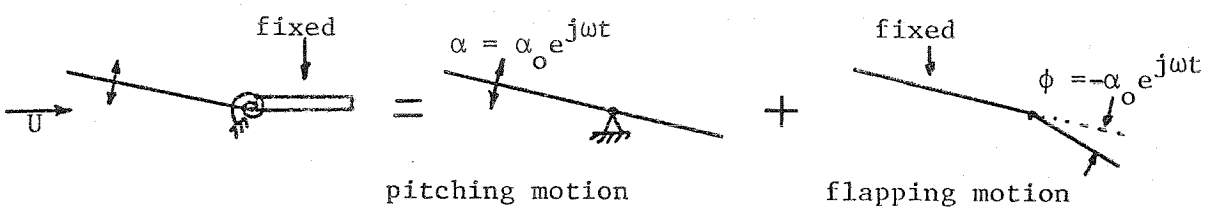

The equation of motion is, of course, the same, the only difference is the reduced flutter frequency. The motion of an oscillating foil with fixed trailing edge may be obtained by superposition of pitching and flapping motion as shown above. The linearized potential flow solution for the pitching motion is outlined in Appendix E. The linearized potential flow problem for the flapping motion has been solved by C. S. Song (ref.22). The moment at the hinge due to the leading edge portion of the chord may be obtained by superposition of the solutions for pitching and flapping motion.

IV-4. Noncavitating Wake Flow

It is well known that a noncavitating wake flow is similar to the

supercavitating flow at least as far as the steady state lift and drag are concerned. For an oscillating foil, the two flows are different in some respects. First of all the apparent mass of the noncavitating flow is almost twice as great as the apparent mass of a supercavitating foil. Dynamically the noncavitating wake flow should be similar to the non-separated airfoil since in both cases the oscillation of the foil results in perturbations of the flow over and under the foil itself. In contrast, an oscillating supercavitating foil will create perturbation of the flow that is mainly confined to the region below the foil. If one accepts this qualitative argument, then the noncavitating wake flow case should not flutter since a rigid airfoil hinged at the trailing edge does not flutter (experimentally or within the context of potential flow theory).

V. FUTURE EXPERIMENTS

The single degree of freedom model demonstrated that a rigid foil pivoted at an axis beyond 0.6 chord from the leading edge can flutter. It would be interesting to test this model experimentally. The motivation for this experiment comes from the fact that the foils tested here exhibited a dependency on the mass ratio parameter while the single degree of freedom model and the cantilevered model predicts otherwise. The dependency of the critical value of the reduced frequency on the mass ratio could come from the differences in the experimental mode of oscillation or the fact that the unsteady flow is not dependent solely on the reduced frequency (or both). By testing a rigid chord foil, the first cause is isolated and the second cause may be investigated. This may be easily done by adding mass to the foil.

It was mentioned in the introduction that leading edge flutter can also occur in supercavitating pumps. Because of the close proximity of the blades, it is expected that the flutter boundary will differ from an isolated blade case. An experiment with cascade flexible foils in the 2-D test section of the HSWT would lead the way in understanding the more complex problem of the supercavitating pump.

VI. SUMMARY AND CONCLUSIONS

The problem of leading edge flutter of a supercavitating hydrofoil has been studied experimentally and theoretically. The experiments were carried out in the Free Surface Water Tunnel and in the High Speed Water Tunnel of the California Institute of Technology Hydrodynamic Laboratory.

The experiment determined the flutter boundary of an idealized flat plat hydrofoil. The flutter boundary was very distinct in the High Speed Water Tunnel. The study assumed that the problem of leading edge flutter could be represented sufficiently well by the reduced velocity, cavity length or cavitation number, mass ratio, ratio of flexible chord to overall chord and the angle of attack. For "infinitely" long cavity case or zero cavitation number, the mass ratio and the chord ratio have an opposite effect on the reduced velocity over the range of parameters tested. Increasing mass ratio increases the reduced velocity and increasing chord ratio decreases the reduced velocity. Flutter velocity was observed to be dependent on the angle of attack and minimum at 10°-11°.

At a moderate to short cavity length (say, less than 5 chords), leading edge flutter phenomenon was influenced by the cavity closure condition. During flutter, leading edge oscillation caused pinching of the rear end of the cavity. The resonances of flutter amplitude with respect to cavity length could be a manifestation of the role played by the cavity closure. The inherent unsteadiness of flow with short cavity also influenced the hydro-elastic response of the foil. Flutter velocity of a foil with short cavity was lower than its asymptotic value at an

infinitely long cavity. The reduction of flutter velocity could be as much as 50%. For all the foils tested, the reduced velocity lies between 0.15 to 0.25. The reduced velocity is defined as $U/\omega b$ where U is the free stream velocity, ω is the angular flutter frequency and b is the chord length.

The analytical study models the leading edge flutter problem as a rigid chord foil hinged at the trailing edge. The linearized problem was studied for the zero cavitation number flow. For the idealized problem, the reduced flutter velocity is not a function of the mass ratio, angle of attack and the chord ratio. The theoretical value of the reduced flutter velocity is 0.143 and somewhat lower than that obtained experimentally. The calculated flutter velocity is approximately 36% lower than that observed and the theory overestimates the flutter frequency by an average of 28%. The analysis also predicts that flutter occurred before divergence which was confirmed experimentally.

Frequency (cps)	Mode	
210	1st bending (possibly a sub-harmonic excitation)	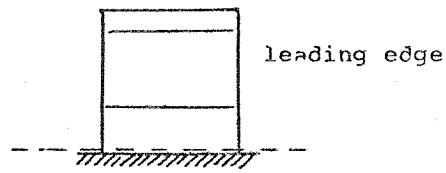
410	1st bending	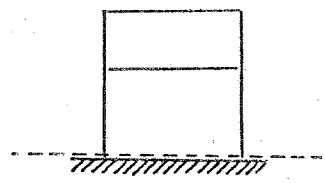
530	chordwise deformation	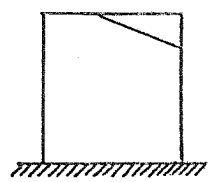
860	1st torsional mode	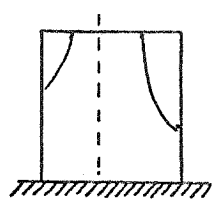
1725	chordwise deformation	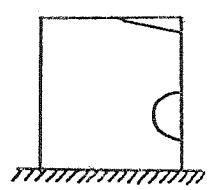
2600	- " -	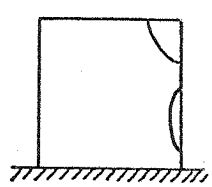

Note: solid lines are contour lines
dashed lines are nodal lines

Table 1. Natural frequencies and modes of CIT 35-435 mod II foil in air.

MODE	Theory in vacuum, cps				Experiment in air, cps			
	foil # 1	foil #2	foil#3A	foil #3	foil# 1	foil #2	foil #3A	foil #3
first bending	34.7	67.2	132.2	192.9	37.0	69.0		230.4
first torsion	42.1	81.6	160.5	234.2				266.8
second torsion	69.3	134.4	264.4	385.8				353.6
second bending	217.5	421.4	829.4	1210.2				

MODE	Theory in water, cps				Experiment in water, cps			
	foil #1	foil #2	foil#3A	foil #3	foil#1	foil #2	foil#3A	foil #3
first bending	2.2	5.9	16.1	28.2	6.3	14.0	37.5	62.5
first torsion	4.3	11.5	31.5	55.0		19.2	50.5	89.0
second torsion	7.6	20.5	55.8	97.4		32.2	77.5	
second bending	13.6	36.6	100.8	176.9				

Note: All foils have 6" span and 6" overall chord length and are made of 6061 T-6 aluminum. The thicknesses of foil 1; 2; 3A and 3 are 0.016"; 0.031"; 0.061" and 0.089" respectively.

TABLE 2. DIMENSIONS AND NATURAL FREQUENCIES OF FOILS TESTED IN THE FREE SURFACE WATER TUNNEL.

Foil No.	Thickness inch	Length of flexible chord & % of total chord length.	1st bending natural frequency in air c.p.s. exp. value	1st bending natural frequency in a super-cavitating flow, c.p.s. exp. value
2	0.031	3.5" , 58%	71.2	destroyed
3AA	0.068	3.5" , 58%	159.4	44
3	0.089	3.5" , 58%	195.7	60
4	0.125	3.5" , 58%	294.0	83
5	0.050	2.5" , 42%	192.3	53
6	0.125	4.23", 71%	200.0	60

Note: All foils have 6" span and 6" chord and are made of 6061 T-6 aluminum.

TABLE 3 . Dimensions and natural frequencies of the foils tested in HSWT.

FOIL #	THICKNESS IN INCH	FLUTTER FREQ., cps	$\frac{1}{k} = \frac{U}{\omega b}$	$\mu = \frac{\rho_s t}{\rho_w b}$	$\frac{1}{k^*} = \frac{U}{\omega a}$	$\mu^* = \frac{\rho_s t}{\rho_w a}$	$\frac{a}{b}$
3	0.089	60	0.20	μ_3	0.34	μ_3^*	58%
4	0.125	83	0.25	$1.40\mu_3$	0.43	$1.4\mu_3^*$	58%
5	0.050	53	0.18	$0.56\mu_3$	0.43	$0.78\mu_3^*$	42%
6	0.125	60	0.25	$1.40\mu_3$	0.35	$1.15\mu_3^*$	71%

NOTE: $\mu_3 = 0.04$ $\mu_3^* = 0.069$

values of the reduced velocity are at $\alpha = 7^\circ$

TABLE 4. TABLE OF THE REDUCED VELOCITIES, MASS RATIO AND THE PARAMETER a/b.

Foil #	$\alpha = 7^o$	$\alpha = 8^o$	$\alpha = 10^o$	$\alpha = 13^o$	FREQ. C.P.S.
3AA	36(0.26)[1]				44
3	38(0.20)		28(0.15)	32.3(0.17)	60.6
4	65(0.25)[2]		52(0.2)		83.3
5	30(0.18)[3]				53.3
6		47(0.25)[4]	36(0.19)	39.6(0.21)	60

NOTE: The first figure is the flutter velocity in f.p.s., and figure in parenthesis is the reduced velocity $U/\omega b$.

1) Extrapolated value. The last experimental value is 23 f.p.s. at $\ell/b = 2$
2) Extrapolated value. The last experimental value is 60.2 f.p.s. at $\ell/b = 2.7$
3) Extrapolated value. The last experimental value is 20 f.p.s. at $\ell/b = 2.5$
4) Extrapolated value. The last experimental value is 37.7 f.p.s. at $\ell/b = 3.5$

TABLE 5. FLUTTER VELOCITY AND THE REDUCED FLUTTER VELOCITY $U/\omega b$ AT $\ell/b > 6$ AND VARIOUS ANGLES OF ATTACK

FOIL #	THEORETICAL FULLY WETTED, NON-SEPARATED		EXPERIMENTAL NON-CAVITATING WAKE FLOW	THEORETICAL SUPERCAVITATING FLOW	
	W/CAMBER EFFECT	W/O CAMBER EFFECT		W/CAMBER EFFECT	W/O CAMBER EFFECT
1	7.9	3.8	4	15.0	5.3
2	21.1	10.5	6.8	40.5	14.3
3A	58.2	29.1	*	111.8	39.5
3	102.5	51.3	*	197.0	69.7

Note: All values are in feet per second.

* Foils became ventilated above 16 fps; no divergence was observed up to the maximum tunnel speed of 26 fps.

TABLE 6. THE THEORETICAL AND EXPERIMENTAL DIVERGENCE SPEEDS

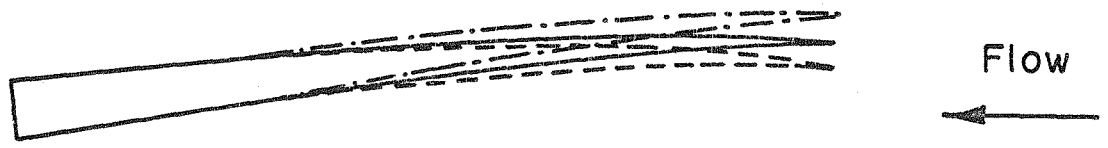

FIG. I TYPICAL PROFILE OF A SUPERCAVITATING HYDROFOIL.
DASHED LINES SHOW THE MODE OF LEADING EDGE FLUTTER

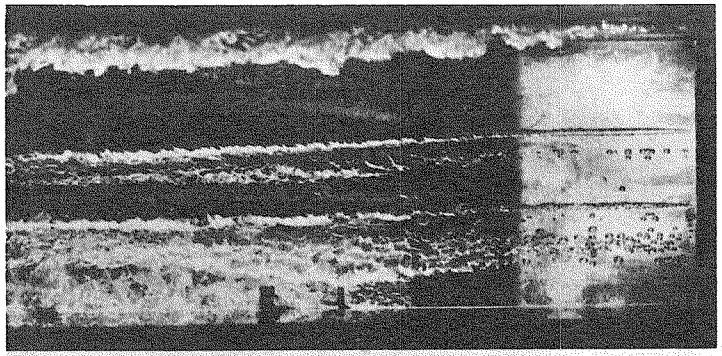

Fig. 30 Upper surface cavitation for $\alpha_a = 2.73^\circ$, $\sigma_v = .07$, $V = 30.0$ fps.

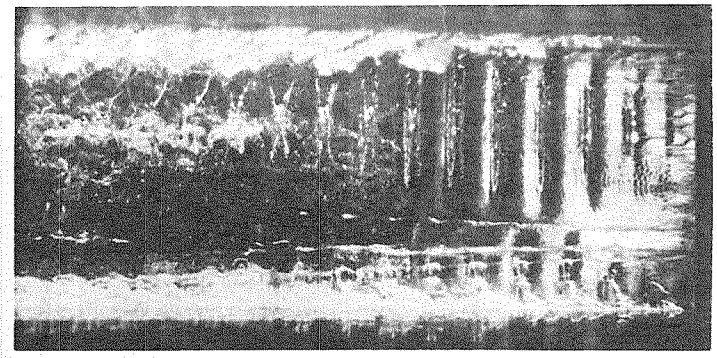

Fig. 32 Upper surface cavitation for $\alpha_a = 5.73^\circ$, $\sigma_v = .12$, $V = 29.2$ fps.

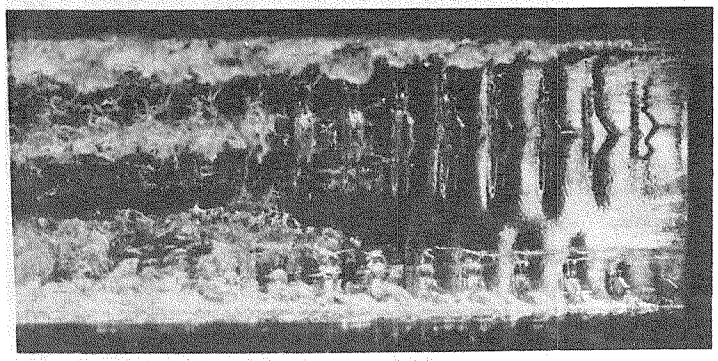

Fig. 31 Upper surface cavitation for $\alpha_a = 5.73^\circ$, $\sigma_v = .20$, $V = 30.8$ fps.

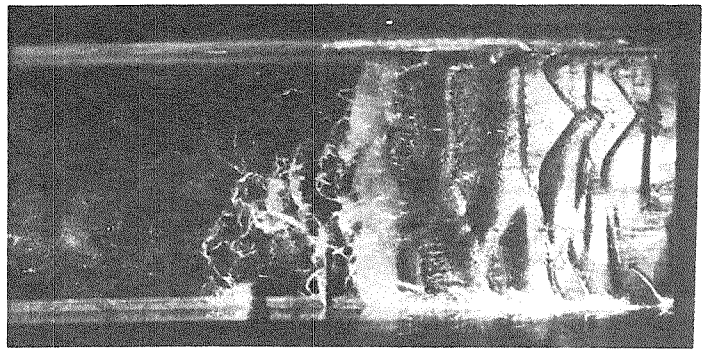

Fig. 33 Upper surface cavitation for $\alpha_a = 2.456^\circ$, $\sigma_v = .28$, $V = 41.0$ fps.

FIG. 2 WAVES ON THE UPPER SURFACE DUE TO LEADING EDGE FLUTTER. (FROM REF. 2)

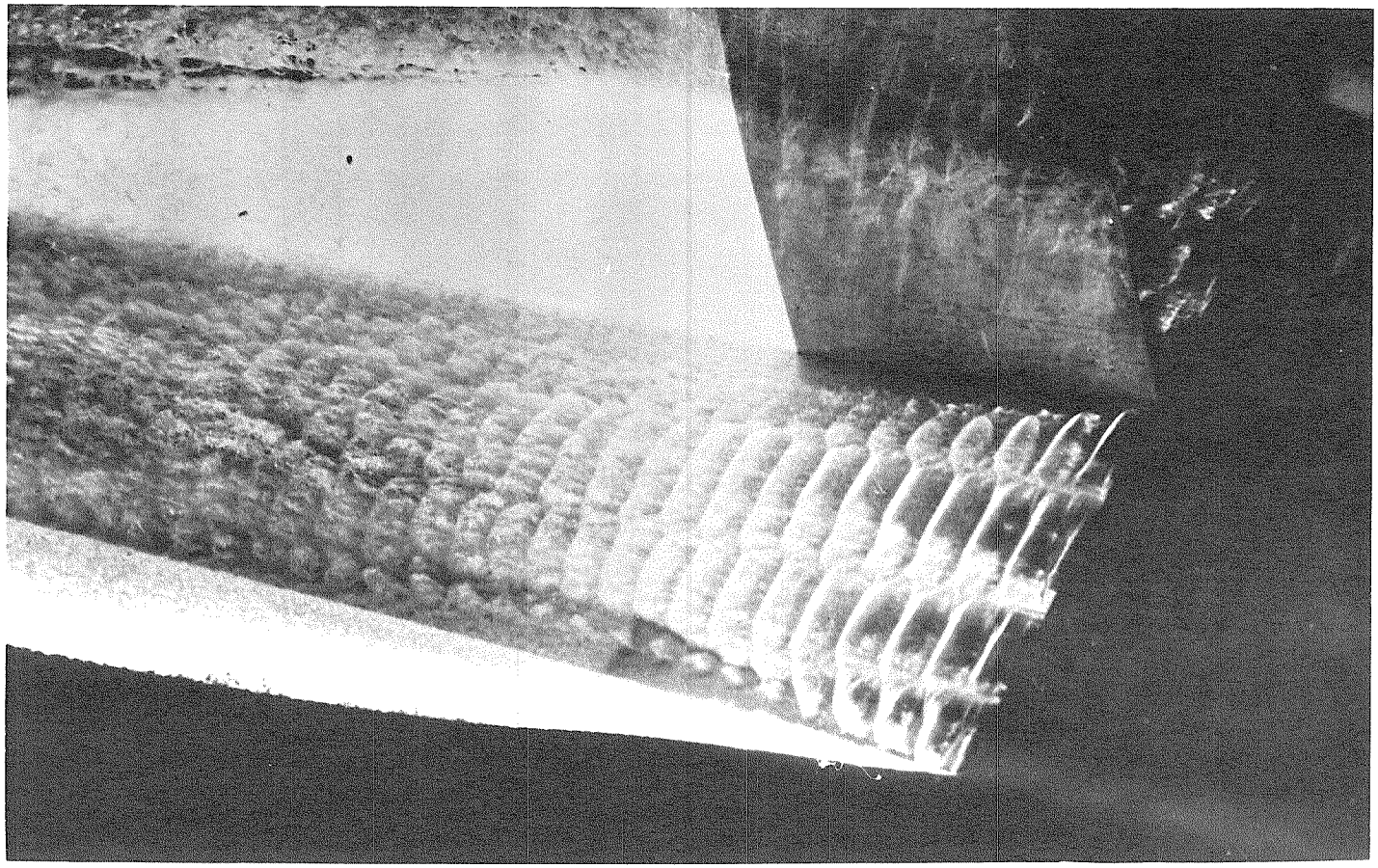

Vibration at d/c = 1.0, α = 7.44 deg, and U = 105.8 fps
(σ = 0.192)

FIG. 3 LEADING EDGE FLUTTER WITH SPANWISE PHASE VARIATION.
(FROM REF. 3)

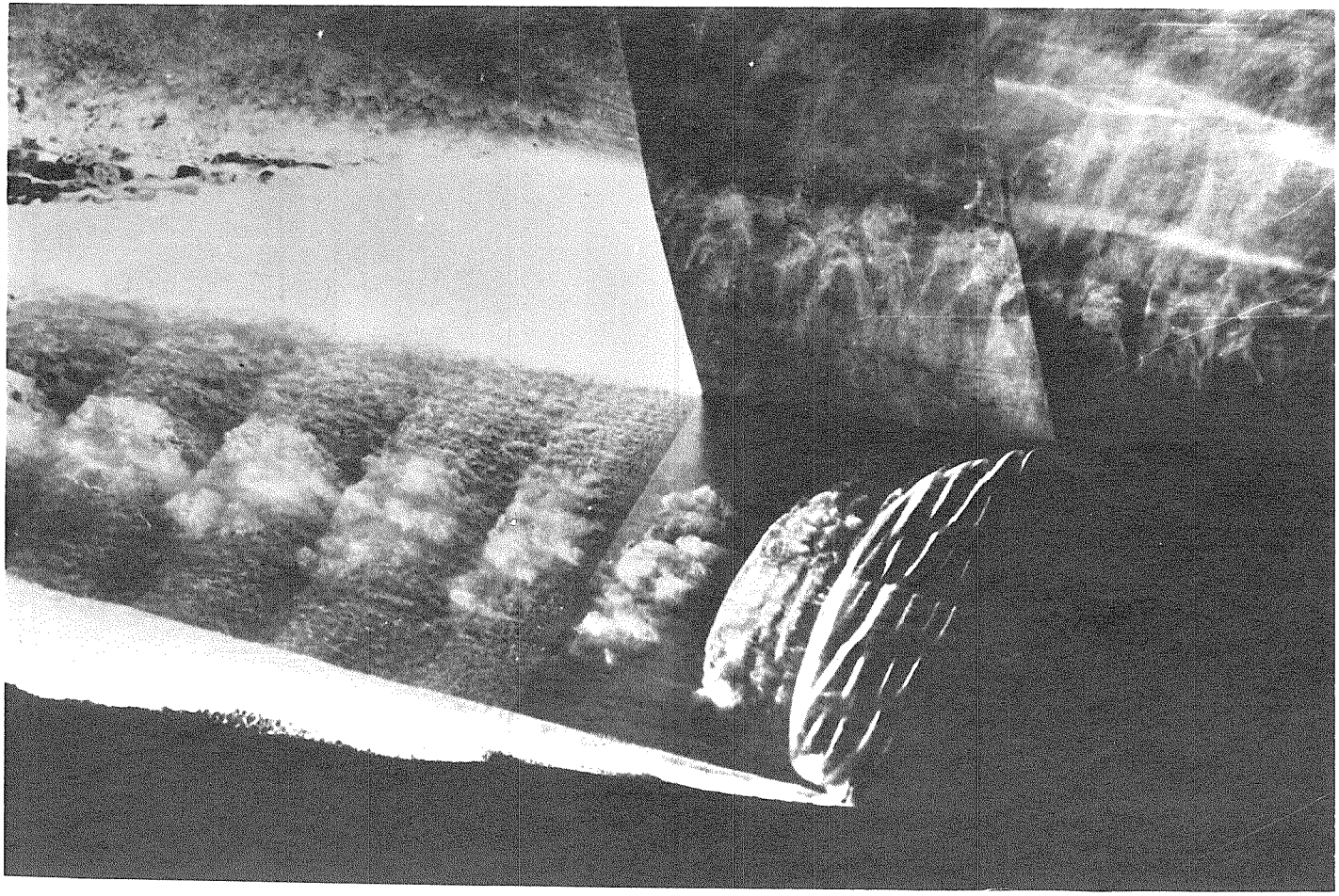

Vibration at d/c = 1.0, α = 7.44 deg, and U = 91.9 fps
(σ_v = 0.257)

FIG. 4 ANOTHER MODE OF LEADING EDGE FLUTTER WITH PERIODIC CAVITY SHEDDING AT THE LEADING EDGE. (FROM REF. 3)

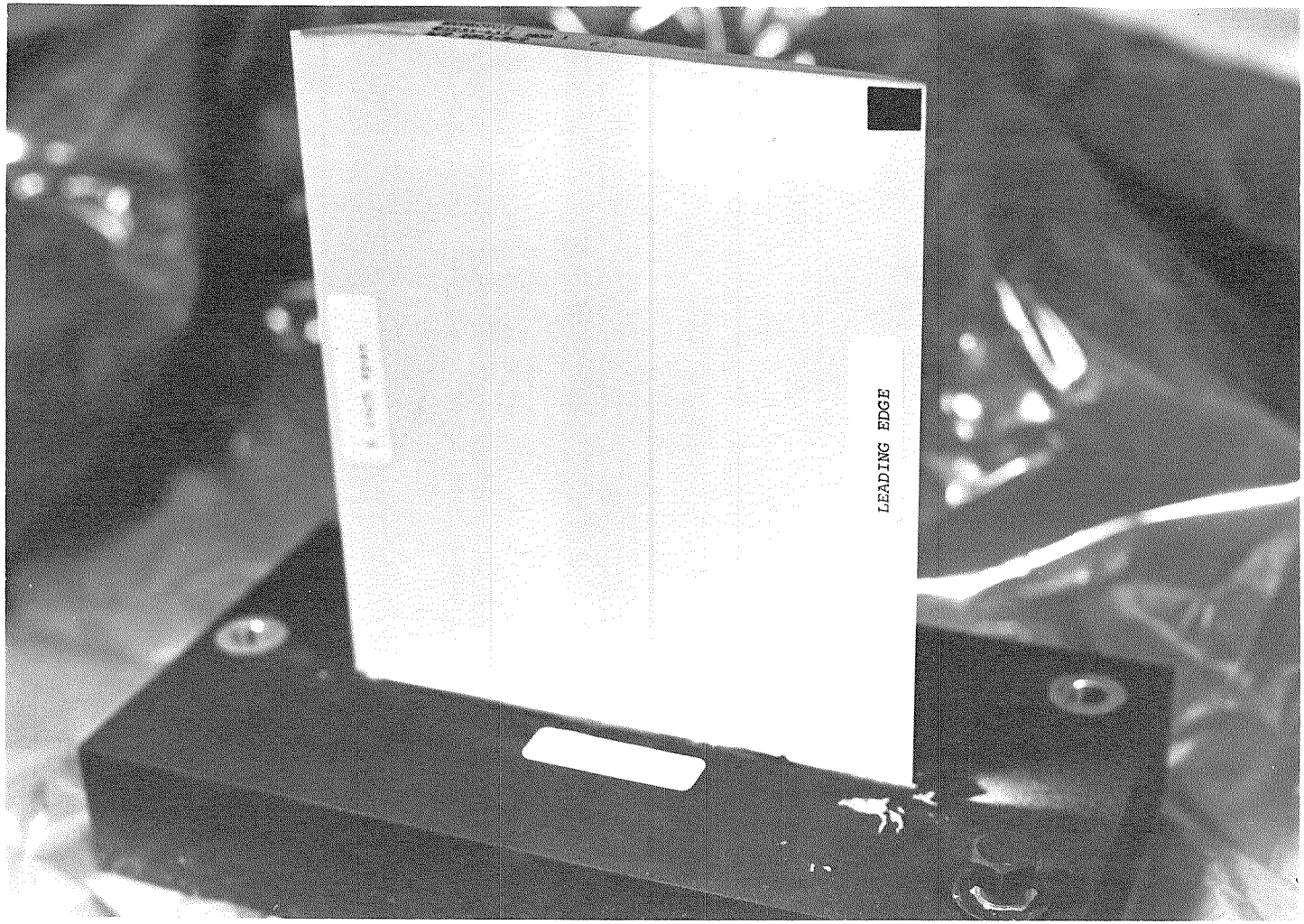

FIG. 5 C.I.T. 35-435 HYDROFOIL

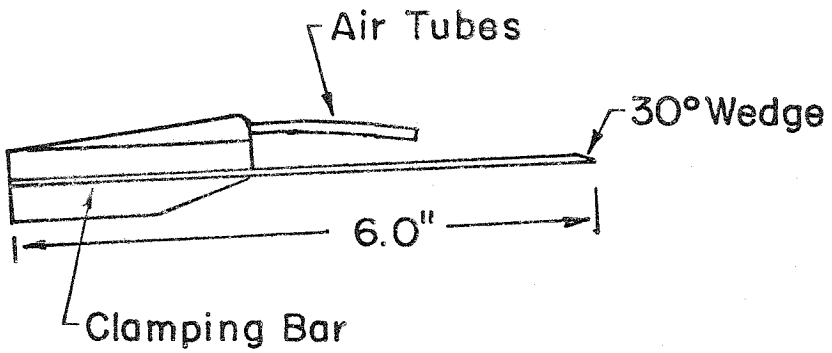

FSWT MODEL 14" SPAN

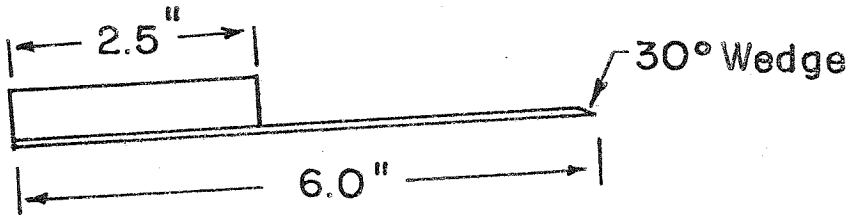

HSWT MODEL 6" SPAN

FIG. 6 CROSS SECTIONS OF MODELS TESTED IN THE FSWT AND HSWT

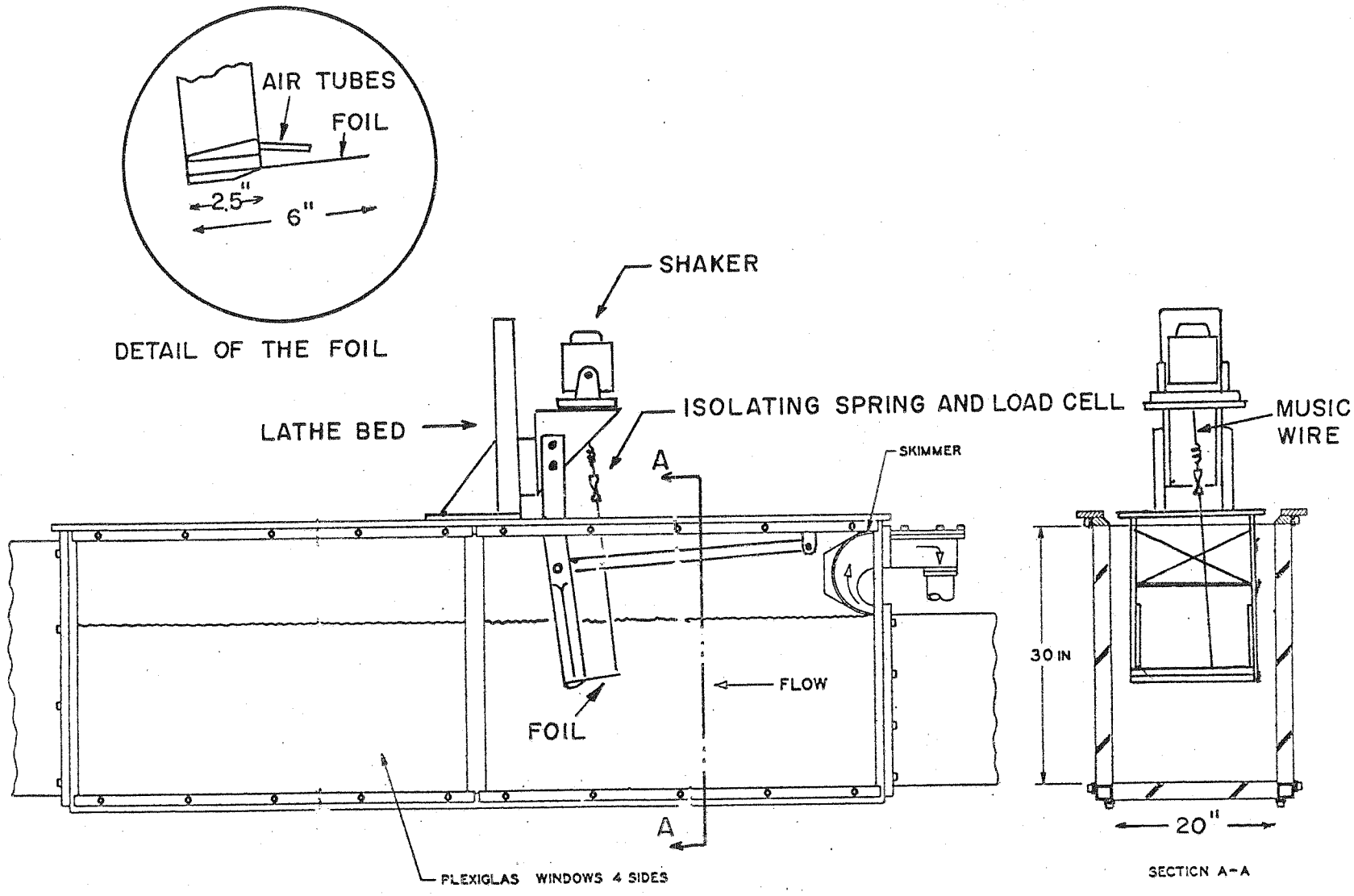

FIG. 7 EXPERIMENTAL SET-UP IN THE F.S.W.T.

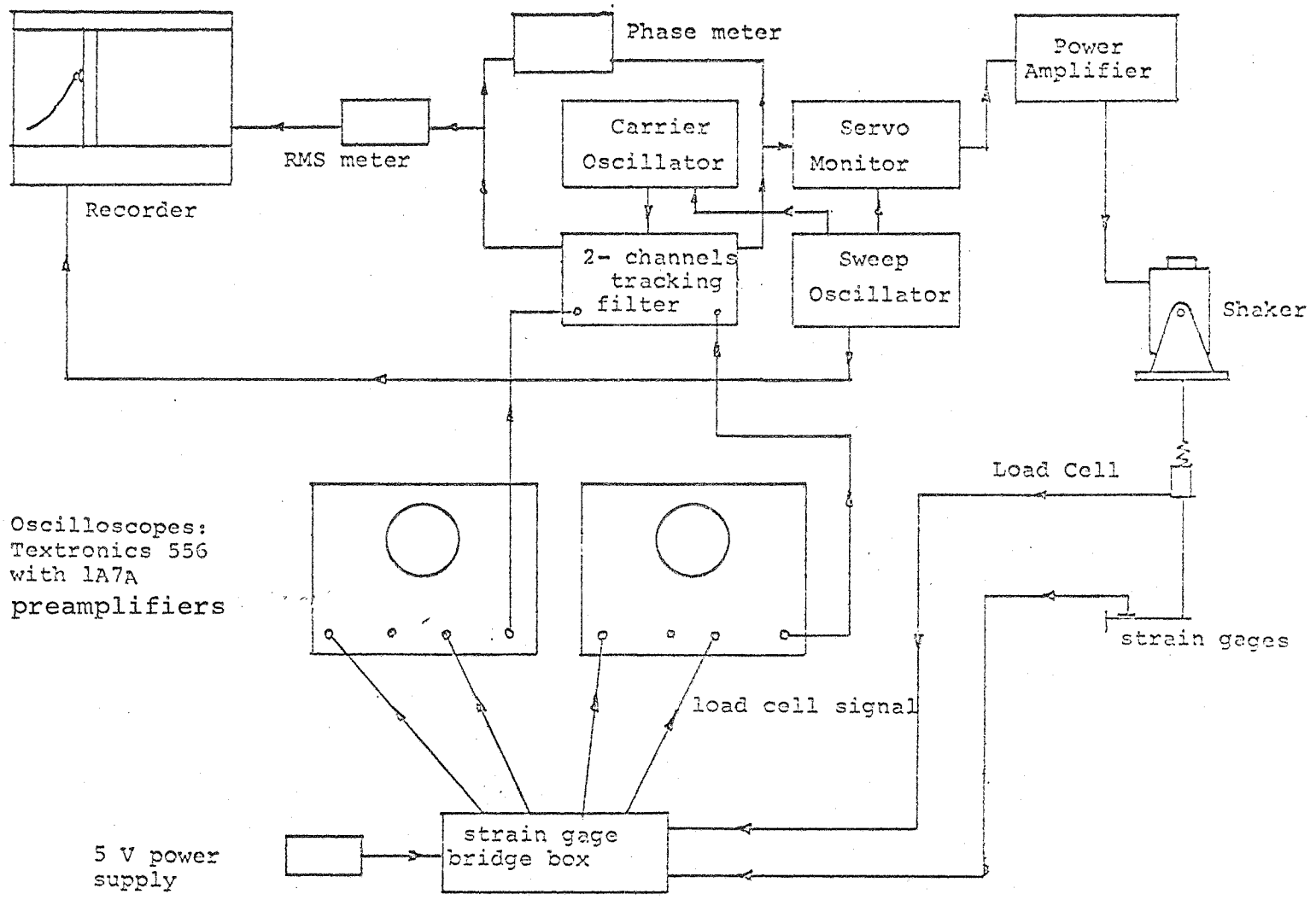

Fig 8. Block diagram of instruments for frequency response measurements.

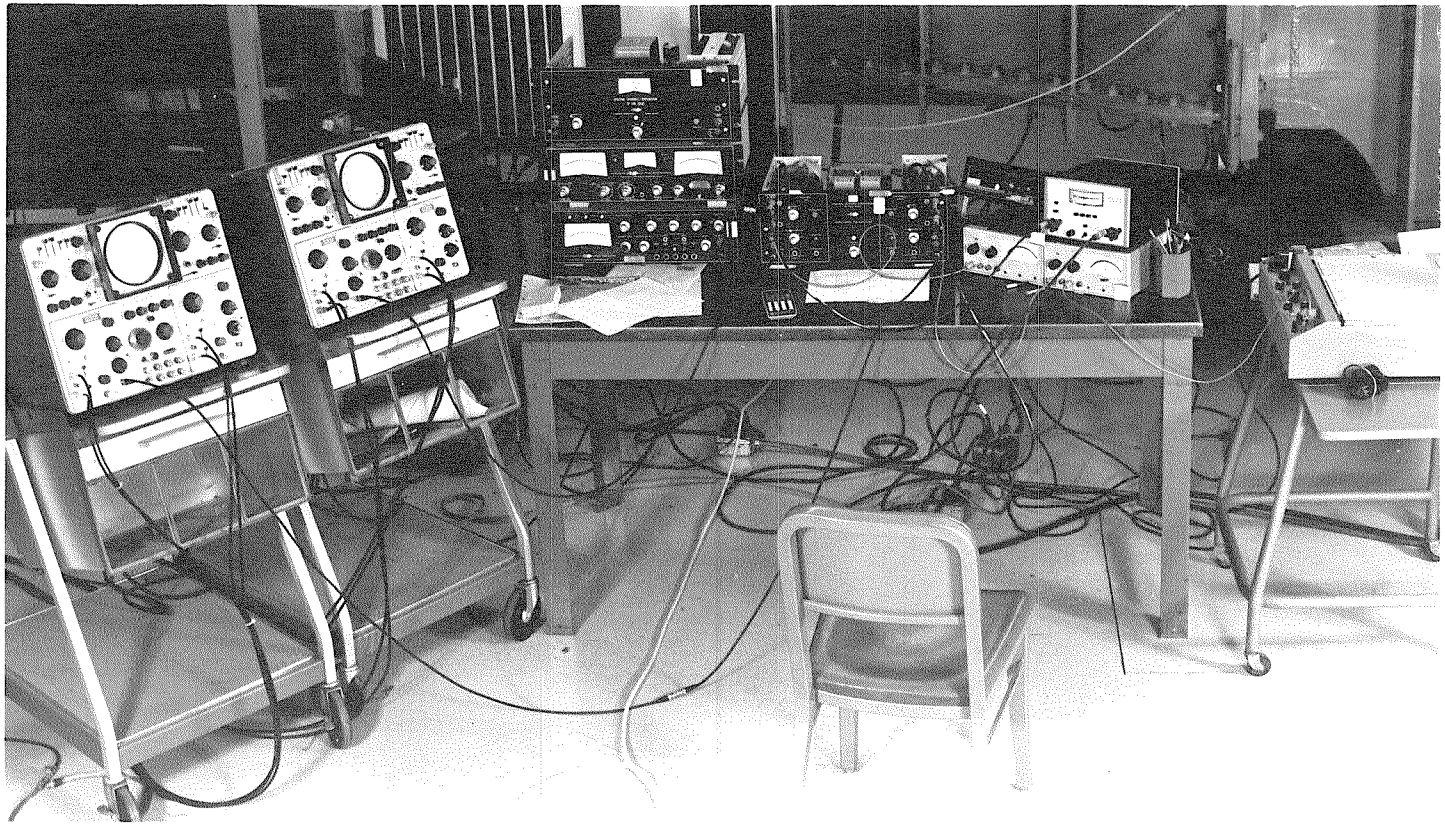

FIG.9 SERVO SYSTEM FOR FREQUENCY RESPONSE MEASUREMENTS

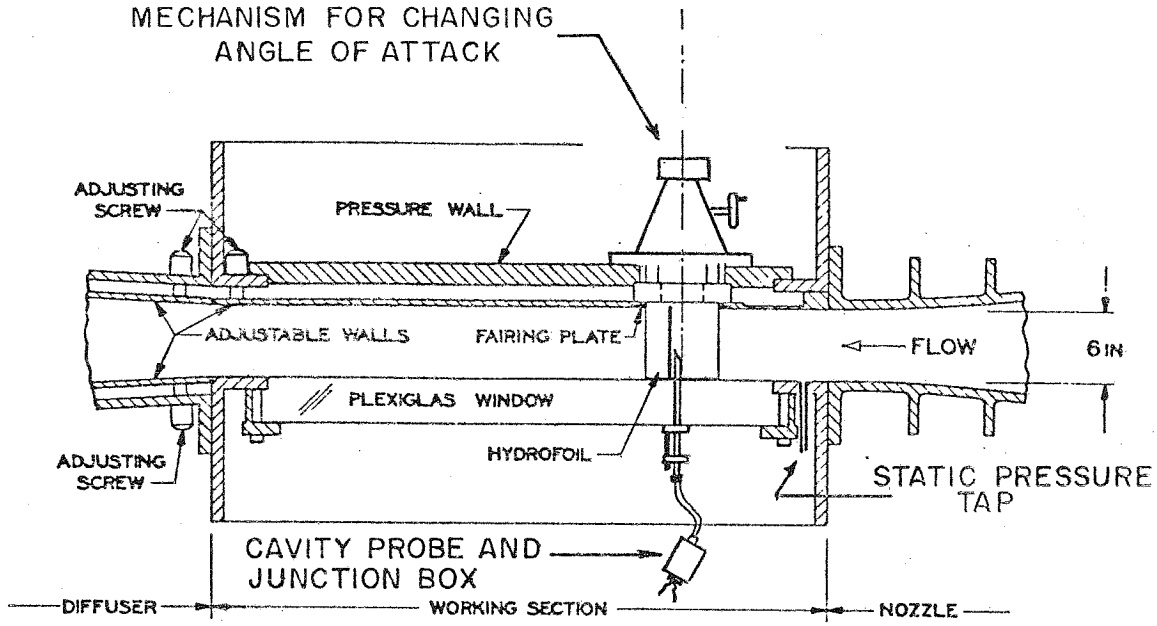

SECTION A-A

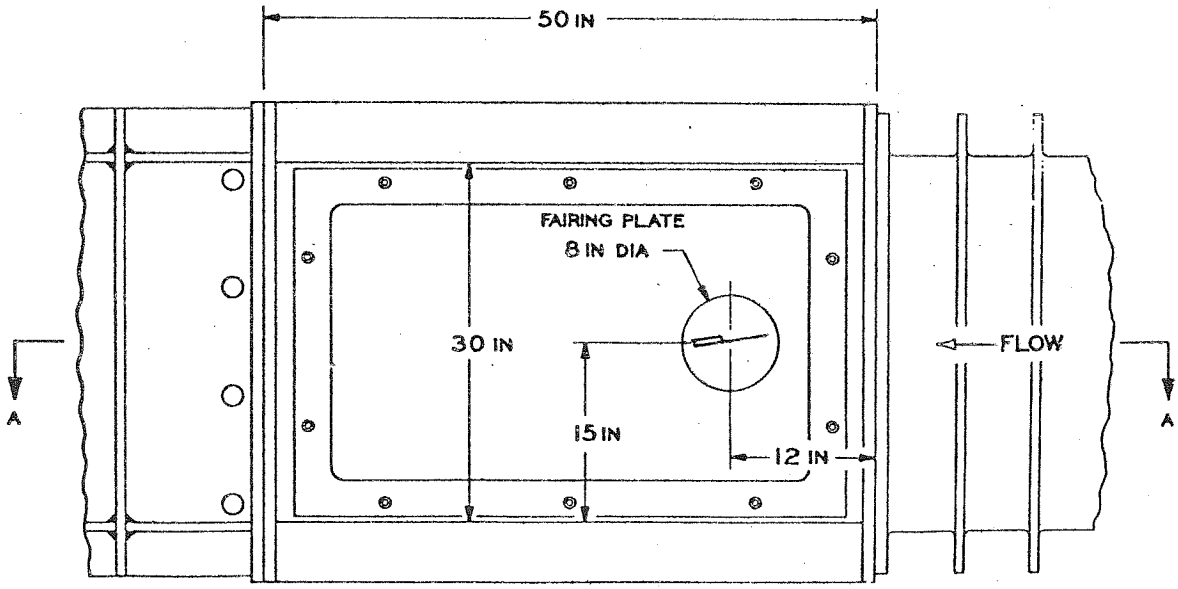

PLEXIGLAS WINDOWS TOP AND BOTTOM

FIG. 10 2-D TEST SECTION OF THE HIGH SPEED WATER TUNNEL

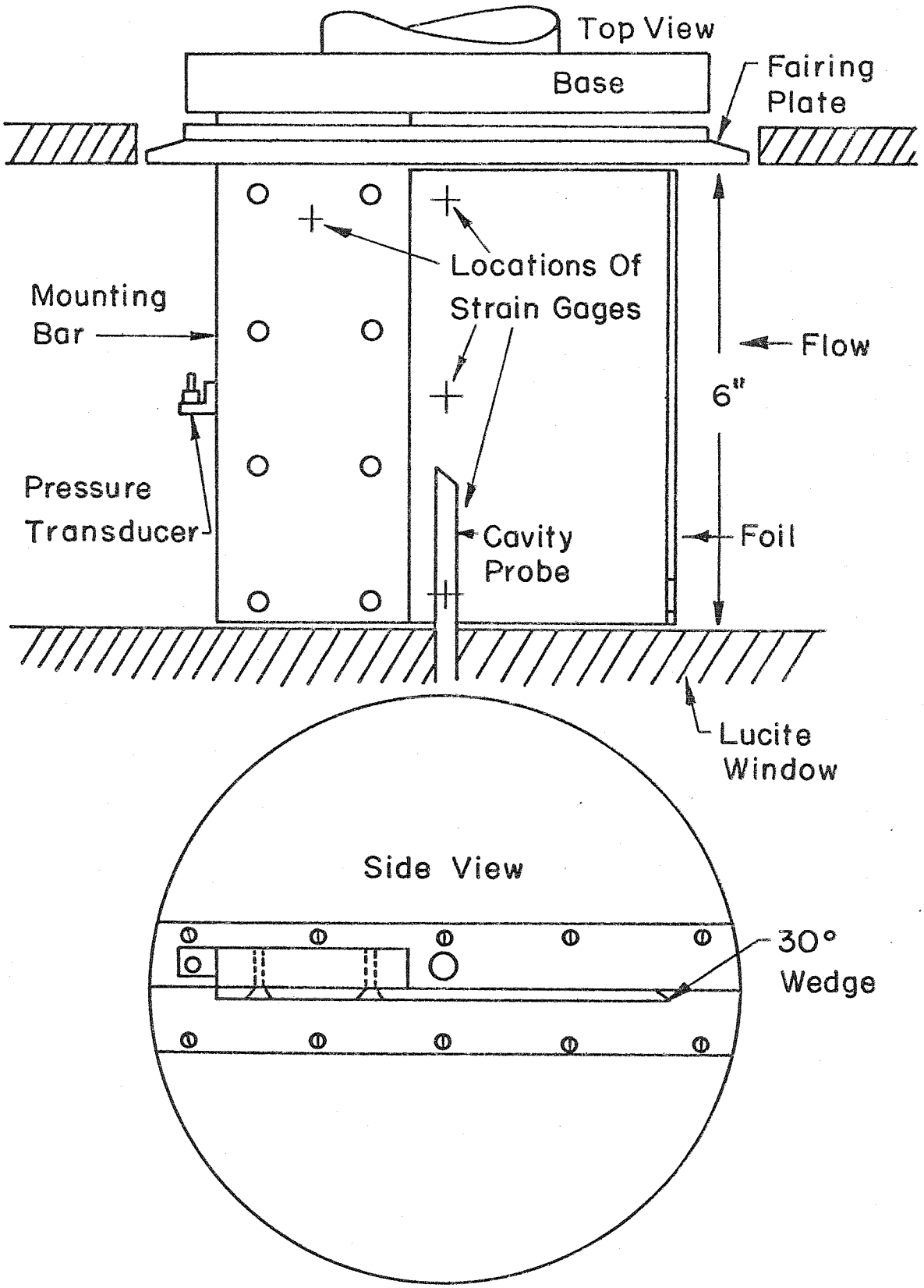

FIG. 11 HYDROFOIL AND ITS MOUNTING BASE

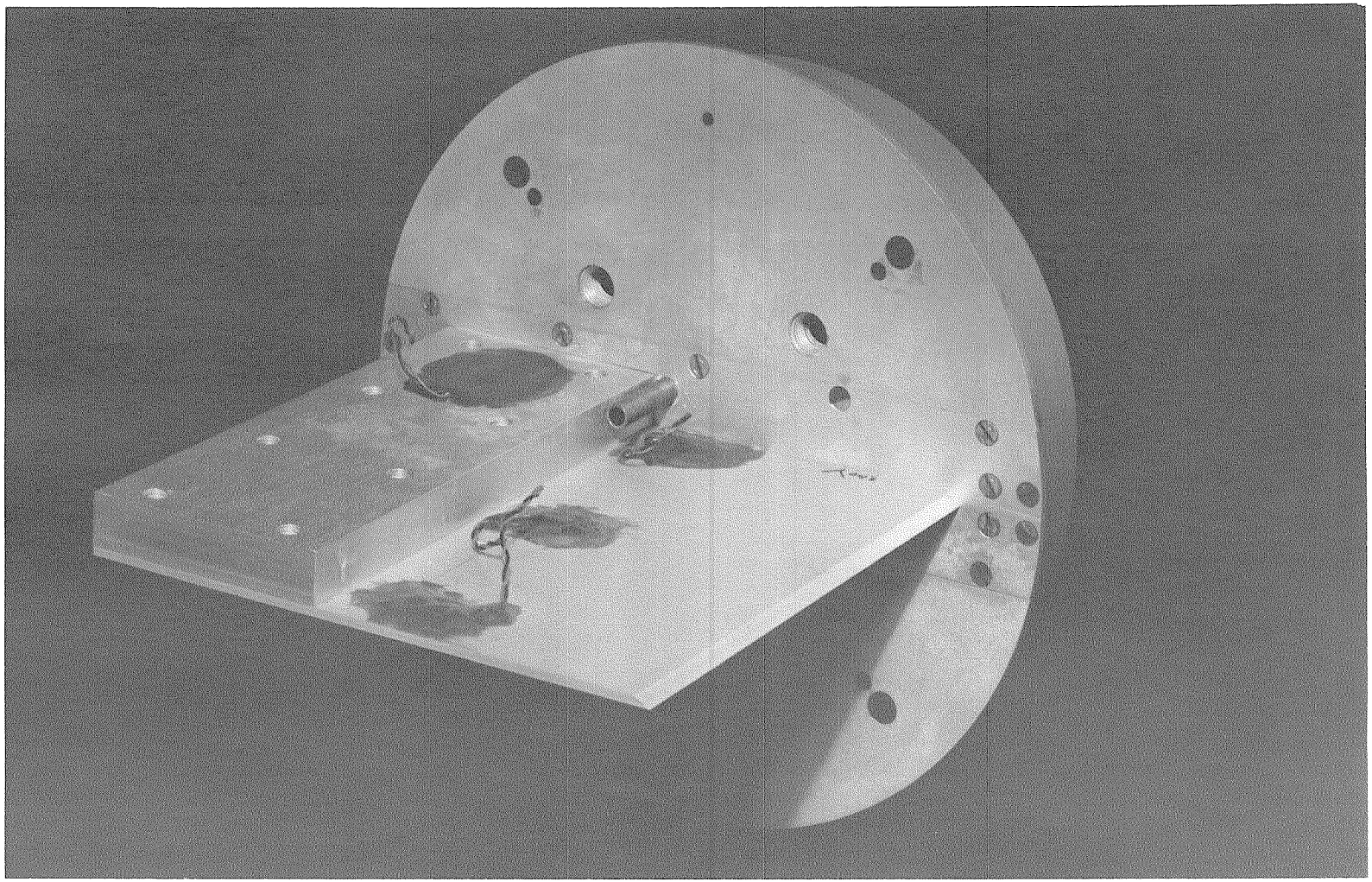

FIG. 12 MODEL TESTED IN THE H.S.W.T.

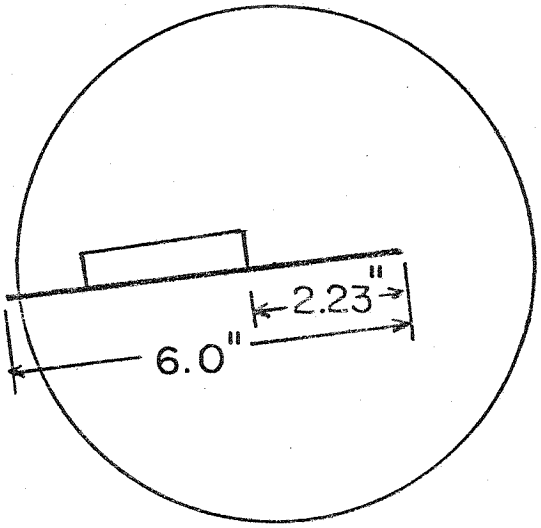

Foil 5

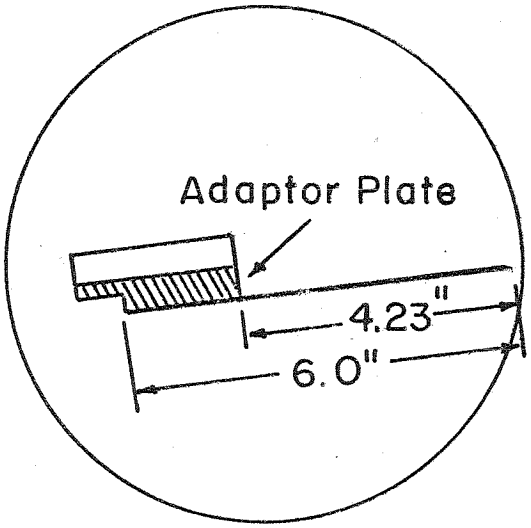

Foil 6

FIG. 13 MOUNTING SYSTEM FOR FOILS 5 AND 6

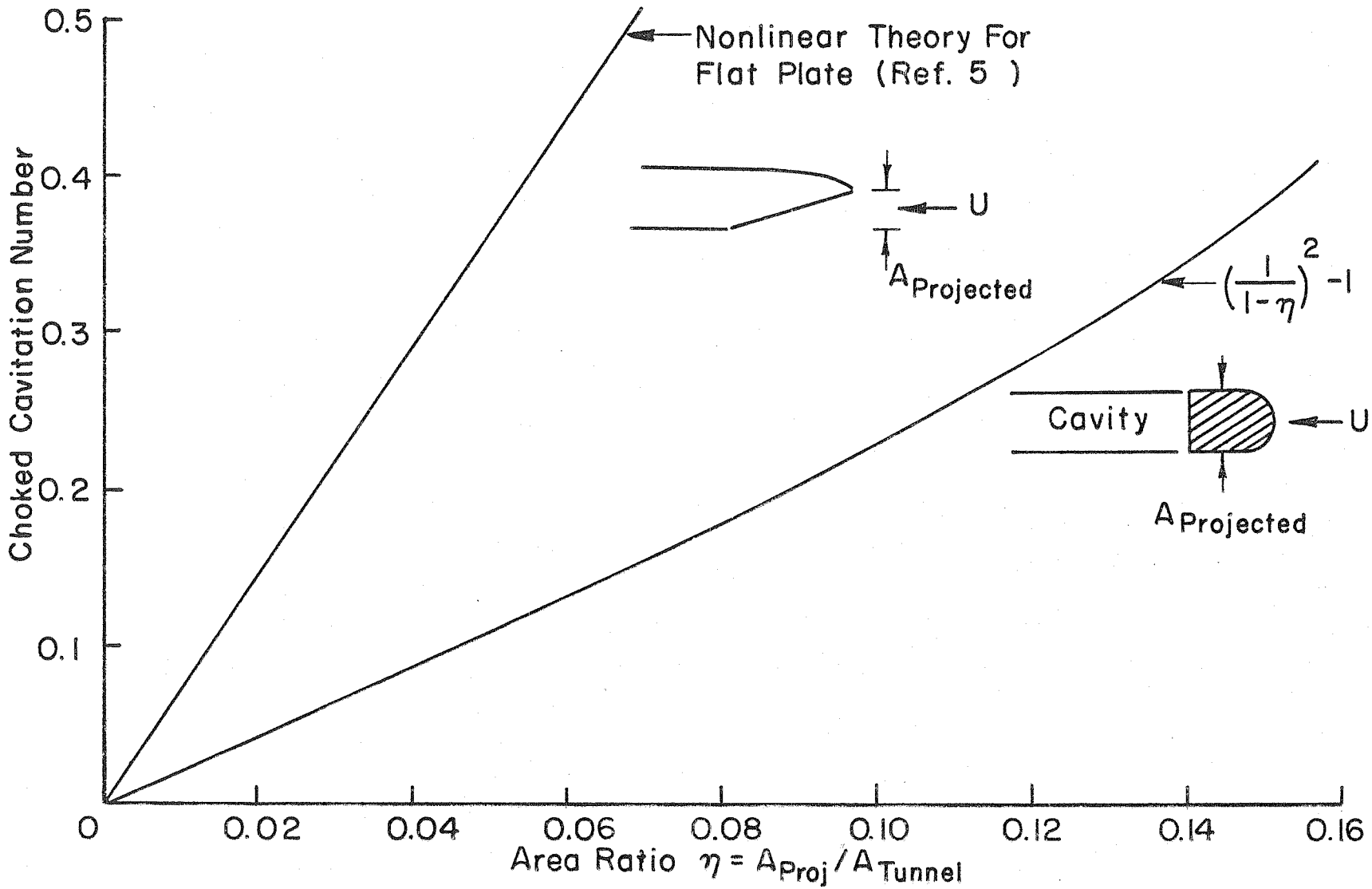

FIG.14 VARIATION OF CHOKED CAVITATION NUMBER WITH AREA RATIO

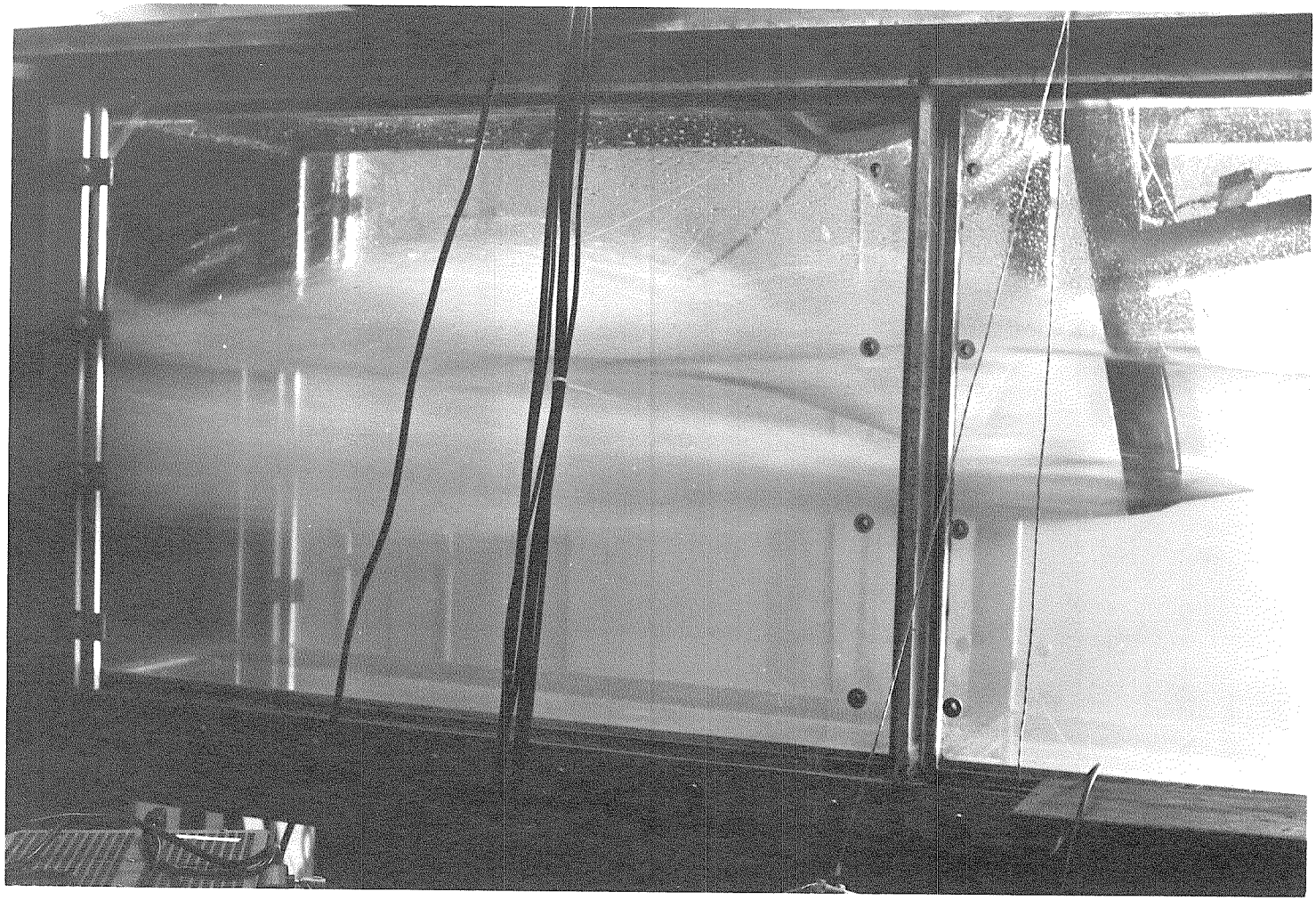

FIG. 15 VENTILATED CAVITY IN THE F.S.W.T.

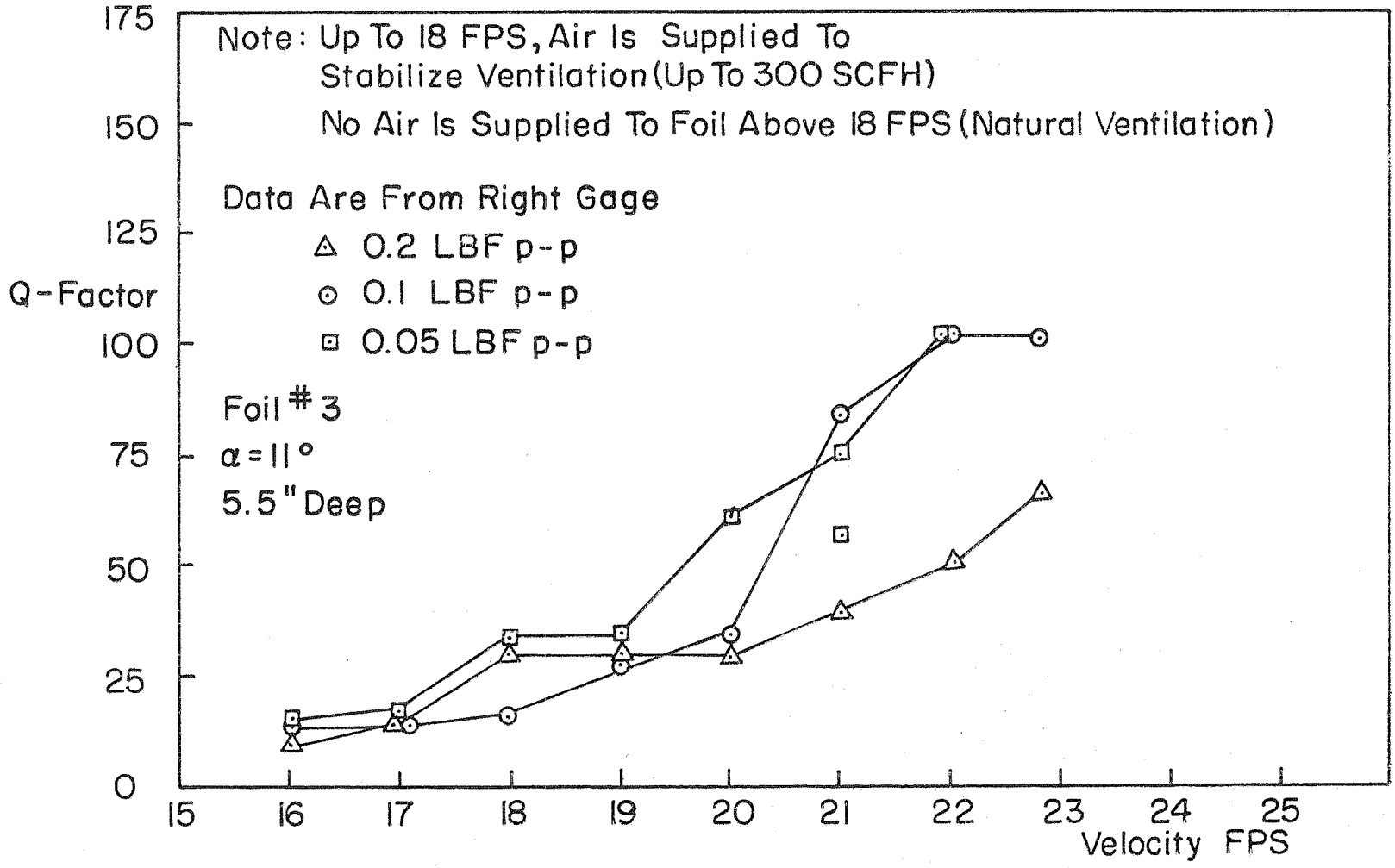

FIG. 16 . Q-FACTOR OF FIRST BENDING MODE AS A FUNCTION OF VELOCITY AT VARIOUS LEVELS OF FORCE FOR FOIL #3.

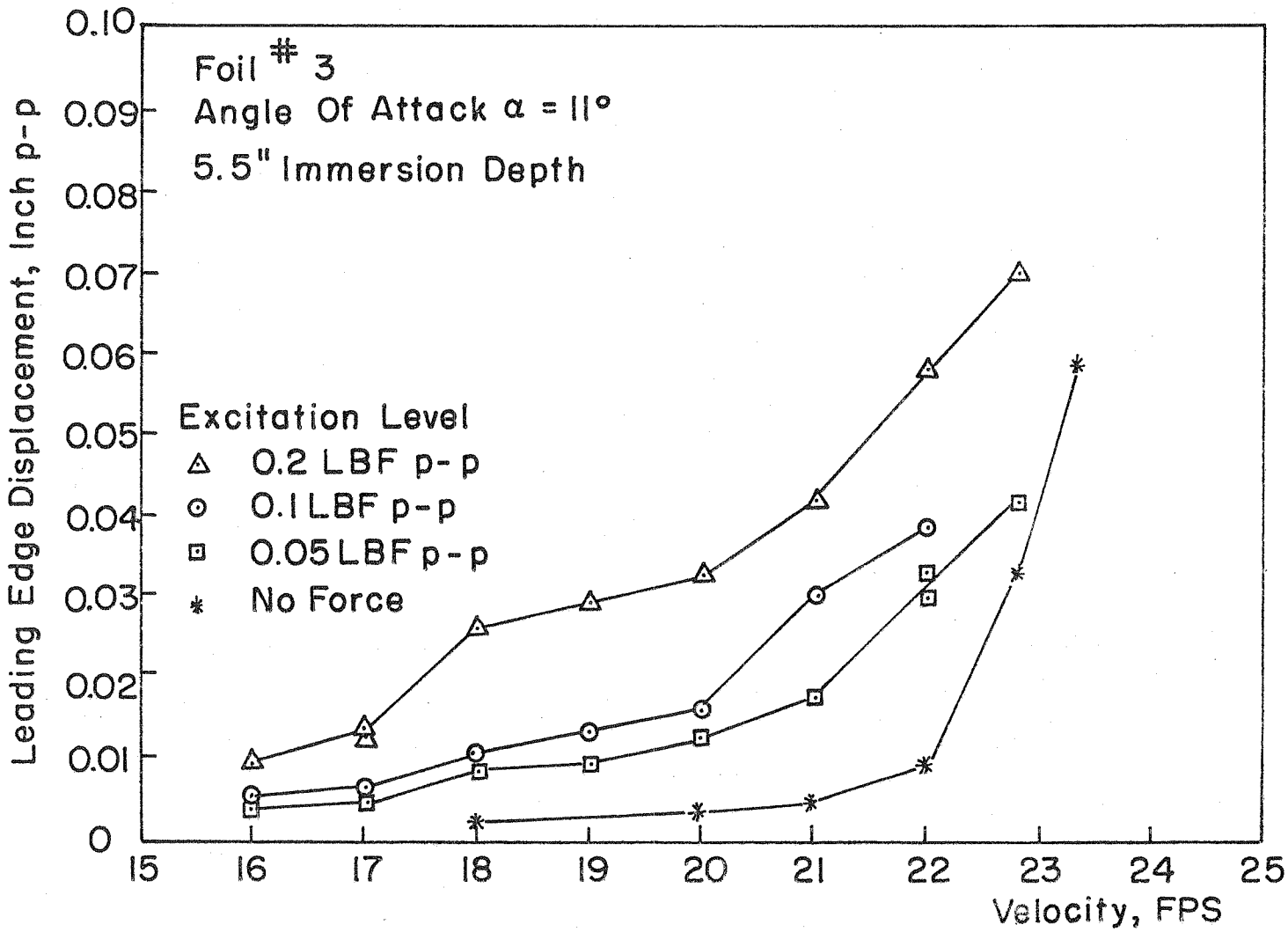

FIG. 17 PEAK TO PEAK AMPLITUDE OF THE LEADING EDGE OSCILLATION AS A FUNCTION OF VELOCITY AND AT VARIOUS LEVELS OF APPLIED FORCE (GIVEN AS PEAK TO PEAK AMPLITUDE IN LBF) FOR FOIL 3. UP TO 18 FPS, SOME AIR IS SUPPLIED TO STABILIZE VENTILATION.

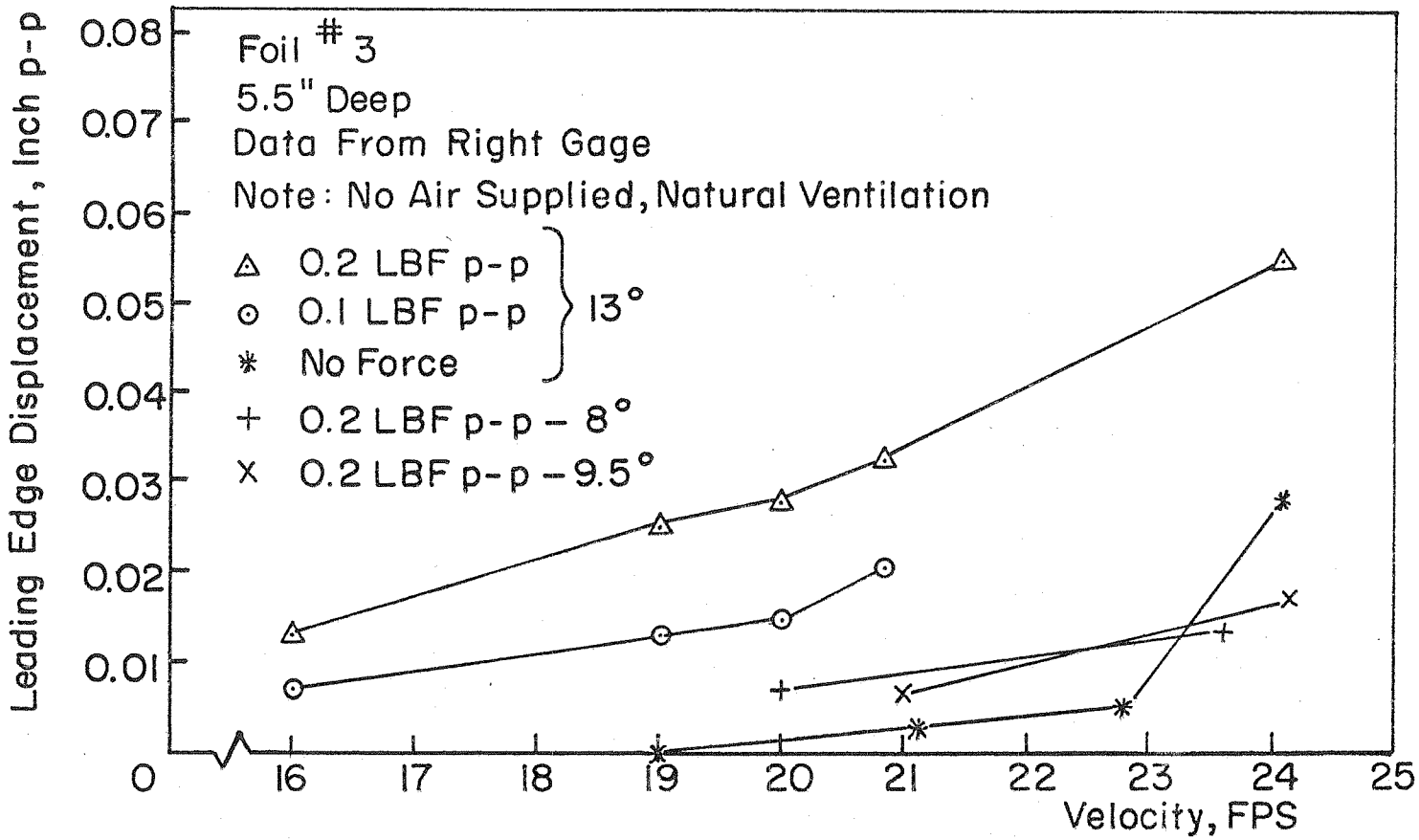

FIG. 18 VARIATION OF PEAK DISPLACEMENT OF FIRST BENDING MODE FOR FOIL # 3 WITH VELOCITY AT VARIOUS ANGLES OF ATTACK AND FORCES

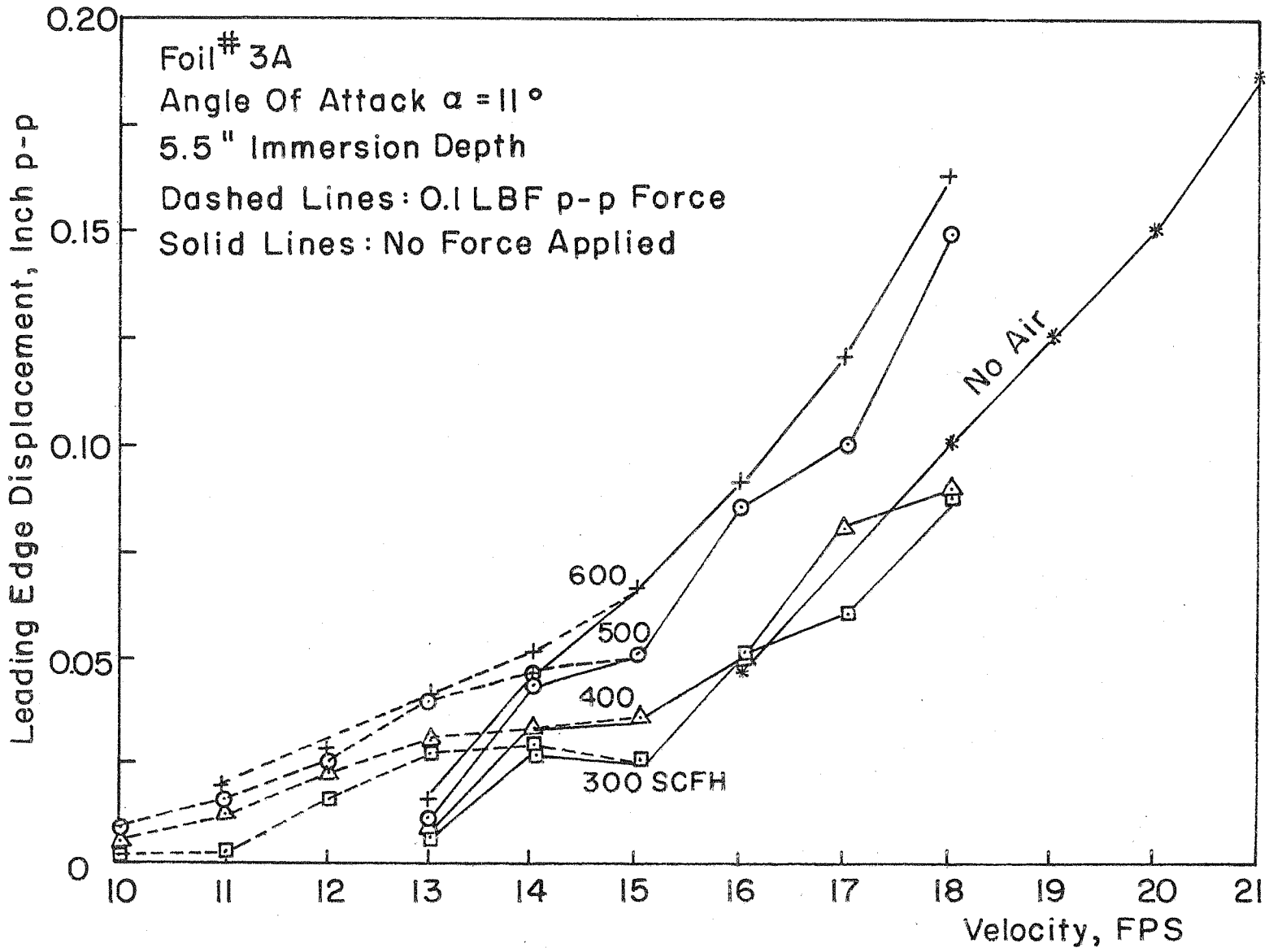

FIG. 19 PEAK TO PEAK AMPLITUDE OF THE LEADING EDGE OSCILLATION AS A FUNCTION OF VELOCITY AND AT VARIOUS RATES OF AIR INJECTED INTO THE CAVITY (IN STANDARD CUBIC FEET PER HOUR, SCFH) FOR FOIL 3A.

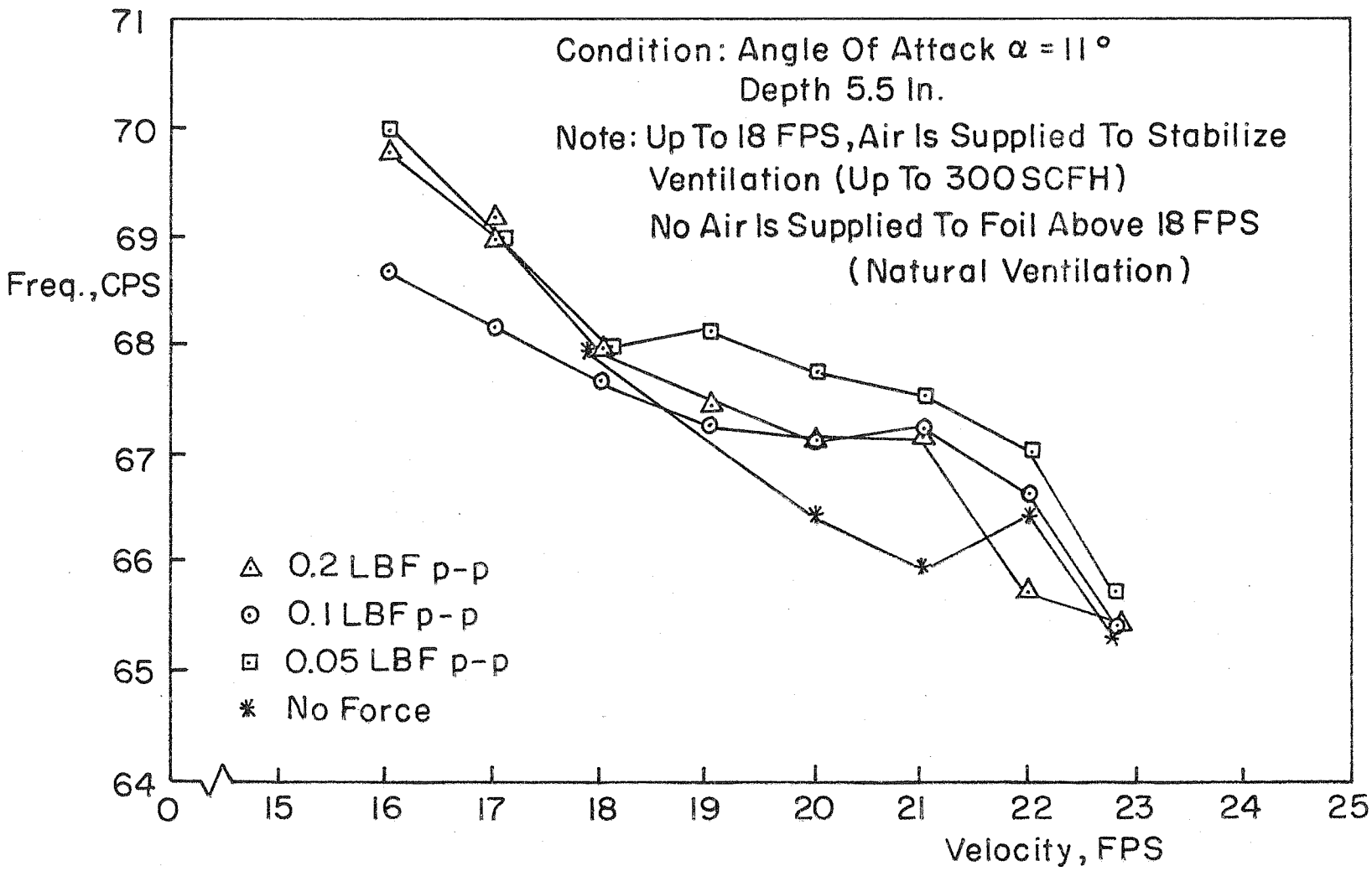

FIG. 20 NATURAL FREQUENCY AS A FUNCTION OF VELOCITY FOR FOIL #3 AT VARIOUS LEVELS OF FORCE.

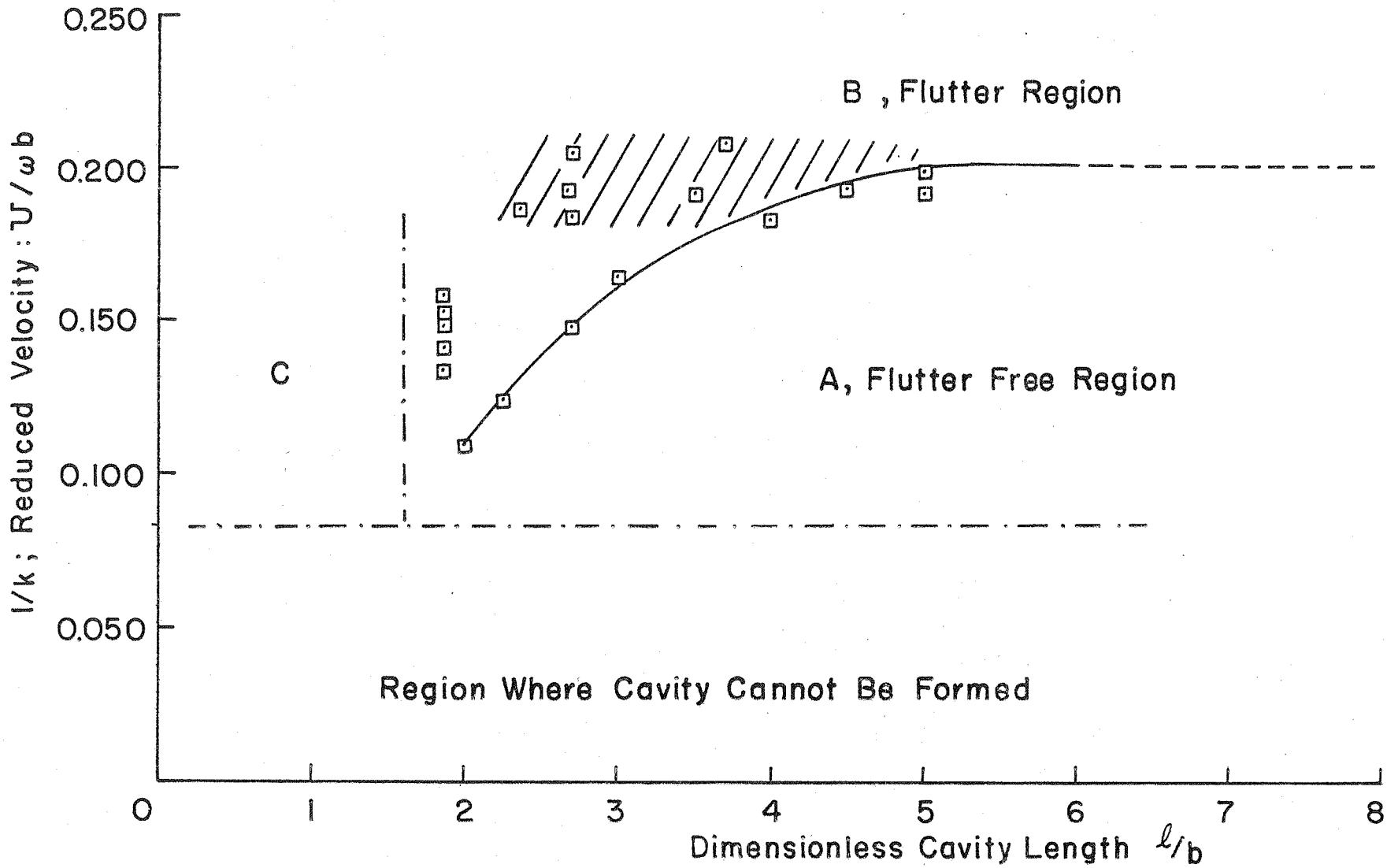

FIG. 21 FLUTTER BOUNDARY OF FOIL 3 AT $\alpha = 7°$

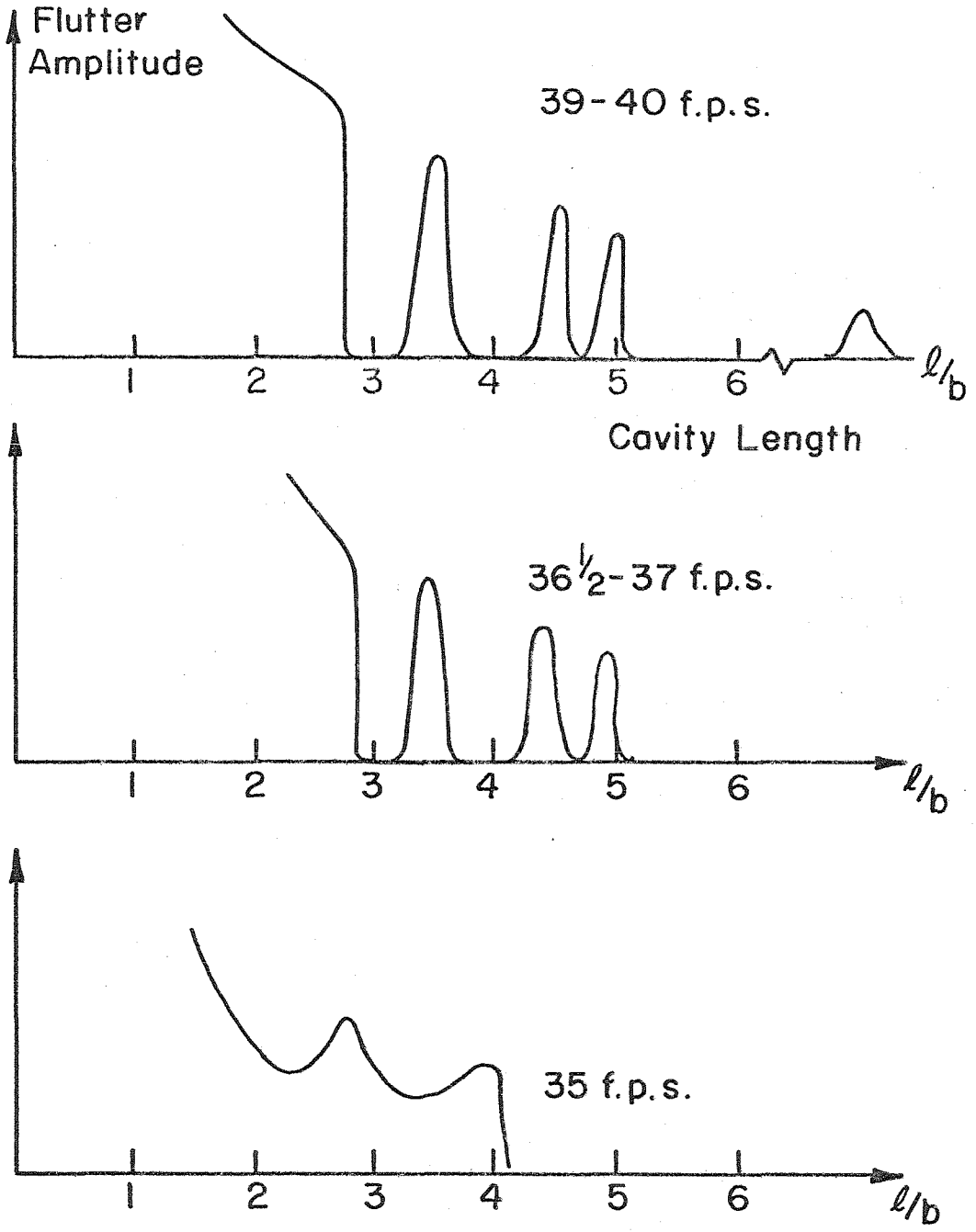

FIG. 22 RESONANCES OF FLUTTER AMPLITUDE WITH CAVITY LENGTH

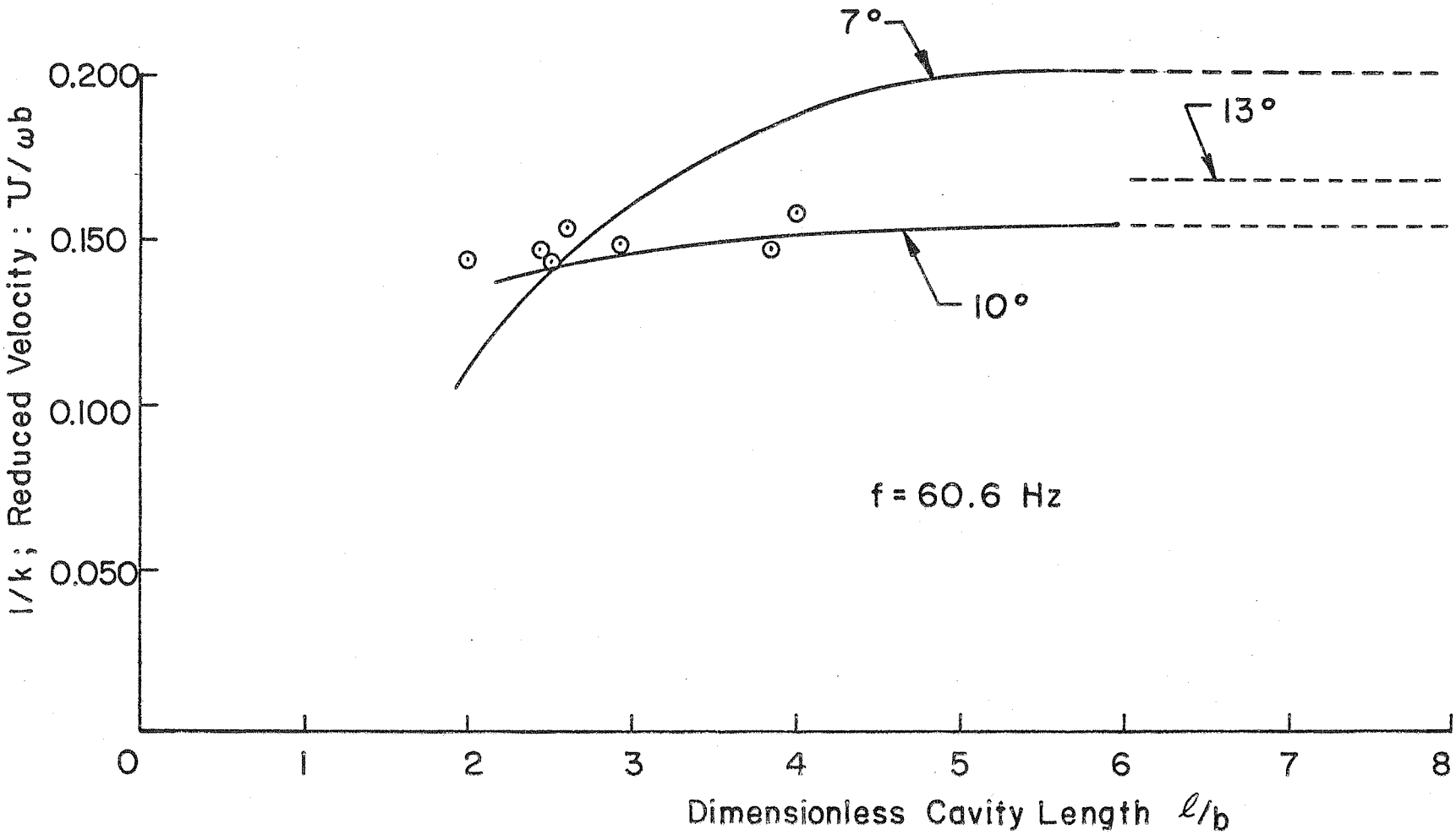

FIG.23 FLUTTER BOUNDARY FOR FOIL 3 AT $\alpha = 7°$, $\alpha = 10°$, AND $\alpha = 13°$

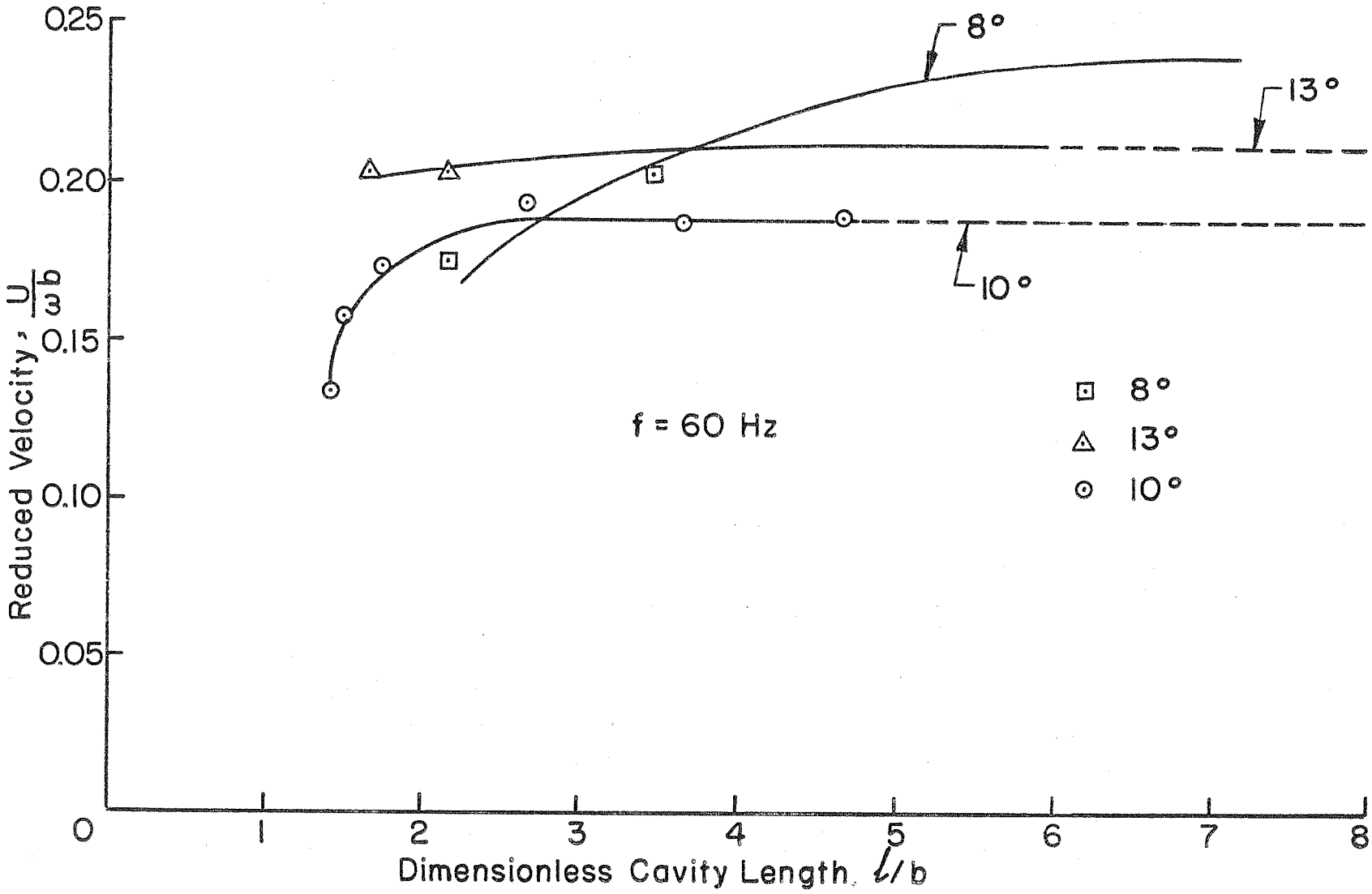

FIG. 24 FLUTTER BOUNDARY FOR FOIL 6 AT $\alpha = 8°$, $\alpha = 10°$, AND $\alpha = 13°$

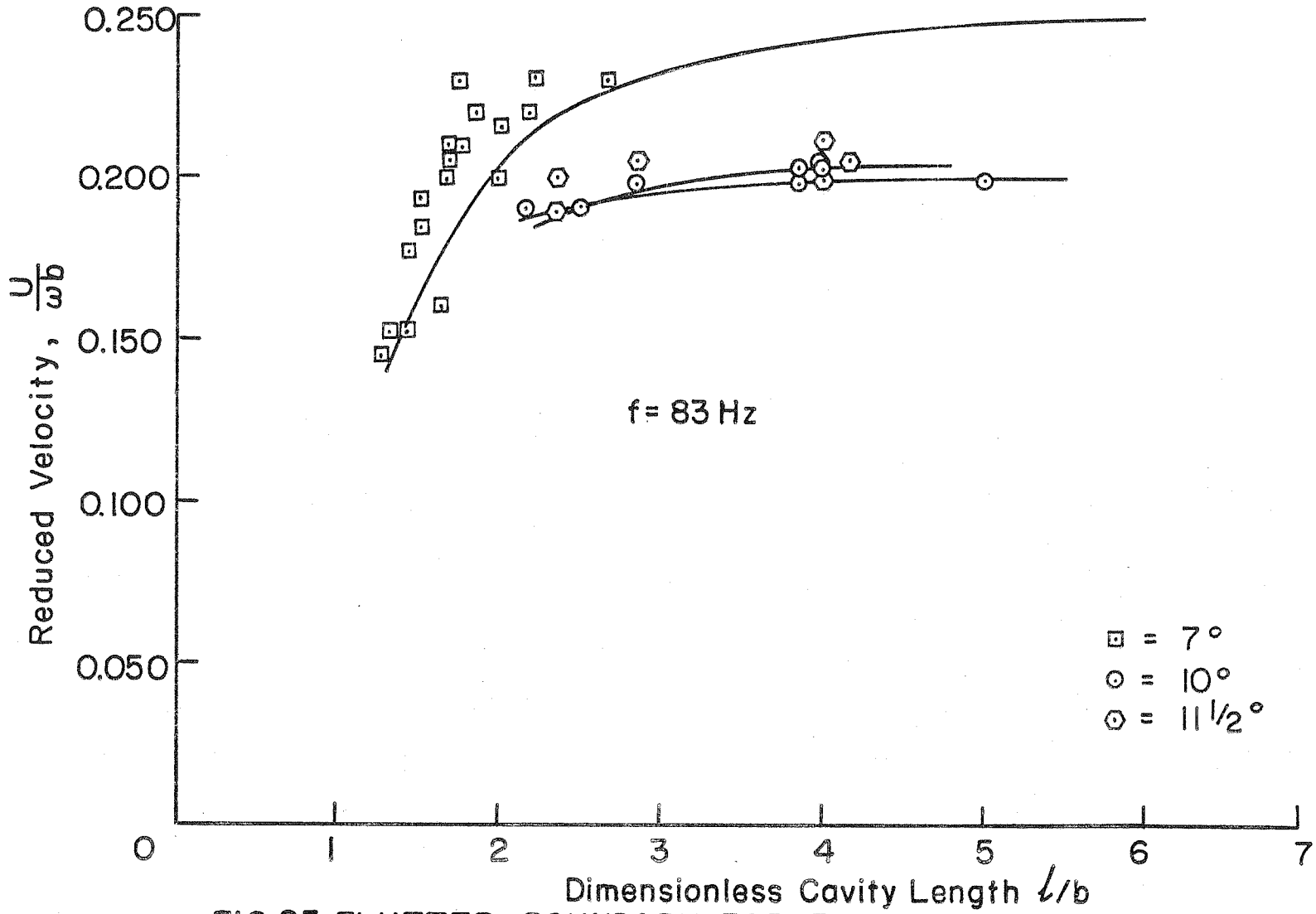

FIG.25 FLUTTER BOUNDARY FOR FOIL 4 AT $\alpha = 7°$, $\alpha = 10°$, and $\alpha = 11\frac{1}{2}°$

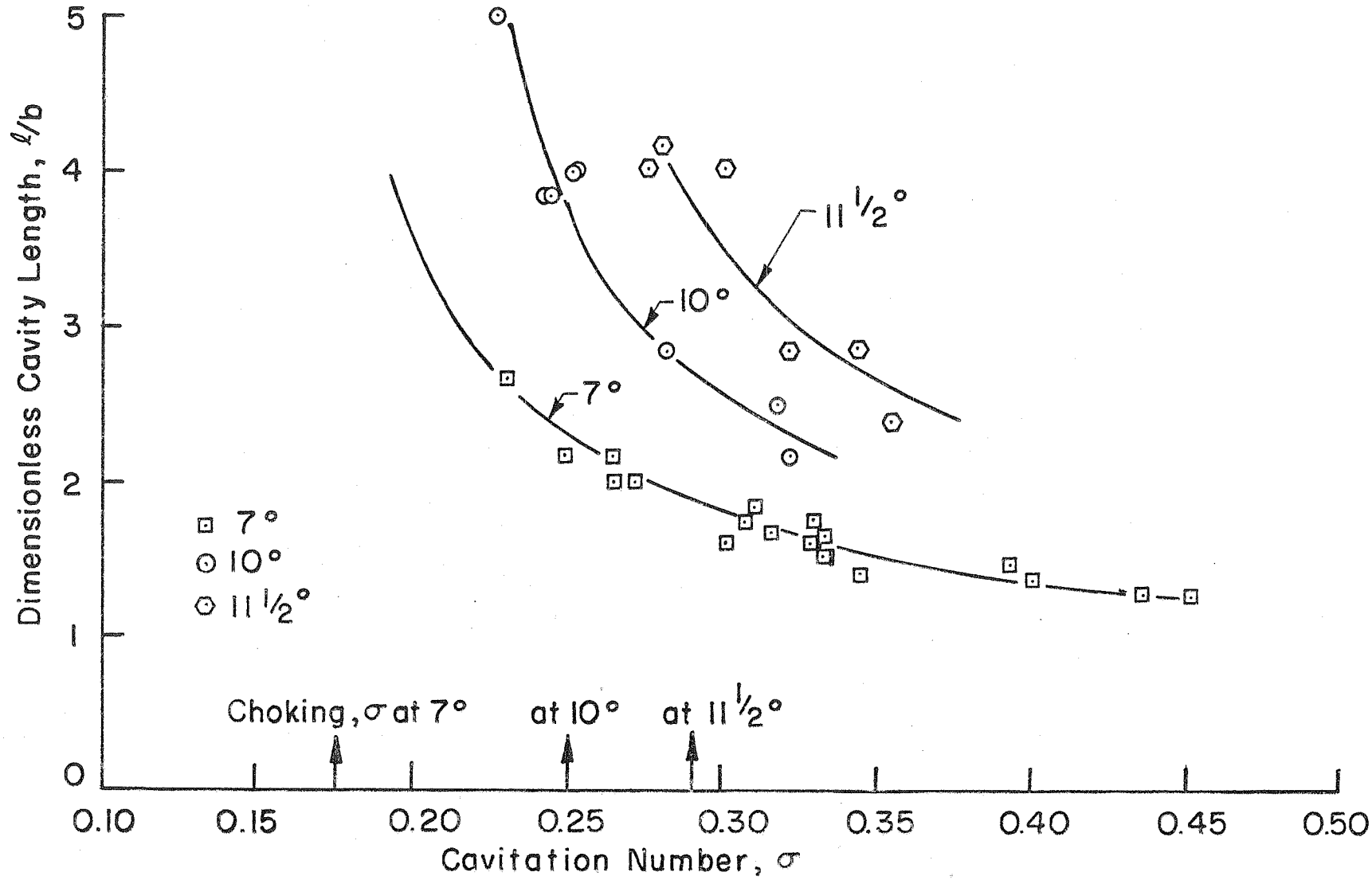

FIG. 26 THE VARIATION OF CAVITATION NUMBER WITH CAVITY LENGTH. FOIL 4

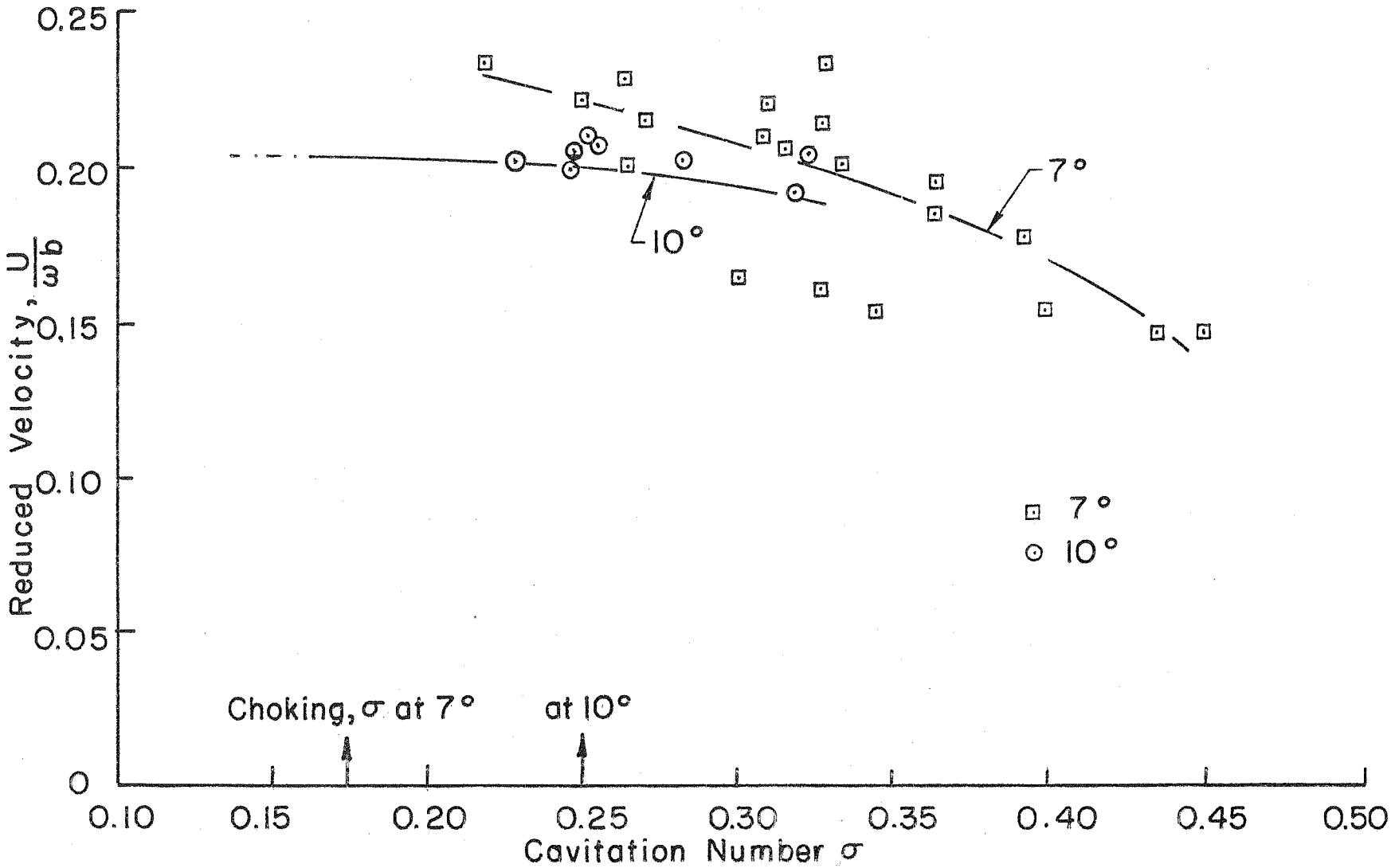

FIG. 27 FLUTTER BOUNDARY AS A FUNCTION OF THE REDUCED VELOCITY AND THE CAVITATION NUMBER. FOIL 4 AT $\alpha = 7°$ AND $\alpha = 10°$.

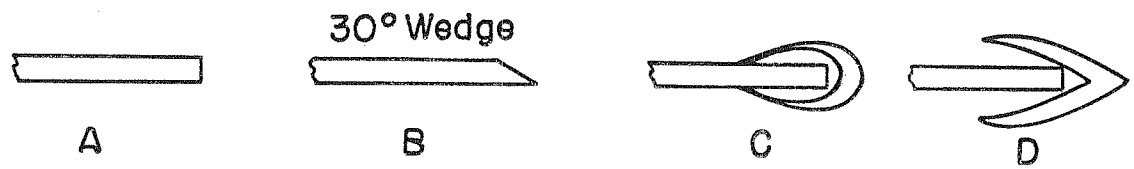

FIG. 28 SHAPES OF LEADING EDGE TESTED IN THE F.S.W.T.

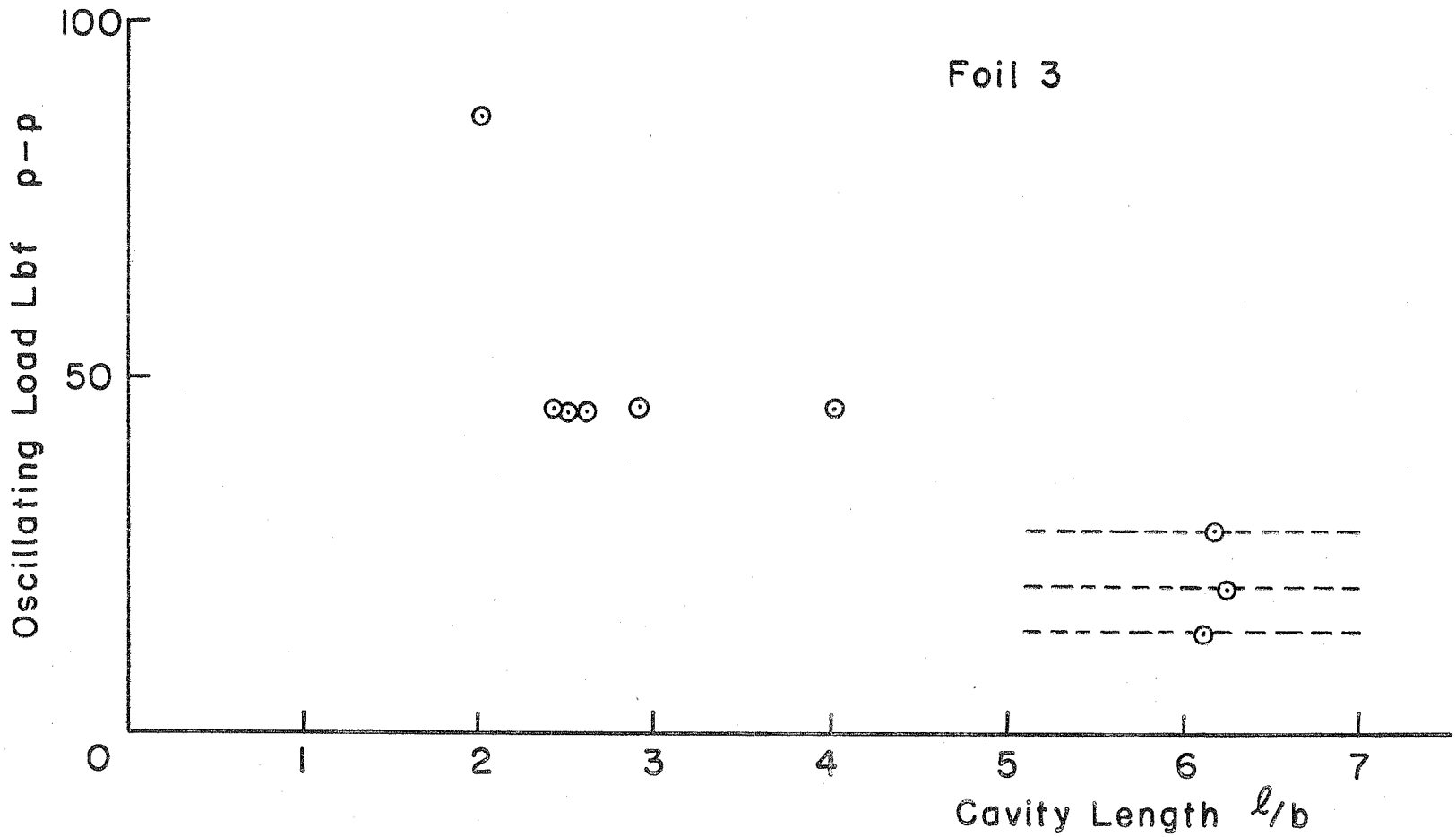

FIG. 29 OSCILLATING LOAD AT $\alpha = 10°$ AND U = 27.5 – 32 FPS

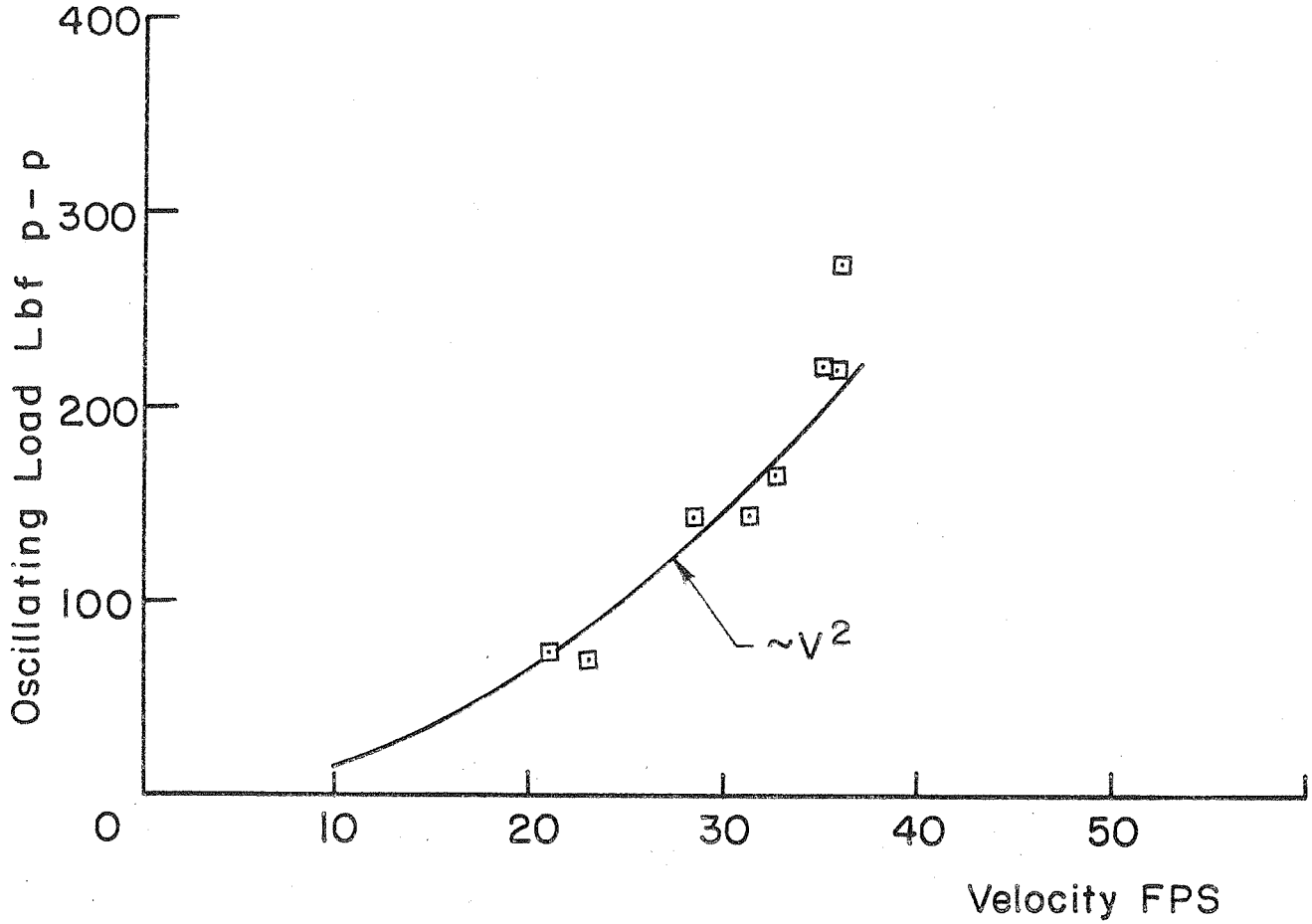

FIG.30 OSCILLATING NORMAL LOAD VS VELOCITY. FOIL 3
AT $\alpha = 7°$

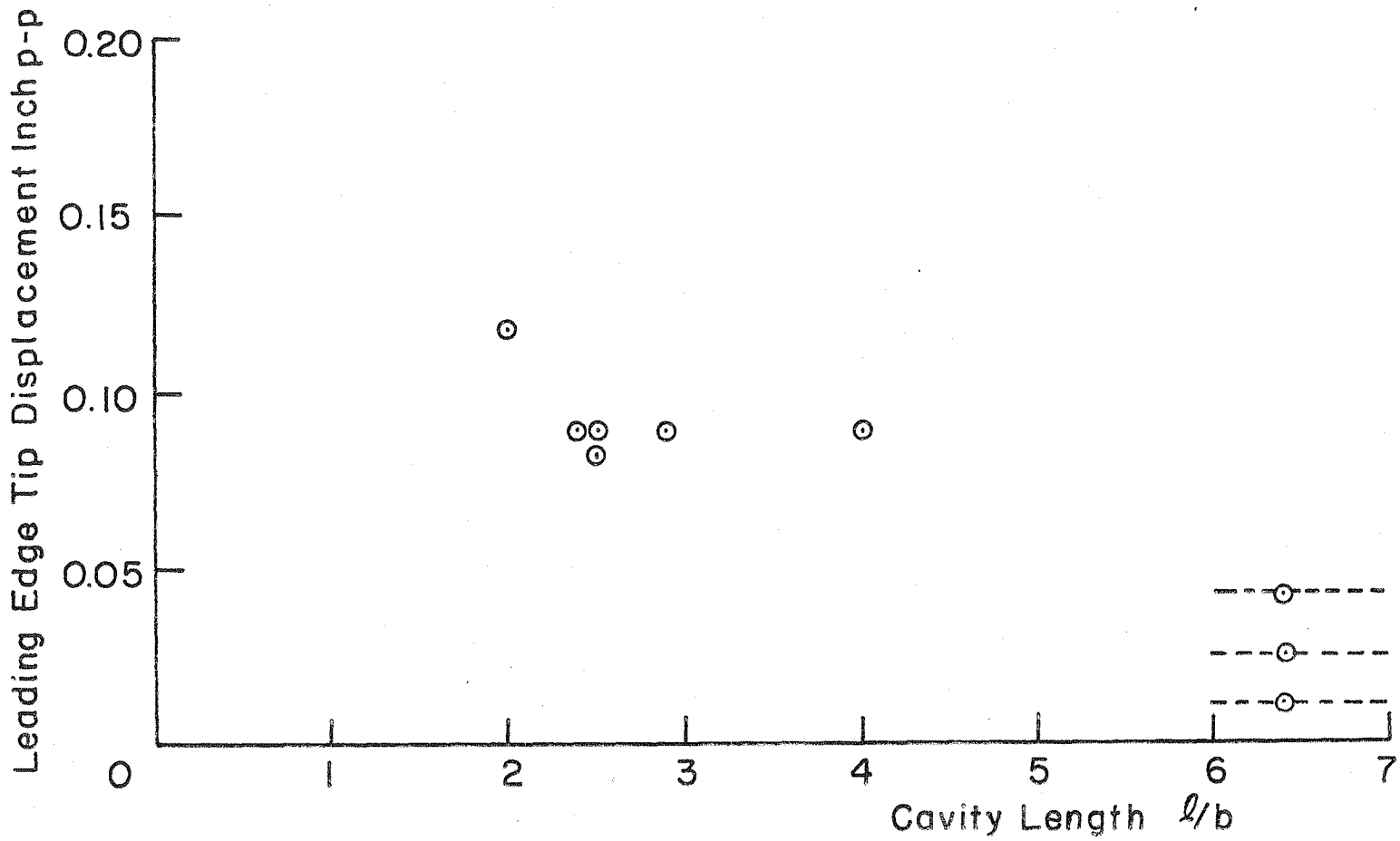

FIG. 31 LEADING EDGE TIP DISPLACEMENT VS CAVITY LENGTH.
FOIL 3 AT $\alpha = 10°$ AND U = 27.5 - 32 FPS

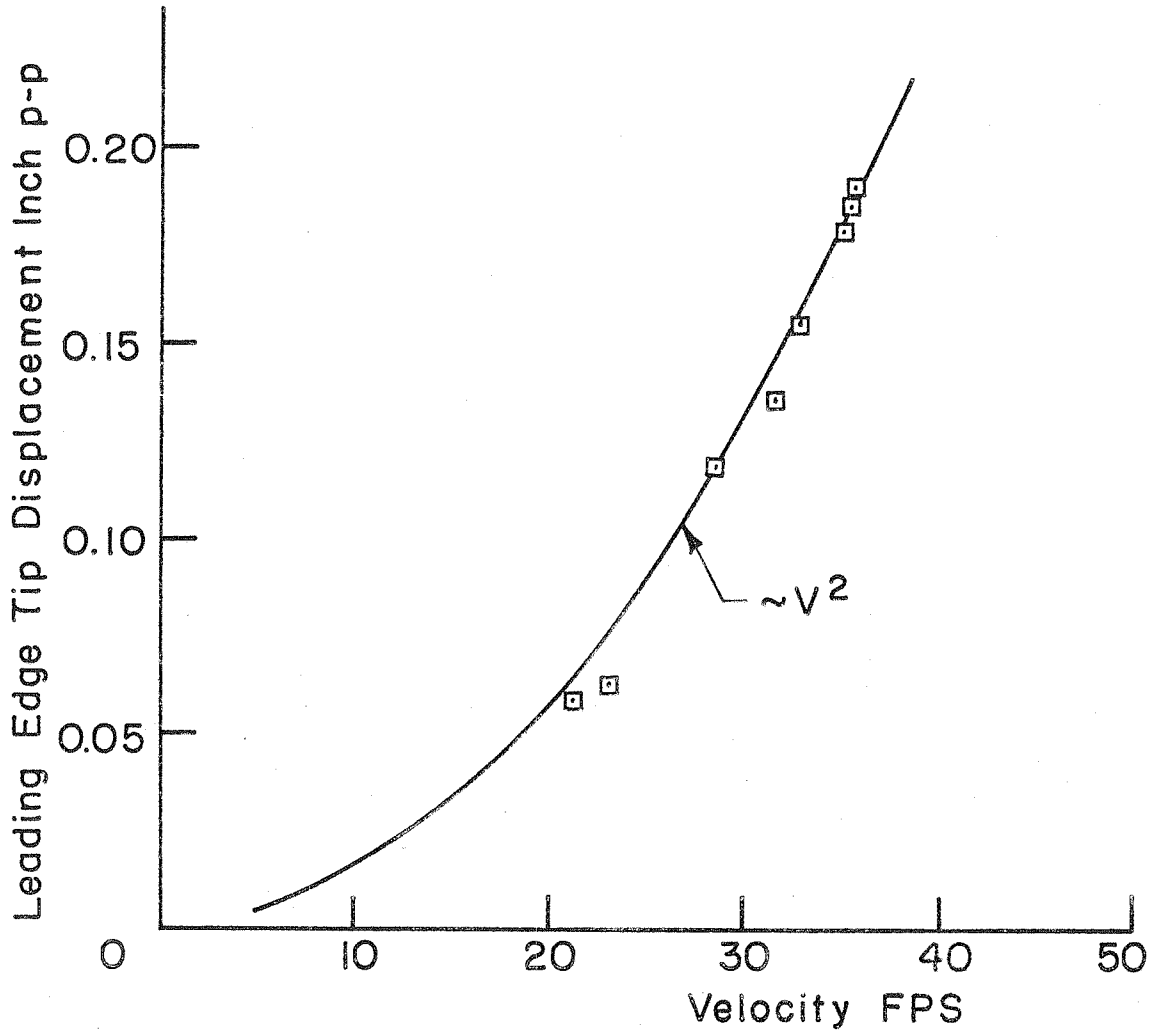

FIG. 32 LEADING EDGE DISPLACEMENT AS A FUNCTION OF VELOCITY
FOIL 3 AT $\alpha = 7°$. CAVITY LENGTH $\ell/b = 2 - 4$

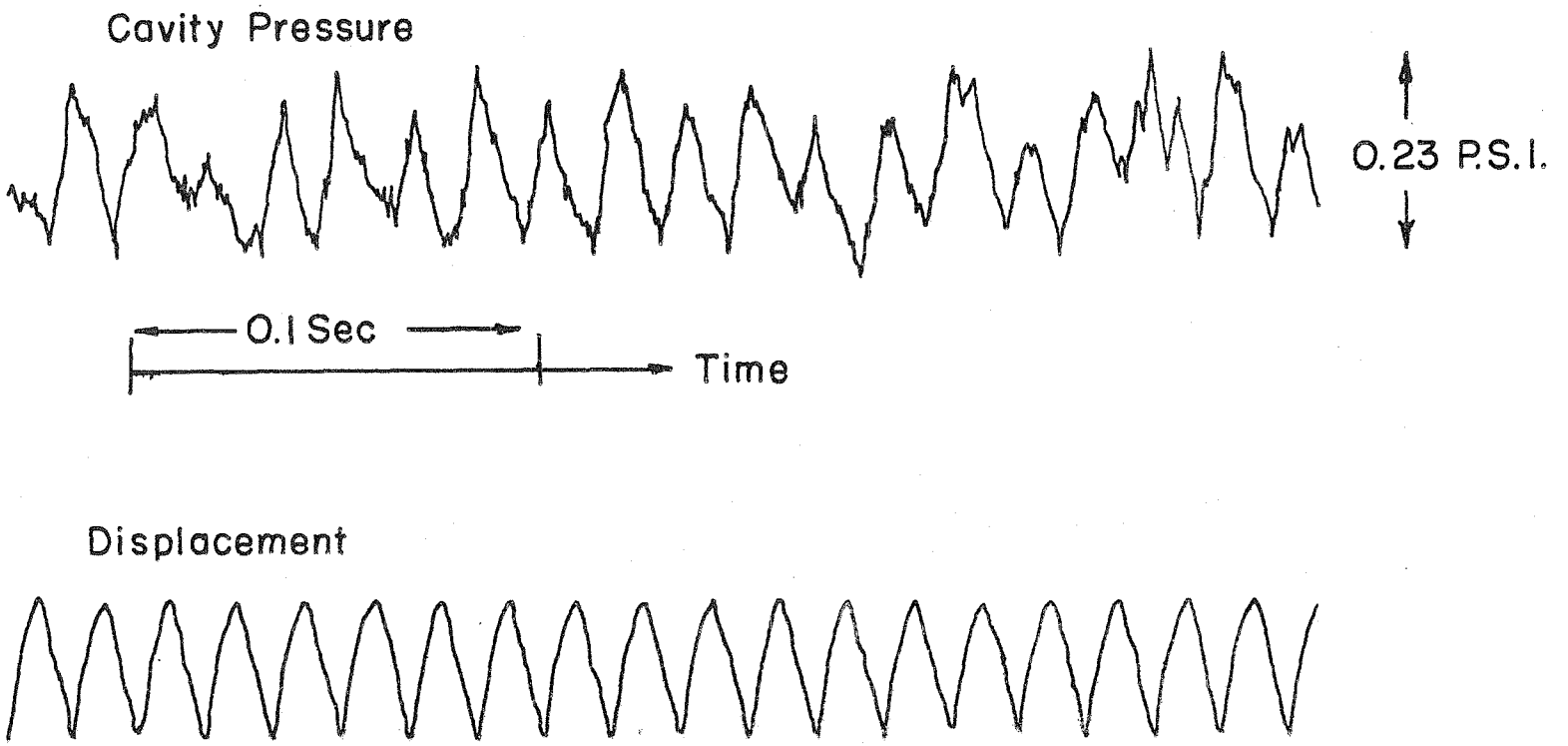

FIG. 33 OSCILLATION IN CAVITY PRESSURE DURING FLUTTER

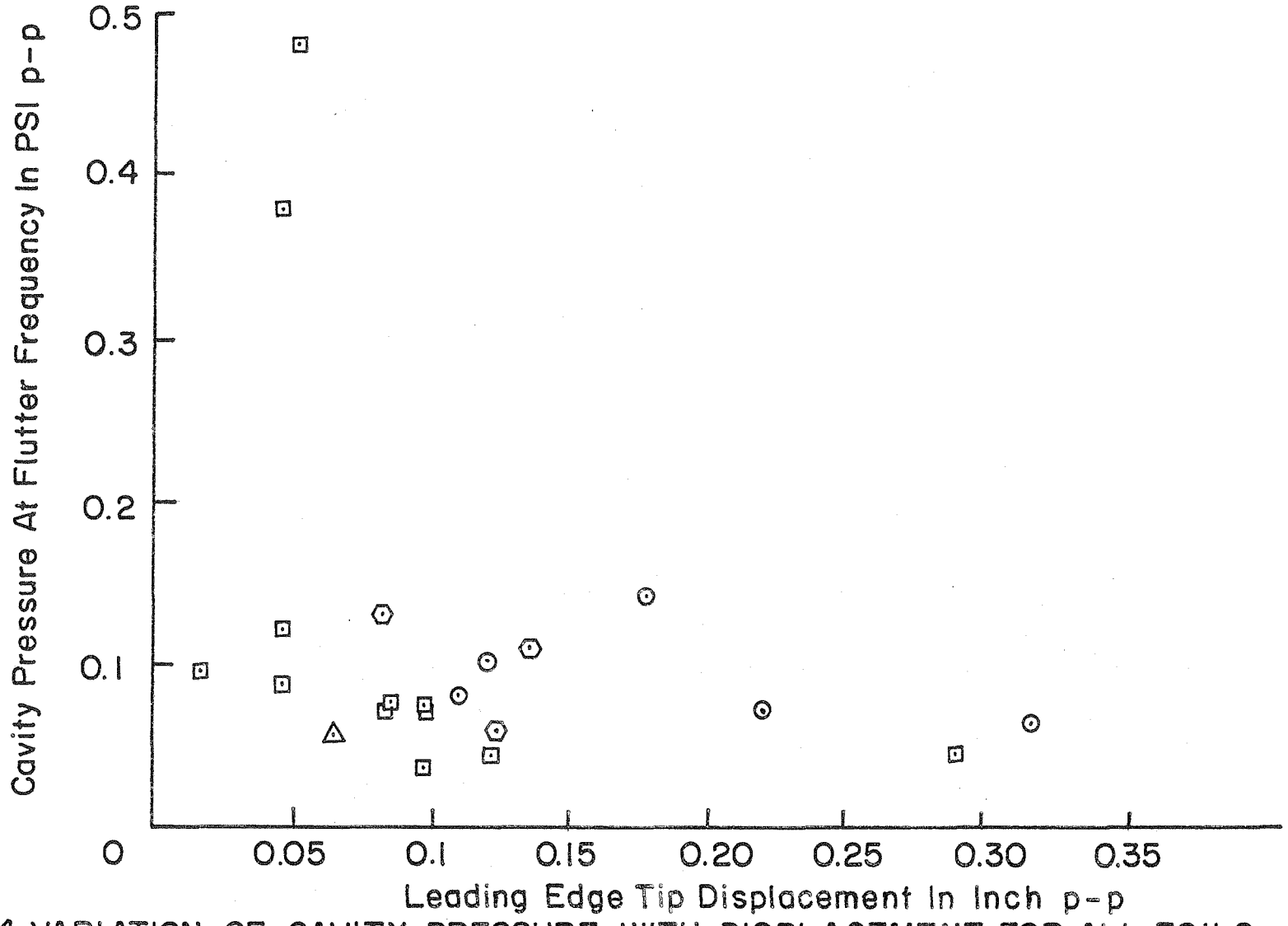

FIG.34 VARIATION OF CAVITY PRESSURE WITH DISPLACEMENT FOR ALL FOILS

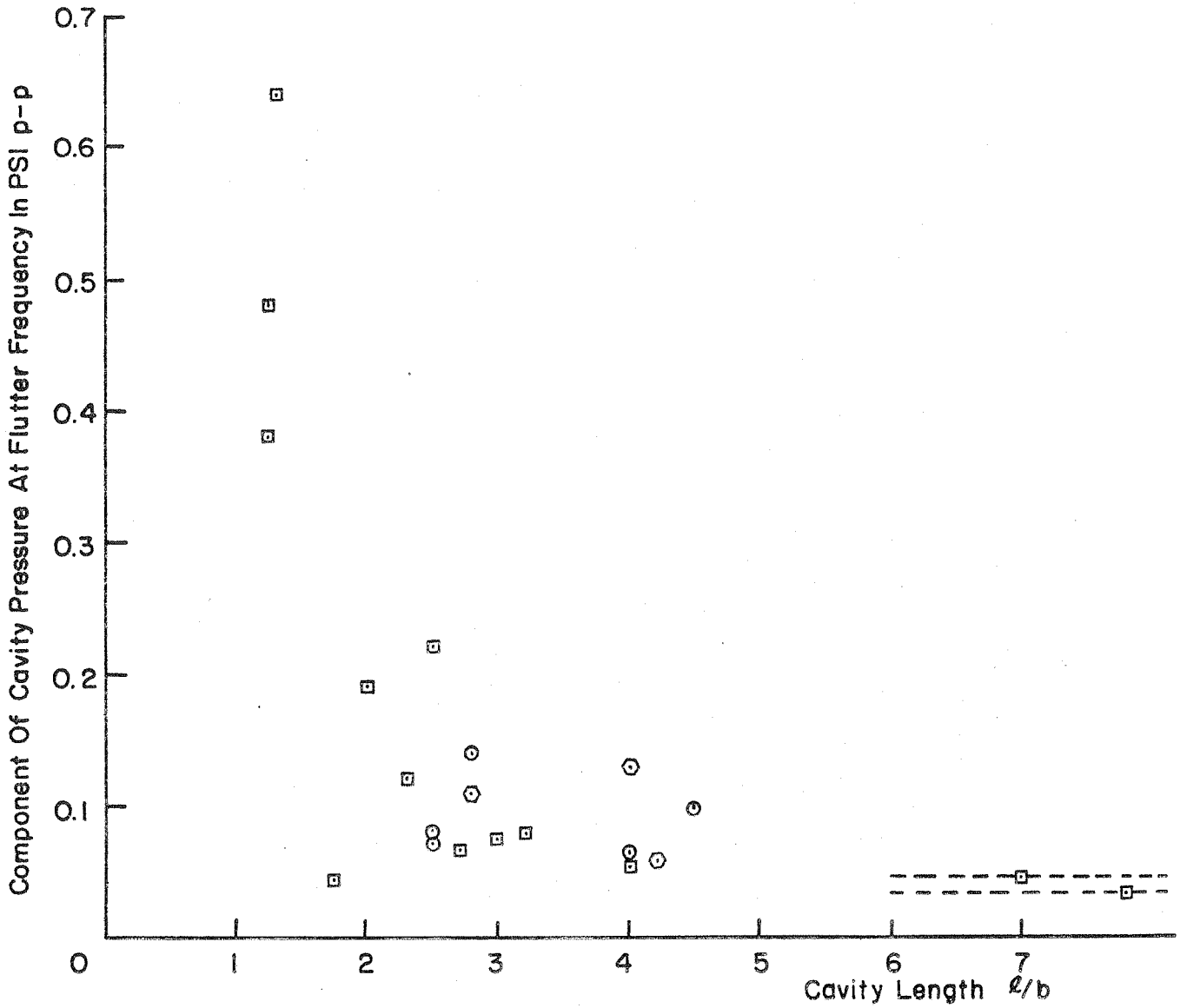

FIG. 35 CAVITY PRESSURE VS CAVITY LENGTH FOR ALL FOILS TESTED

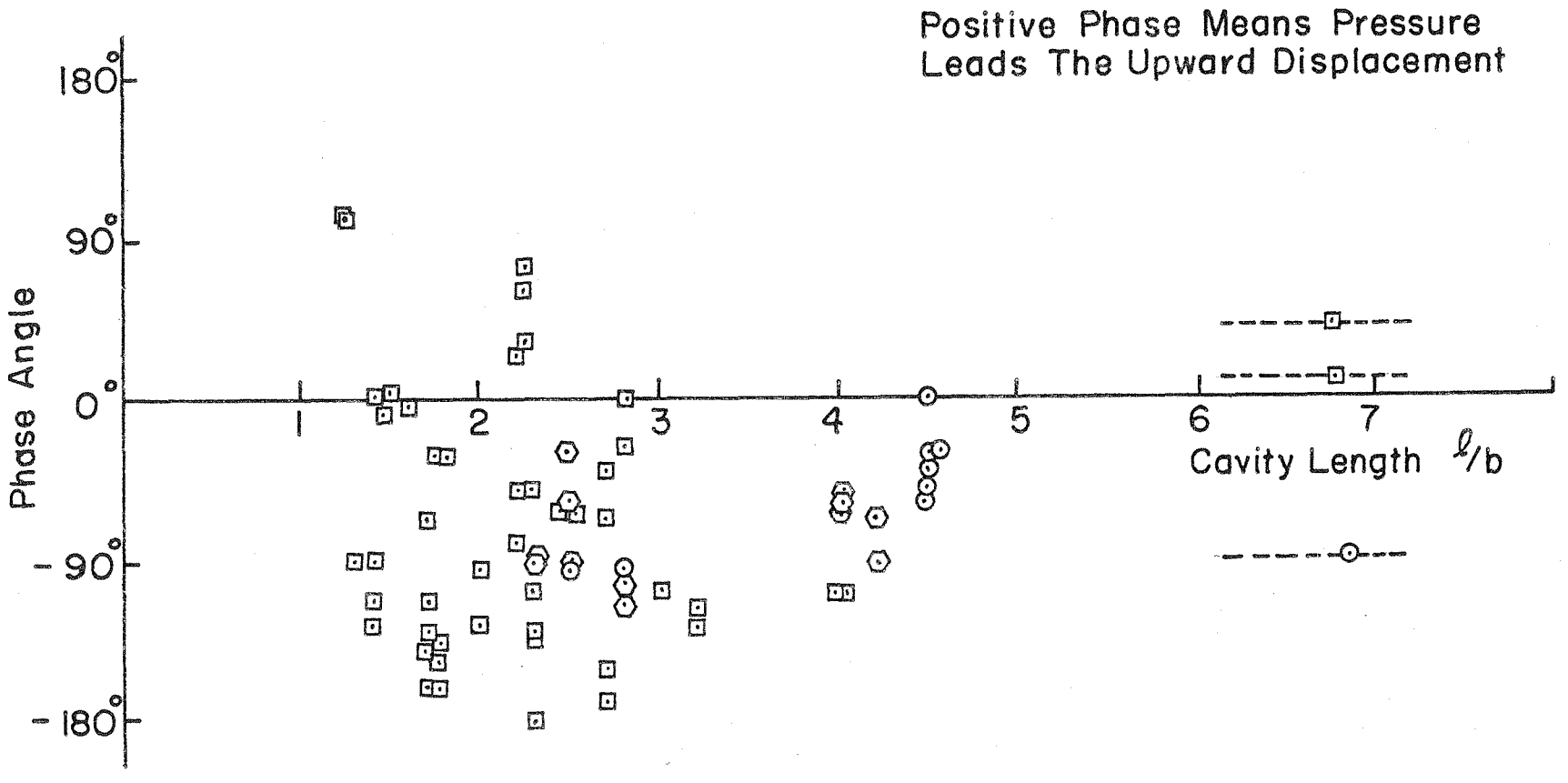

FIG.36 PHASE BETWEEN CAVITY PRESSURE AND DISPLACEMENT OF THE FOIL

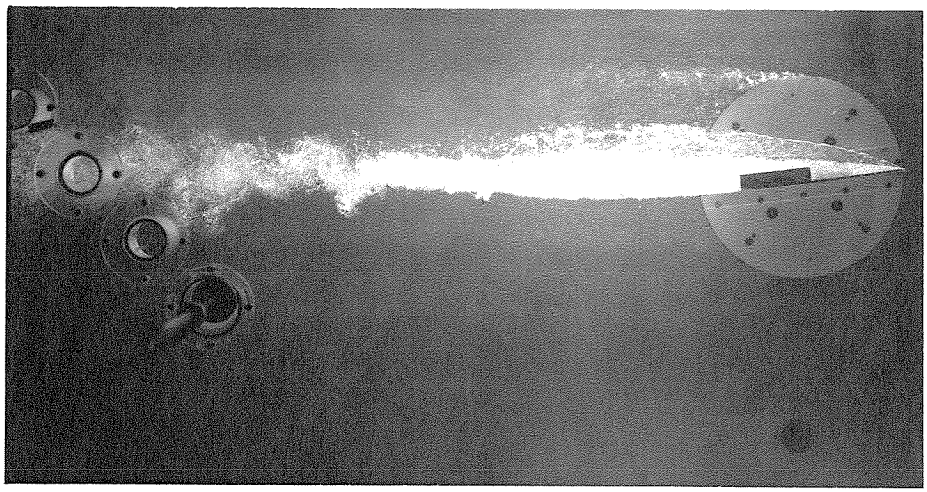

NO FLUTTER

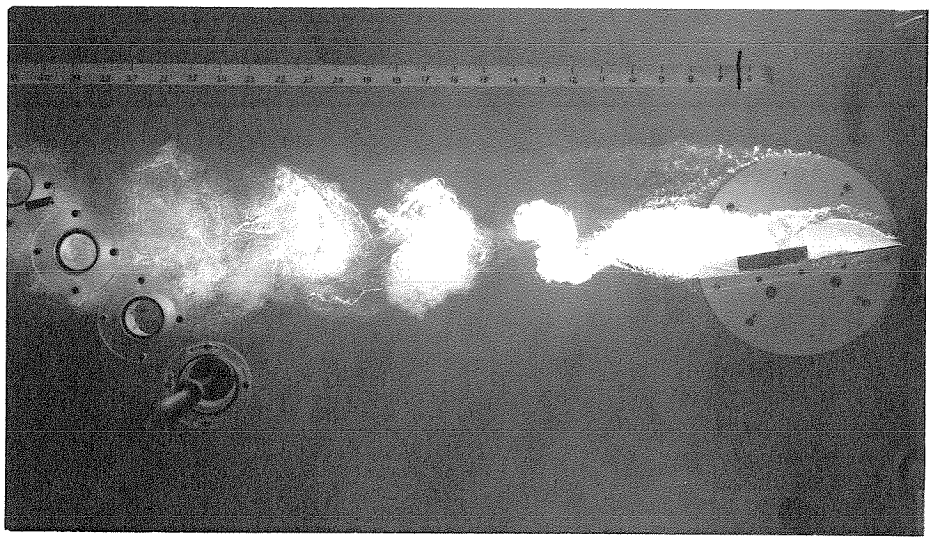

FIG. 37 FLUTTER WITH SHORT CAVITY. NOTICE THE PERIODIC SHEDDING OF THE CLOSURE REGION AS THE RESULT OF CAVITY PINCHING.

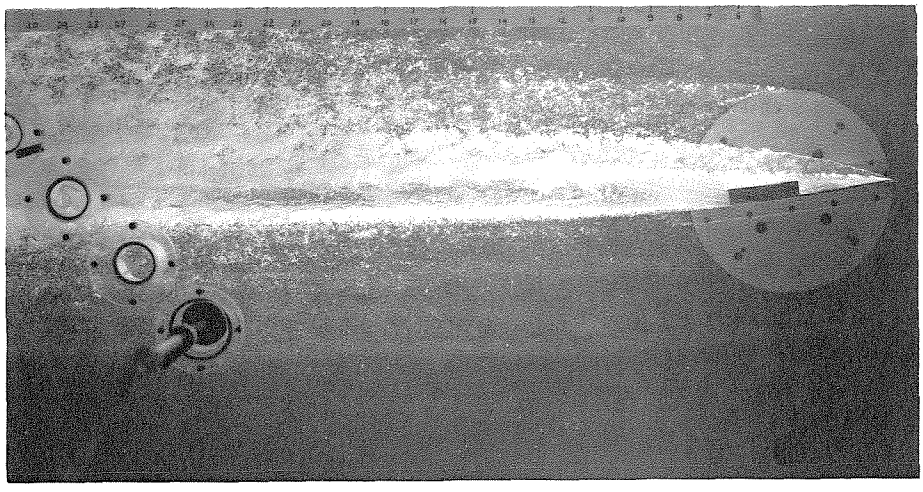

NO FLUTTER

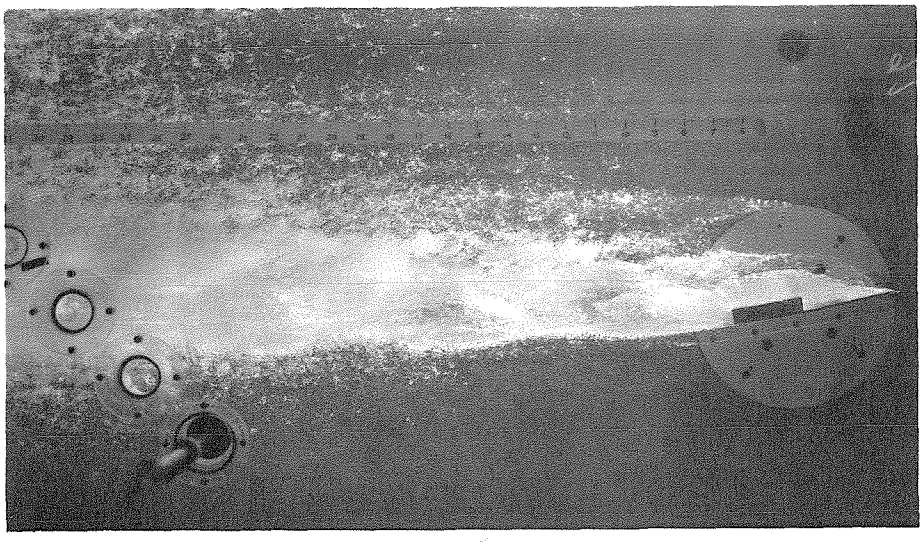

FIG. 38 FLUTTER WITH LONG CAVITY. NOTICE THE WAVES ON THE UPPER SURFACE CREATED BY LEADING EDGE OSCILLATIONS.

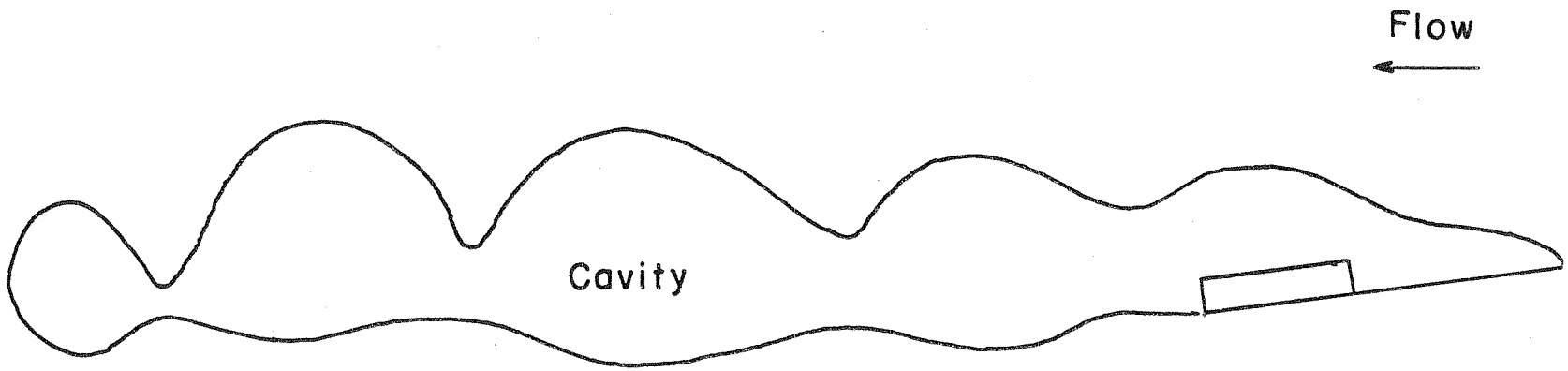

FIG. 39 A SKETCH OF THE WALL OF THE CAVITY DURING FLUTTER

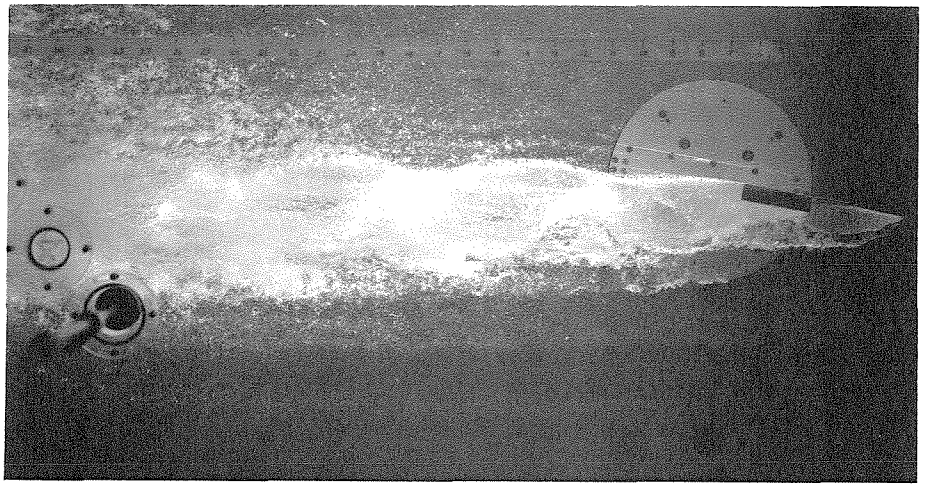

LONG CAVITY

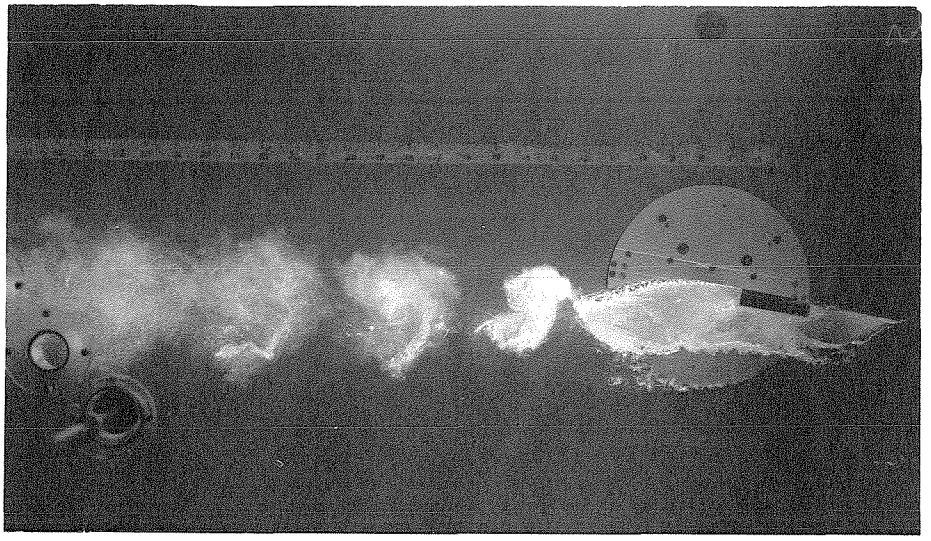

SHORT CAVITY

FIG. 40 FLUTTER AT NEGATIVE ANGLE OF ATTACK

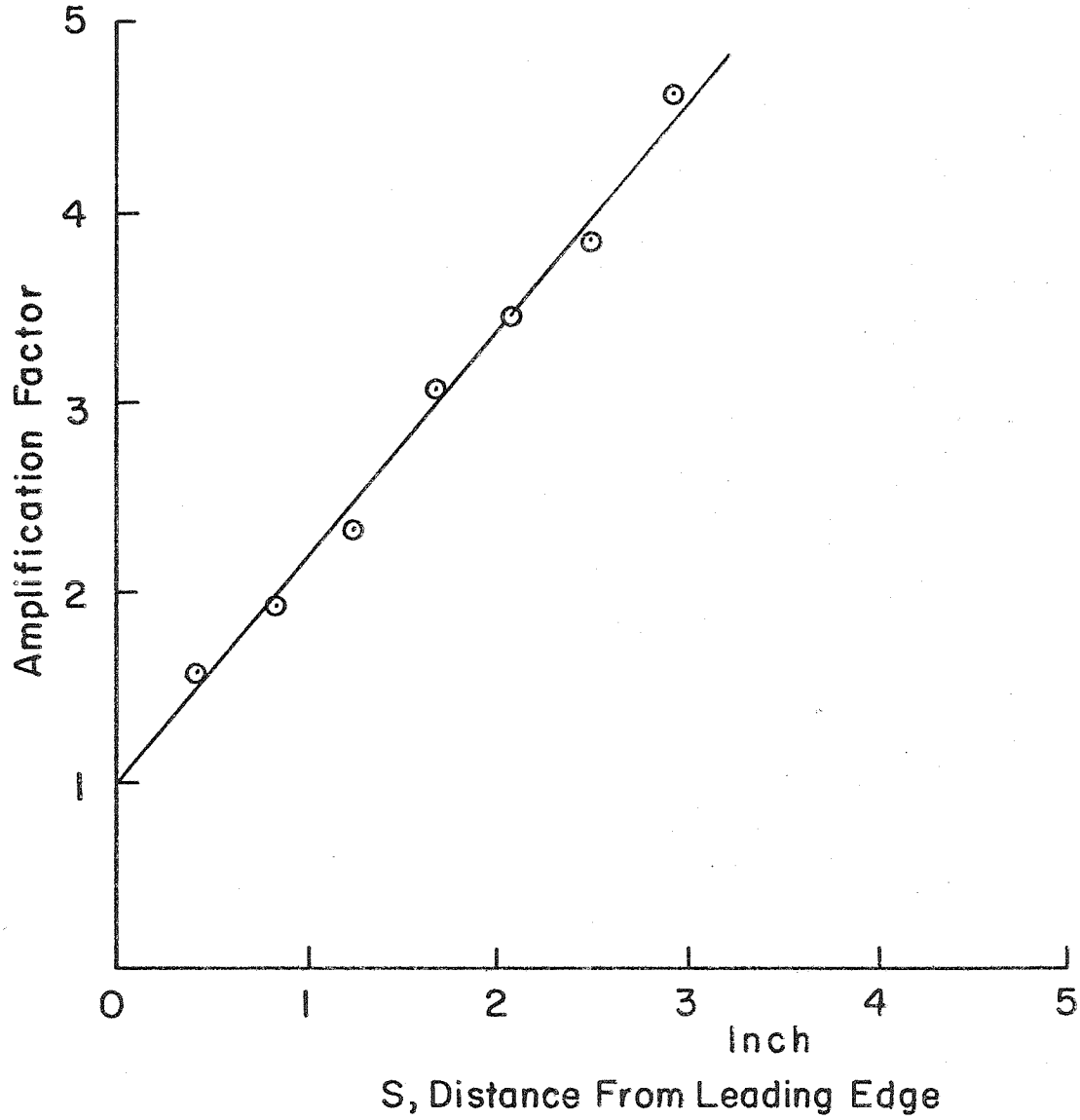

FIG. 41 AMPLIFICATION OF WAVES ON THE UPPER CAVITY

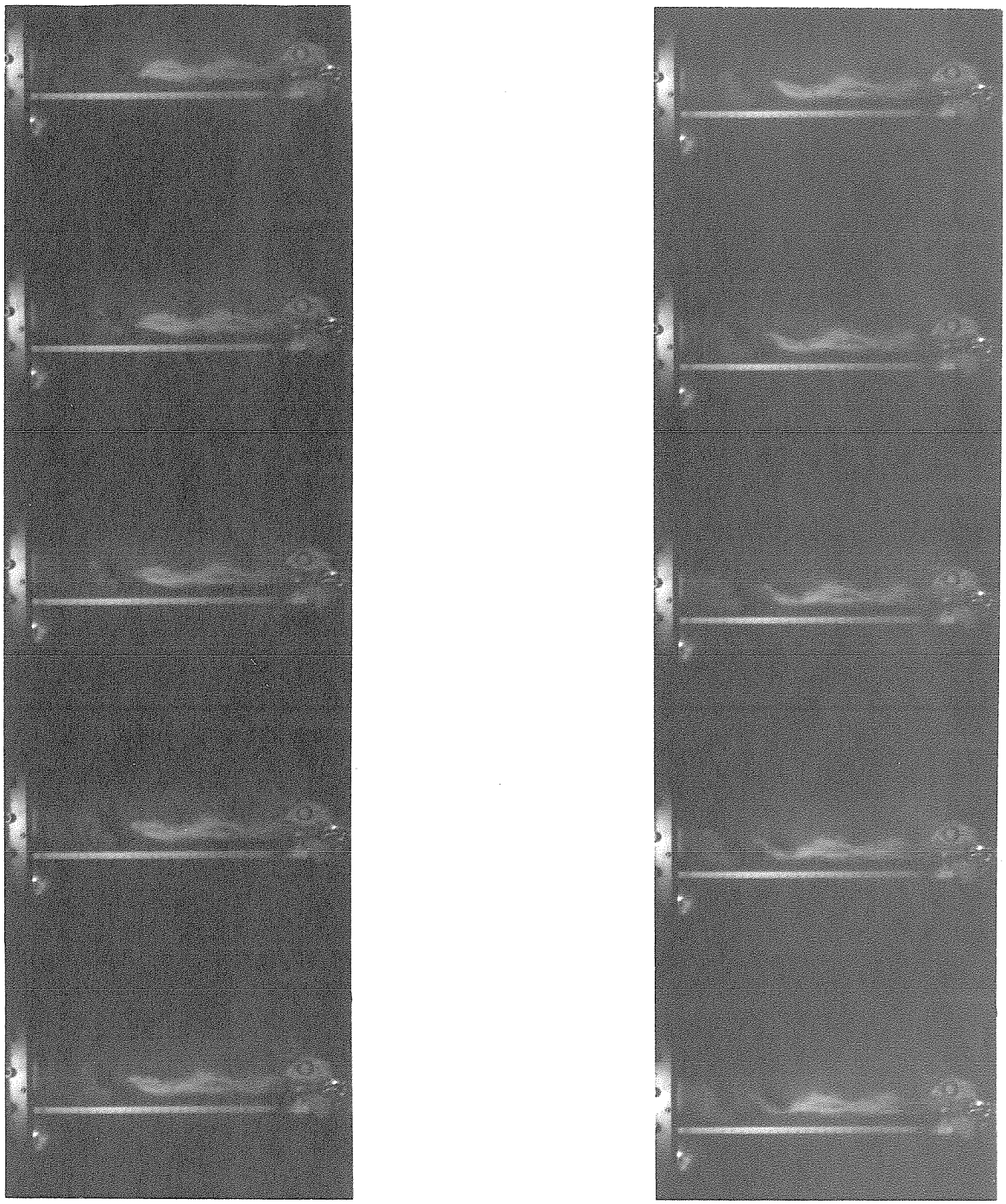

FIG. 42 CAVITY PINCHING PROCESS. TIME BETWEEN FRAMES IS 1/600 SECOND.

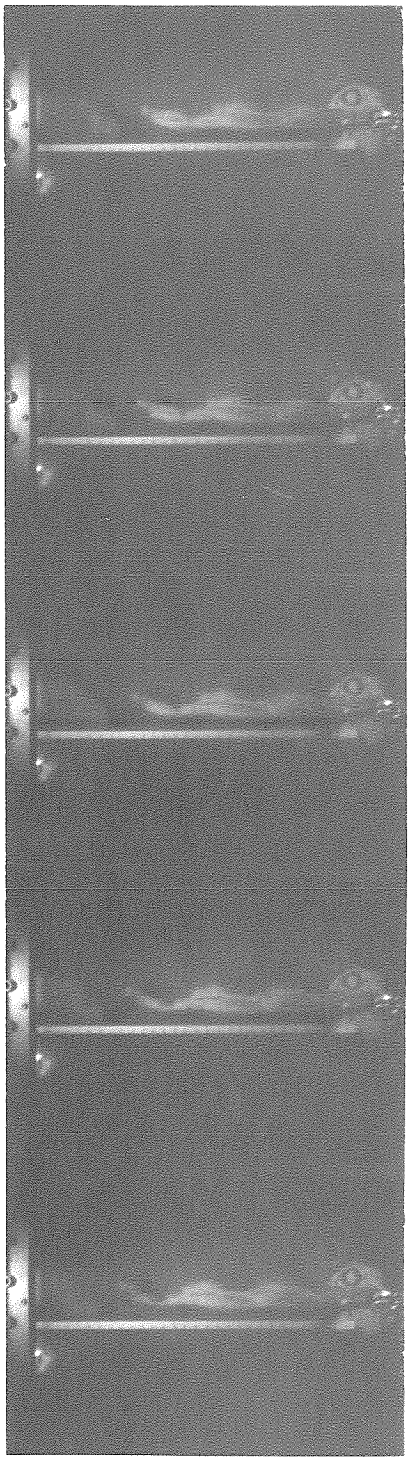

FIG. 42 CONTINUED

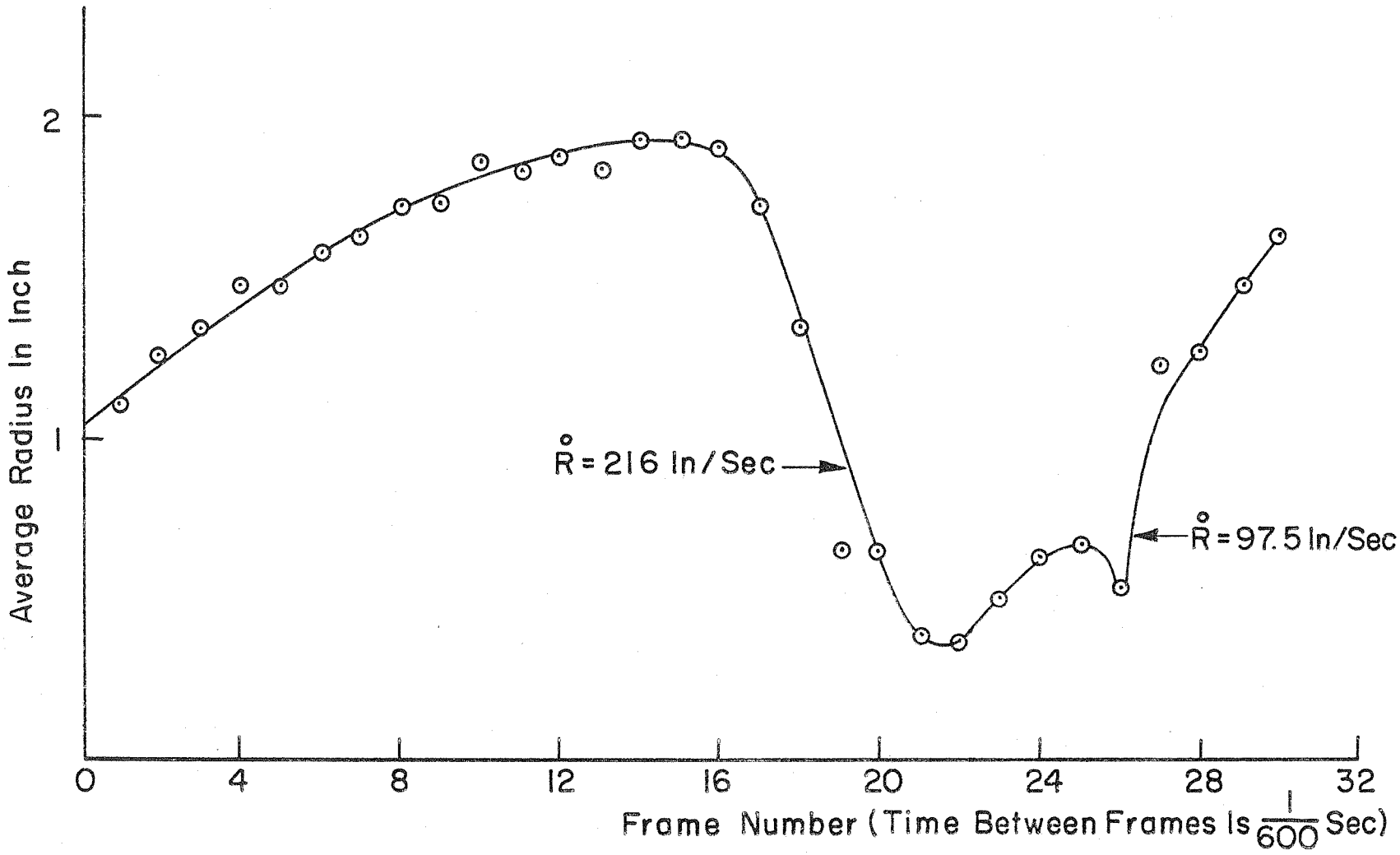

FIG. 43 THE COLLAPSE AND REBOUND OF THE BUBBLY REGION

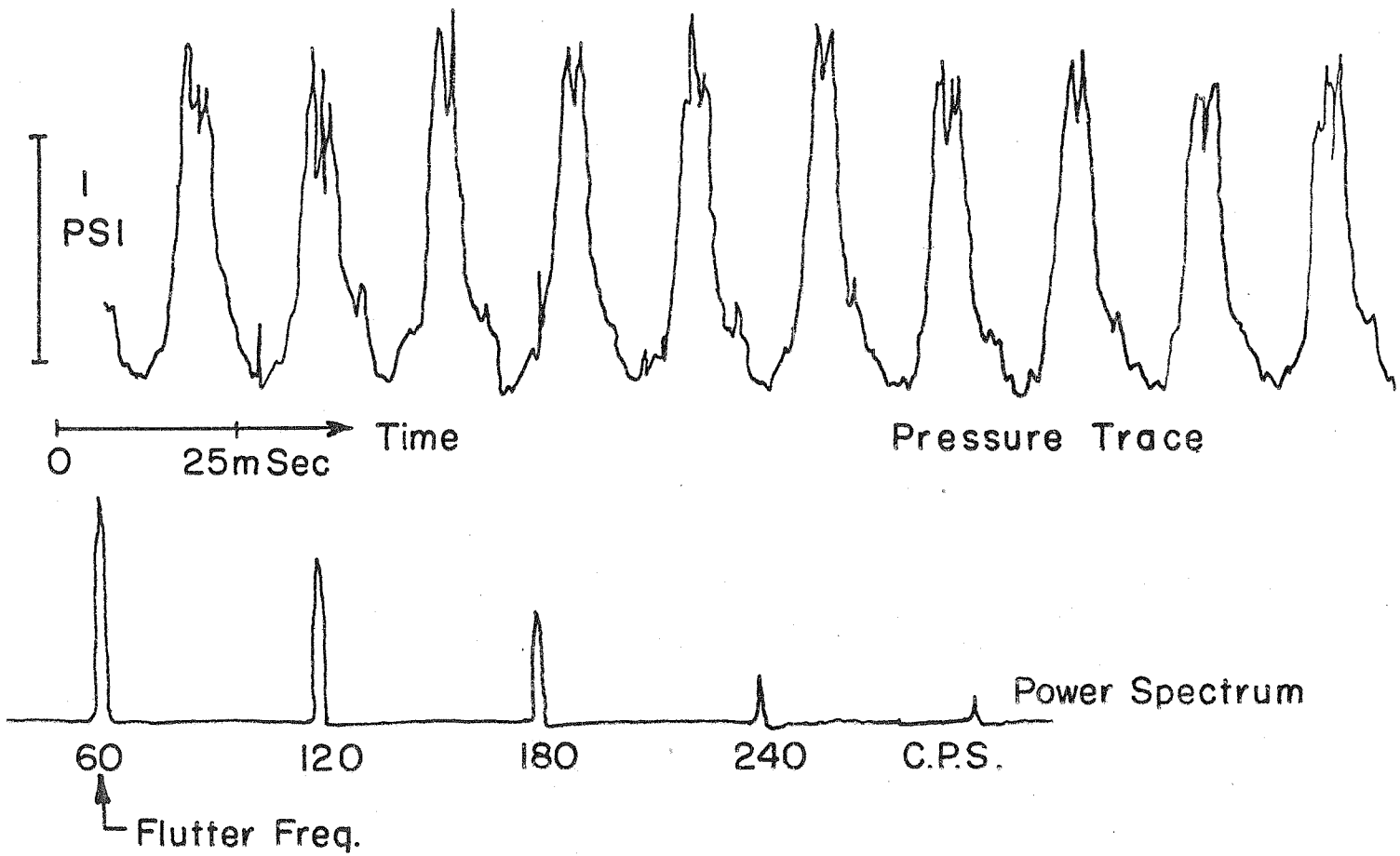

FIG. 44 WATER PRESSURE NEAR THE BUBBLY REGION

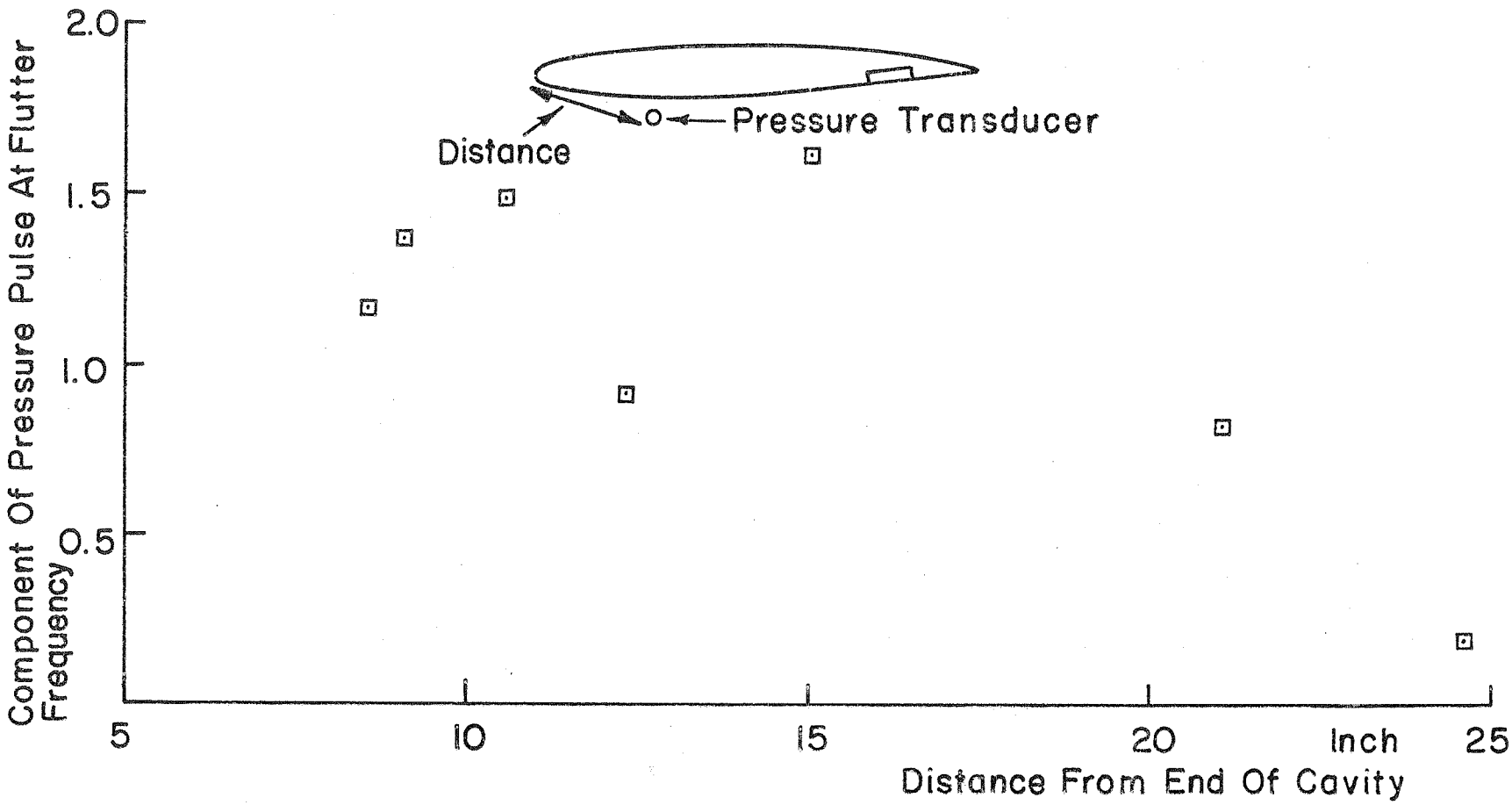

FIG. 45 INTENSITY OF PRESSURE PULSES AS A FUNCTION OF DISTANCE

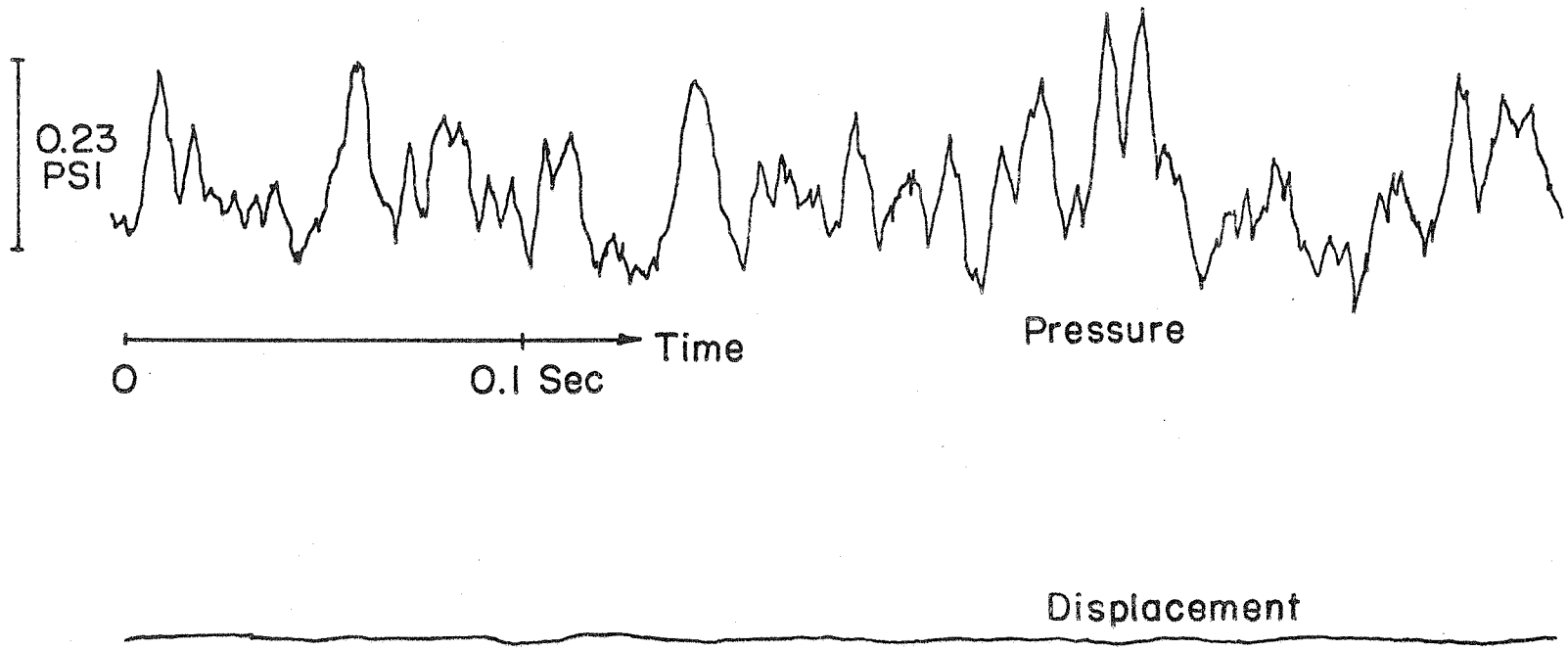

FIG.46a TRACE OF PRESSURE BEHIND A NON-CAVITATING WAKE AND FOIL DISPLACEMENT

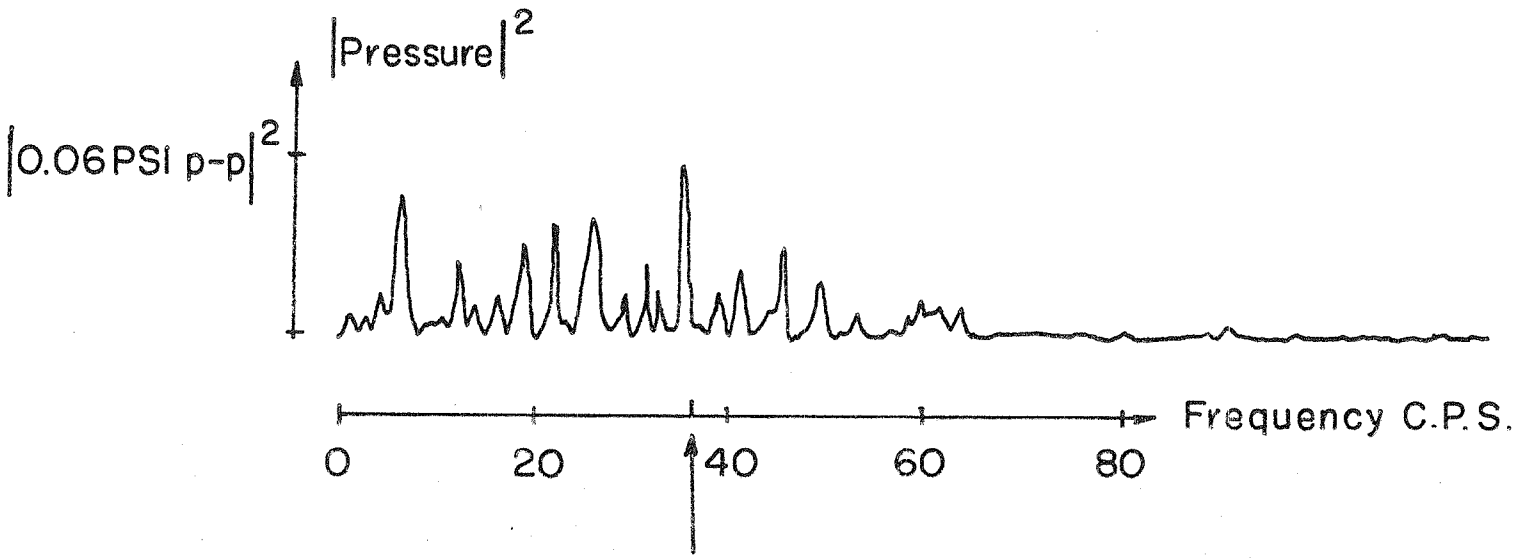

Natural Frequency Of The Foil in A Non - Cavitating Flow

FIG. 46b POWER SPECTRUM OF THE WAKE PRESSURE

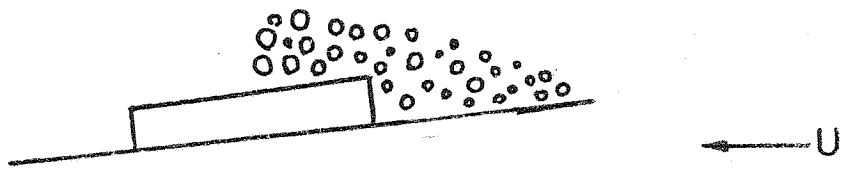

a. Bubbly Partial Cavitation

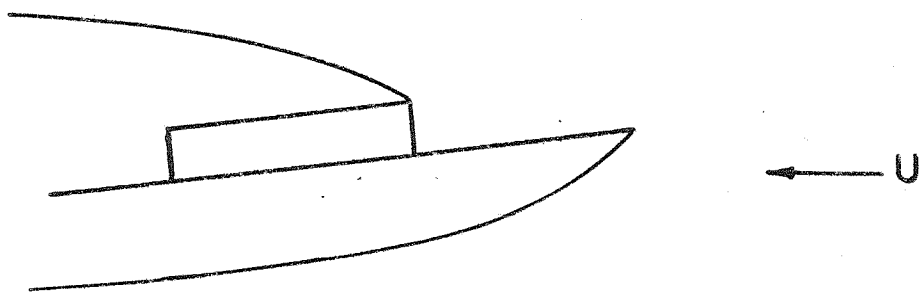

b. Cavitation On The Lower Surface

FIG. 47

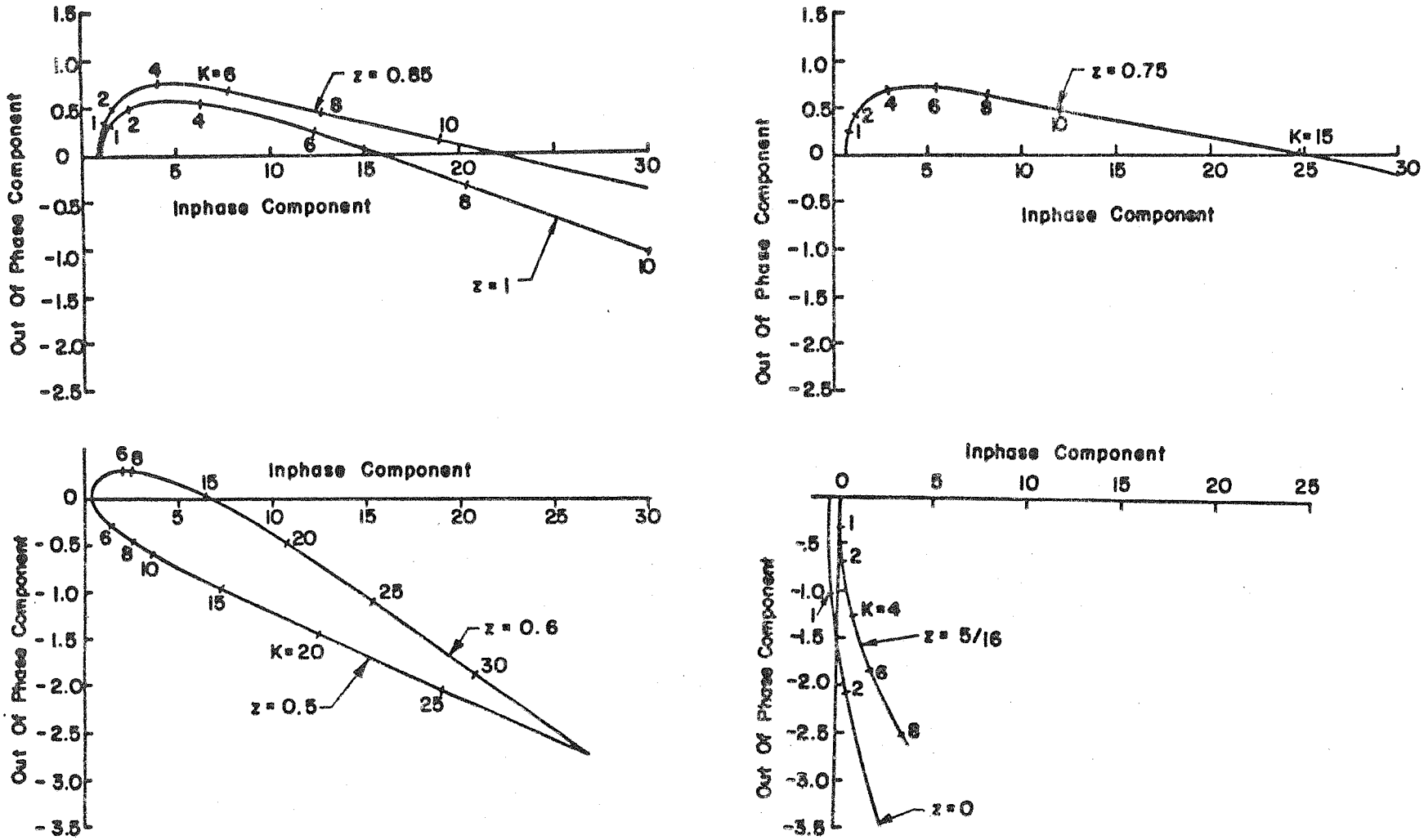

FIG. 48 POLAR PLOT OF $C_{M,\alpha}$ AS A FUNCTION OF THE REDUCED FREQUENCY k AND THE DISTANCE OF THE PITCHING AXIS FROM THE LEADING EDGE z

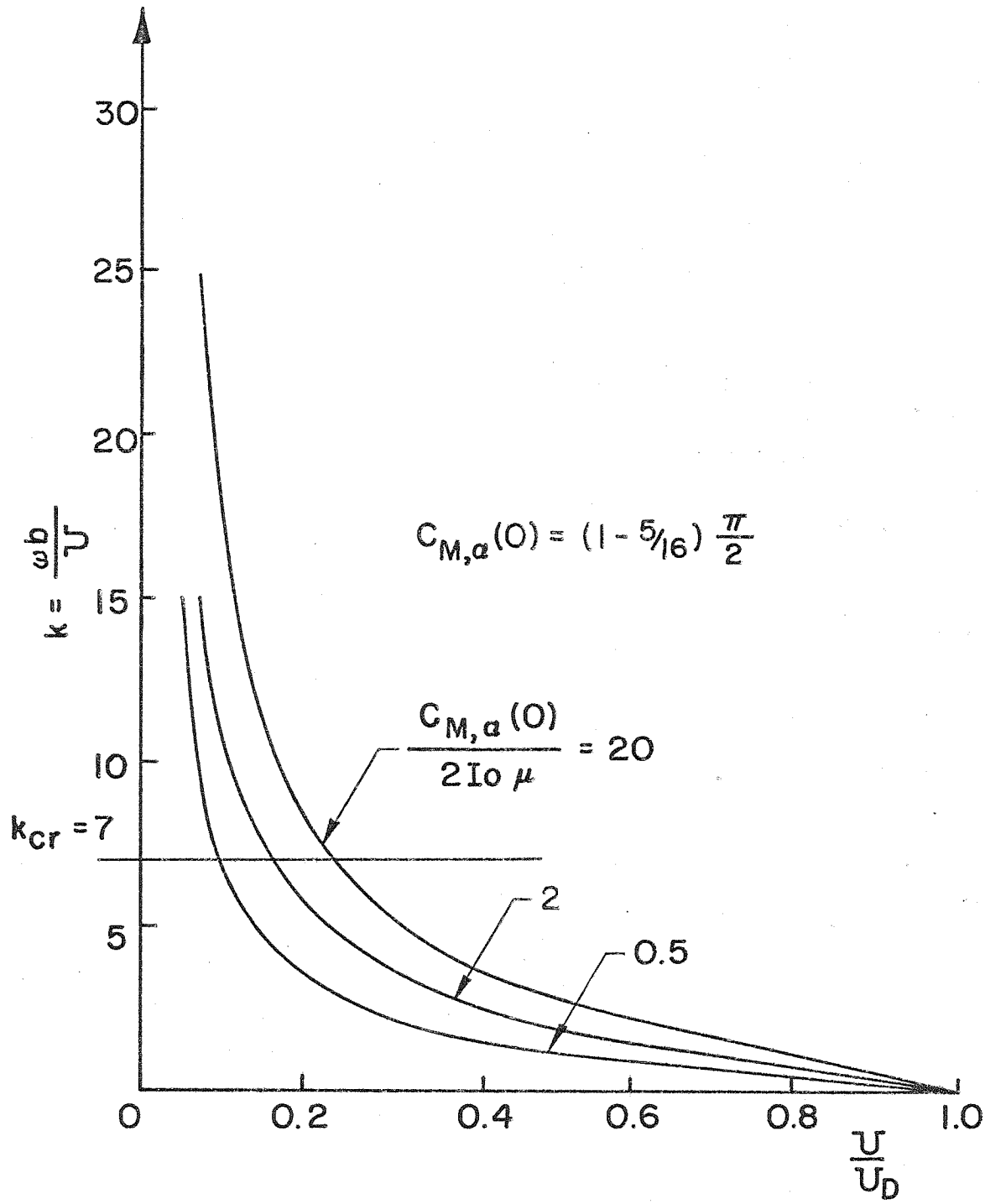

FIG.49 THE VARIATION OF THE REDUCED FREQUENCY WITH VELOCITY FOR A SUPERCAVITATING HYDROFOIL HINGED AT THE TRAILING EDGE

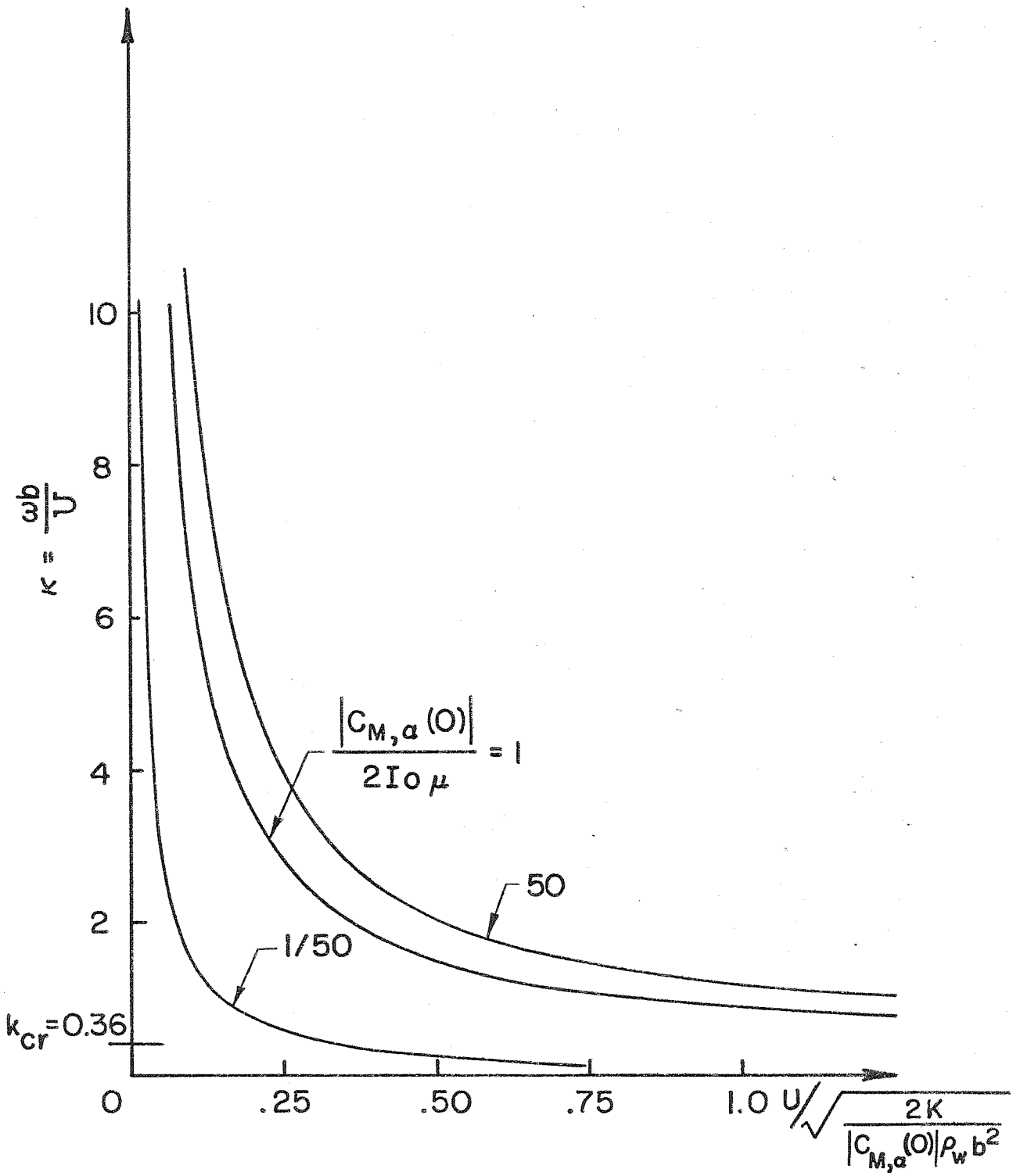

FIG.50 THE VARIATION OF THE REDUCED FREQUENCY WITH VELOCITY FOR AN AIRFOIL HINGED AT THE LEADING EDGE

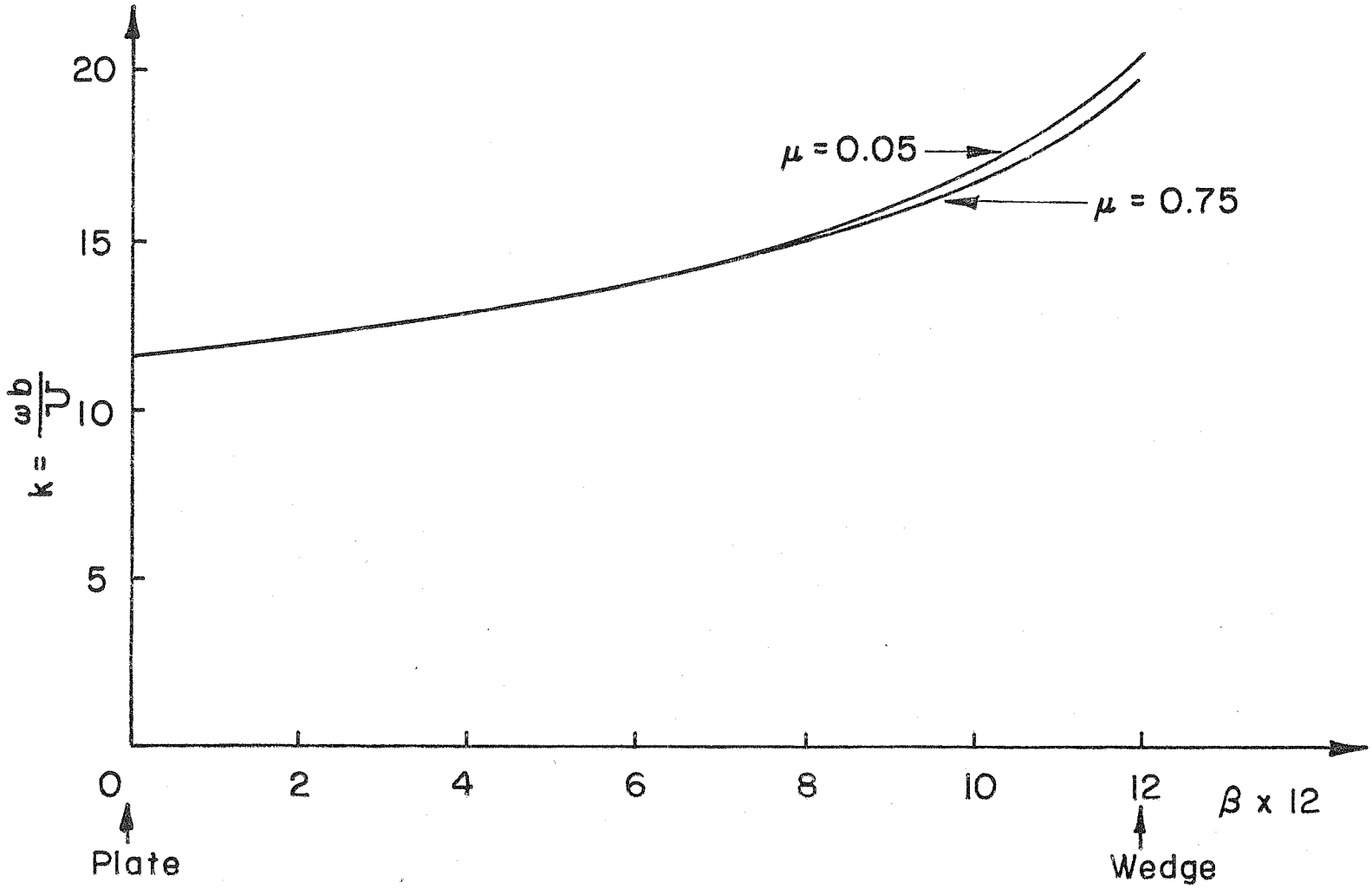

FIG.51 THE THEORETICAL REDUCED FLUTTER FREQUENCY AS A FUNCTION OF THE SHAPE FACTOR β

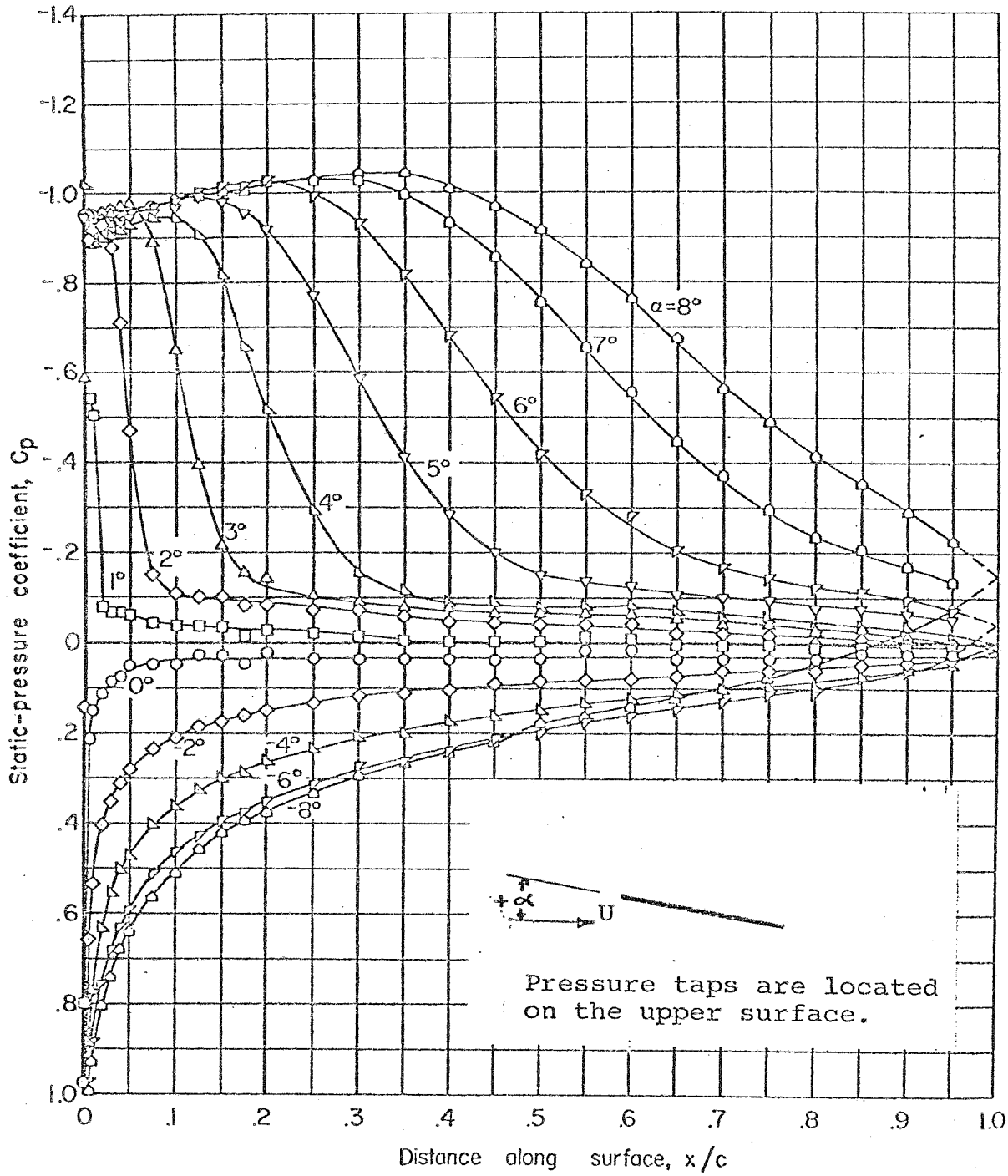

Fig 52. PRESSURE DISTRIBUTION OVER THE UPPER SURFACE OF A FLAT PLATE. (from ref 19)

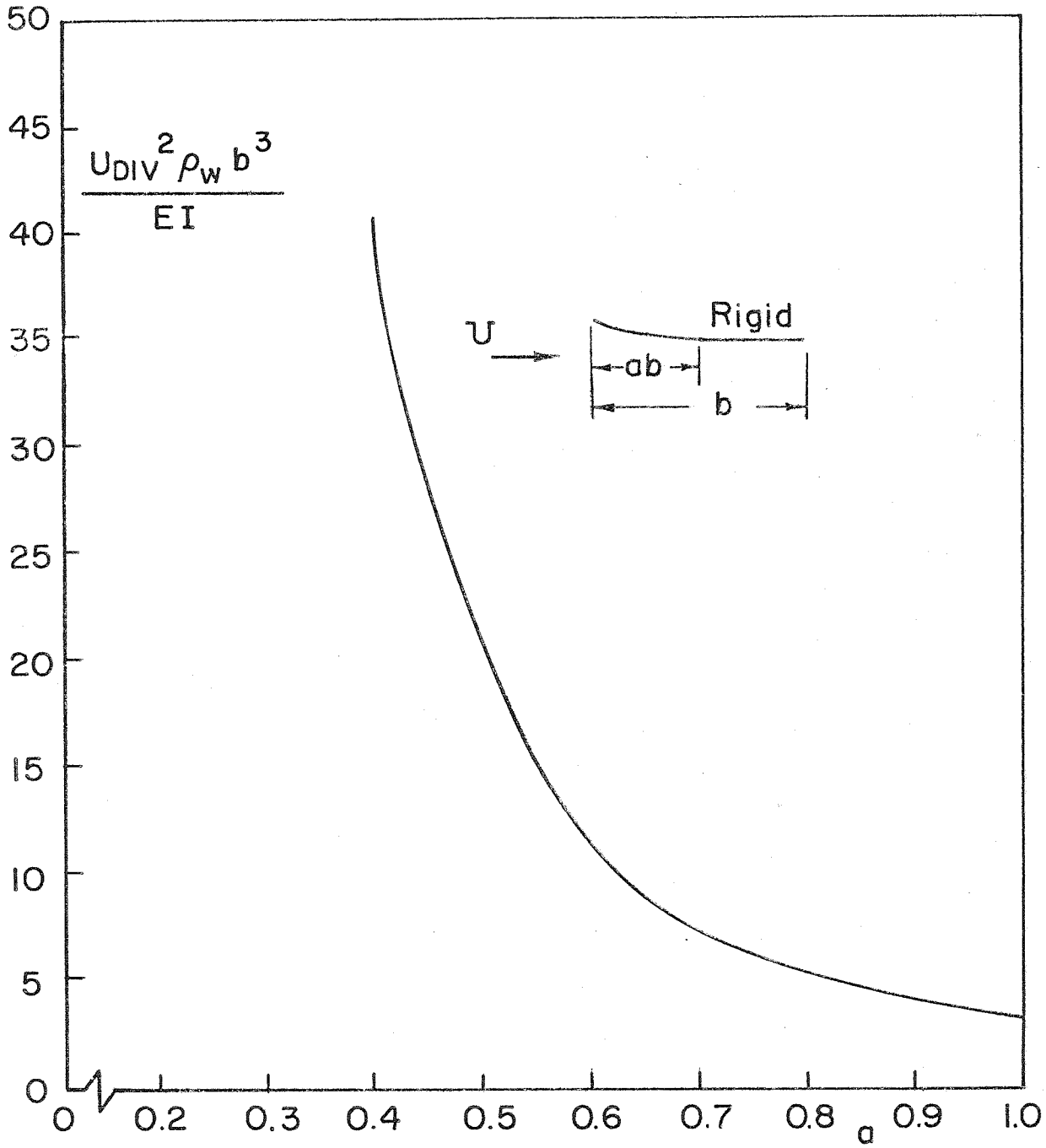

FIG. 53 VARIATION OF DIVERGENCE SPEED WITH LOCATION OF CANTILEVERED POINT FOR FULLY WETTED, NON-SEPARATED FLOW

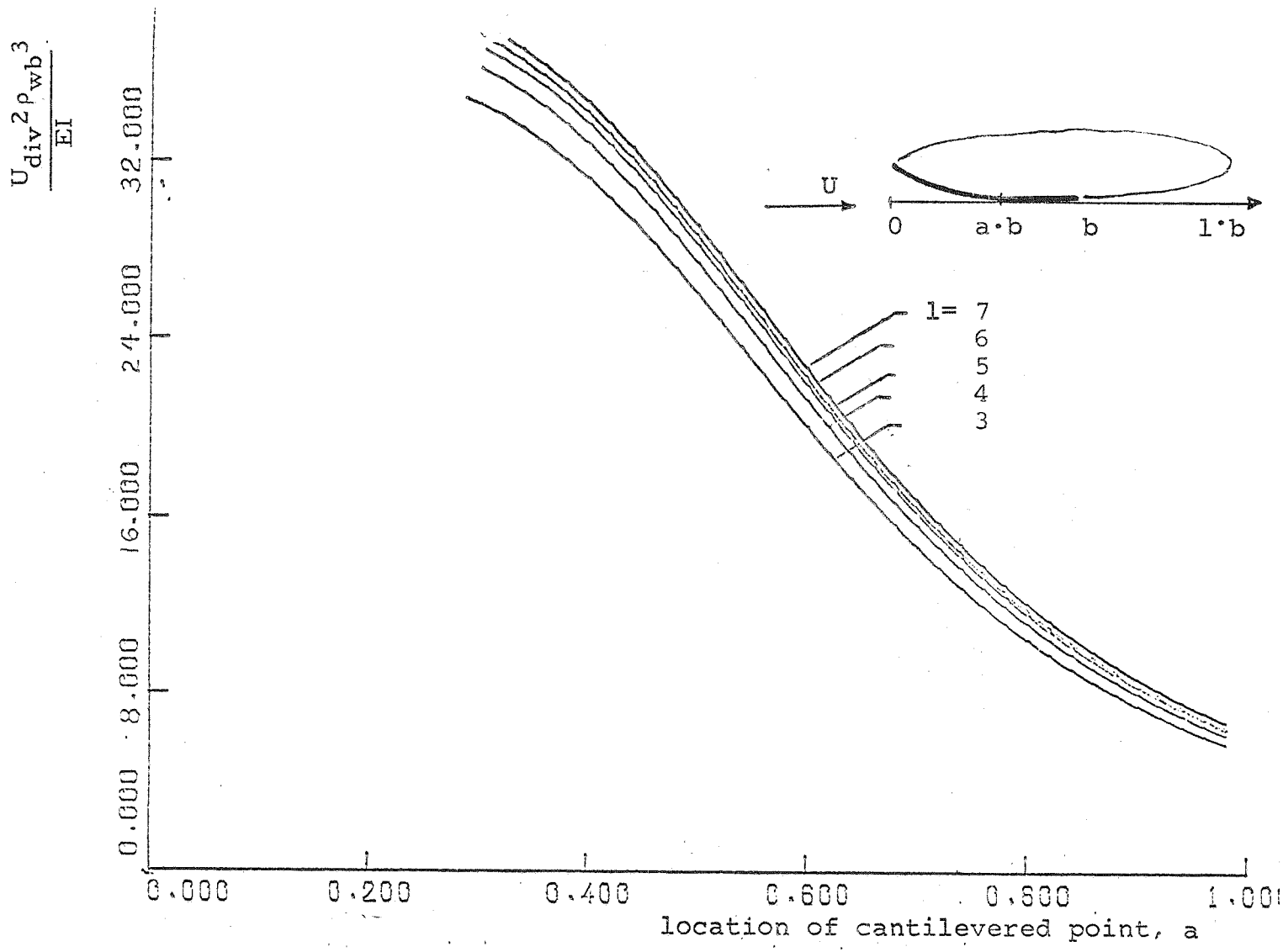

Fig 54. Divergence speed as a function of location of cantilevered point for various cavity lengths.

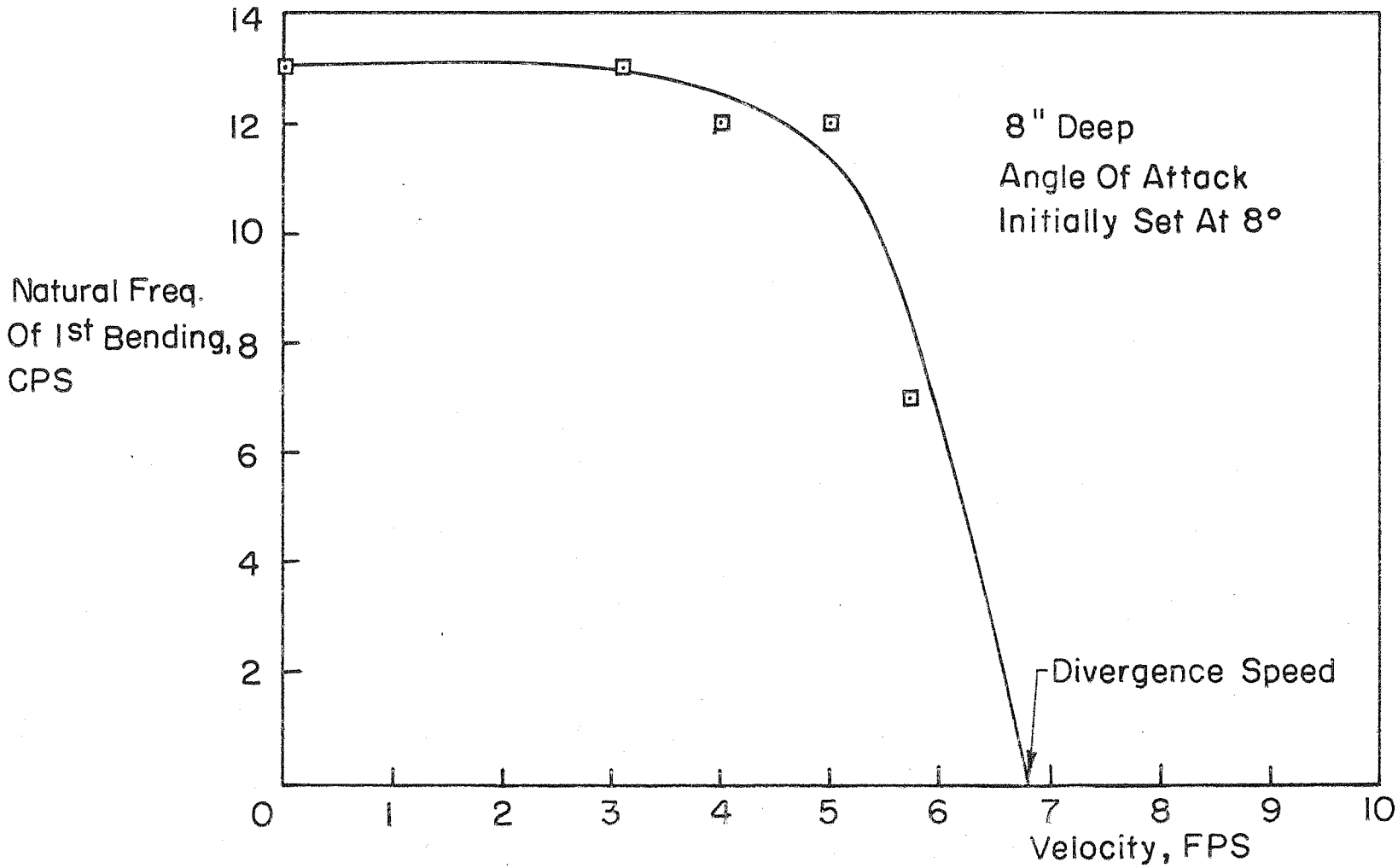

FIG. 55. VARIATION OF FIRST BENDING NATURAL FREQUENCY WITH VELOCITY FOR FOIL #2. NO CAVITY.

APPENDIX A. THE RATIO OF THE RADIATED ENERGY TO KINETIC ENERGY OF THE FOIL

The ratio of acoustical energy radiated due to vibration of the foil to the kinetic or potential energy of the foil is a measure of the importance of acoustic in affecting the leading edge flutter problem. If the acoustical energy radiated is small compared to the kinetic energy of the foil, then leading edge flutter problem may be treated strictly as a hydroelastic problem.

Consider a circular plate of radius a, wetted on one side only as shown below. This could be a model for an underwater speaker or an oscillating supercavitating hydrofoil. According to ref.18 , p. 247, the average energy radiated per unit time is

$$\dot{E} = \tfrac{1}{4}\pi\rho_w c k^2 a^4 \left|\dot{\xi}_{max}\right|^2$$

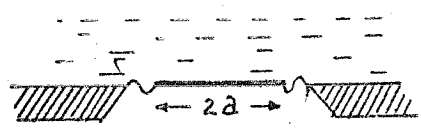

where ρ_w = density of water

c = speed of sound in water

k = wave number $= \frac{1}{\lambda} = \frac{\omega}{2\pi c}$

a = radius of the vibrating plate

$\dot{\xi}$ = velocity of the plate

Energy radiated per cycle of oscillation (period $= \frac{2\pi}{\omega}$) is

$$E = \dot{E}\frac{2\pi}{\omega} = \frac{1}{8}\frac{\rho_w \omega b^4}{c}\left|\dot{\xi}_{max}\right|^2 \quad \left(\frac{\omega}{2\pi c} \text{ has been substituted for } k \text{ and } a = b\right)$$

Kinetic energy of the foil is $KE = \frac{1}{2}\text{mass}\ \dot{\xi}_{max}^{\ 2}$. Typical foil has an average thickness of 10% chord and if we assume low aspect ratio foil then the span may be approximated by the chord, hence mass of the foil is $m = \rho_s b^2 \frac{b}{10}$ where ρ_s = density of foil. Thus the ratio of acoustically radiated energy to the kinetic energy of the foil is $E/KE = (5\rho_w \omega b)/(2\rho_s C)$,

APPENDIX B. A SEMI-EMPIRICAL FORMULA FOR THE NATURAL FREQUENCY OF THE FOIL IN A CAVITATING FOIL

In this appendix, a semi-empirical formula for calculating the first bending natural frequency of a supercavitating foil of arbitrary chord length and thickness is derived. The figure below shows a supercavitating foil with all relevant parameters.

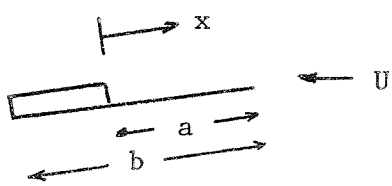

E: Young's modulus
t: thickness
ρ_s: density of the foil
a: flexible chord length
b: overall chord length

The Lagrange's equation of motion of the foil is:

$$\left[\int_0^a \rho_s t(a\eta(x))^2\, dx + \int_0^a ac(x)(a\eta(x))^2\, dx\right]\omega^2 = \int_0^a Et^3 \left(a\frac{d^2\eta(x)}{dx^2}\right)^2 dx$$

where: $a\eta(x)$: mode of vibration and $\int_0^1 \eta^2(\xi)\, d\xi = 1$

$ac(x)$: the distributed apparent mass and $\int_0^1 c(\xi)\, d\xi = 1$

Since we are only interested inhow the frequency varies with a and t, the above equation may be written as:

$$\left[\rho_s t a^3 \int_0^1 \eta^2(\xi)\, d\xi + a^4 \int_0^1 c(\xi)\, \eta^2(\xi)\, d\xi\right]\omega^2 = \frac{Et^3}{a}\int_0^1 \frac{d^2\eta(\xi)}{d\xi^2}\, d\xi$$

The integrals on both sides of the equation are just constants that depends on the mode of vibration and the distribution of the apparent mass; hence the equation may be simplified to:

$$\left[\hat{\rho}_s ta + \hat{c}\, a^2\right] \omega^2 = \frac{\hat{E}\, t^3}{a^3}$$

The constant $\hat{C}$ may be evaluated in terms of $\hat{\rho}_s$ since the frequencies in vacuum and in a supercavitating flow are known for at least one foil. The evaluation of $\hat{C}$ in term of $\hat{\rho}_s$ is valid only if we assume that the modes of vibration in vacuum and in the flow are the same. For foil 3, the experimental frequencies in air and in a supercavitating flow are 195.7 cps and 60.6 cps, respectively. The semi-empirical formula becomes:

$$\frac{1}{f^2} = 1.3782 \times 10^{-9} \left[\frac{a^4}{t^2} + 0.2397\ \frac{a^5}{t^3}\right]$$

where f = frequency in Hz

a = flexible chord in inches

t = thickness in inch

It should be pointed out that changing the flexible chord length, a, while maintaining the overall chord length, b, alters the distribution of the added mass. This distribution is assumed to be fixed regardless of the ratio a/b. However, since the distribution of added mass is concentrated mainly at the leading edge, it is not expected that the variation in a/b will introduce a significant error.

APPENDIX C. DIVERGENCE

Flutter is a dynamic phenomenon involving the interaction between the elastic structure, the hydrodynamic load and the inertia of the foil. Flutter is also called dynamic instability. In contrast to flutter, divergence or static instability involves only the interaction between the elastic restraining force of the structure and the hydrodynamic load. Divergence of a flexible chord hydrofoil in which the leading edge of the foil folds back is a potential problem with thin supercavitating foils and hence it merits special consideration.

Consider a flexible chord hydrofoil oriented in the flow as shown below. The foil has a chord of length b and part of the foil from A to B is rigid (i.e. foil is cantilevered at point B). If the foil were

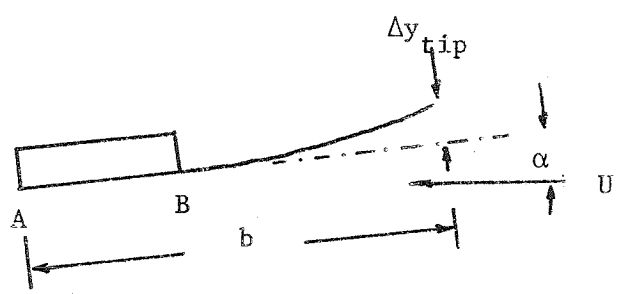

initially set at an angle of attack α without flow, then when the flow is turned on, the flexible part of the foil will deflect upward. However the upward deflection of the foil changes the effective angle of attack and hence increases the load on the foil which causes further deflection. The foil will come to an equilibrium position when the elastic resisting

force (say, the moment at B) balances the hydrodynamic load. Since the structural rigidity is constant and the hydrodynamic loading is proportional to velocity squared, there will be a certain velocity where the deflection becomes unbounded. The velocity, when this occurs, is called the divergence speed.

Two cases of practical interest will be considered. The first case is a fully wetted, nonseparated flow over the foil and the second is the case of supercavitating flow. The first case is, of course, not realizable in practice since the flow over a flat plate at an angle of attack will separate at the leading edge. Figure52, from ref.19, shows the pressure distributions on the upper and lower surfaces of a flat plate with separated flow. Compared to the case of nonseparated flow, this case shows that the center of pressure is located closer to the midchord. Under the same total lift condition the case of separated flow will induce less chordwise deformation and will therefore have a higher divergence speed. Furthermore, at the same angle of attack and velocity, the separated flow produces less lift; hence the analysis with nonseparated cases is useful in establishing a lower limit for the divergence speed. The case of supercavitation is more relevant to the present study. This case is applicable to both the supercavitating flow and non-cavitating wake flow. The theoretical analysis of these two cases is presented below and followed by a discussion on the experimental observation.

C-1 Non-Separated Case

In this case linear potential airfoil theory is used for calculating the hydrodynamic load. Furthermore, the flow is assumed to be two-dimensional and beam theory is used for calculating the deflection of the

foil.

Referring to the figure on the previous page, if the foil was initially set at an angle of attack α without velocity, then the tip deflection of the foil in a flow with velocity U is given by:

$$\Delta y_{tip} = \eta \frac{\rho U^2 b^4}{EI} (\alpha + \Delta\alpha)$$

where η is a coefficient that depends on the location along the chord where the foil is cantilevered and the distribution of the pressure on the foil. However the additional angle of attack $\Delta\alpha$ may be approximated as $\Delta\alpha = C\Delta y_{tip}/b$ where C is a constant is discussed later. Substituting Δy_{tip} in the above expression in terms of $\Delta\alpha$ and solving for $\Delta\alpha$, one obtains:

$$\Delta\alpha = \frac{\eta U^2 b^3 \alpha / EI}{1/C - \eta\rho U^2 b^3/EI}$$

The divergence speed is defined when the additional angle of attack becomes unbounded, i.e., when the denominator of the above expression becomes zero,

$$1/C - \eta\rho U^2 b^3/EI = 0$$

or (I)

$$U_{div} = \sqrt{\frac{EI}{C\eta\rho b^3}}$$

Figure 53 shows the divergence speed when the additional angle of attack is defined as $\Delta\alpha = \Delta y_{tip}/b$, i.e. C=1, and the distribution of pressure over the foil is assumed to be the same as that over a flat airfoil. The calculation of the tip deflection is elementary and the pressure distribution over a flat plate airfoil may be found in any book on aerodynamics;

hence the calculation will not be outlined here.

The proper way to define the angle of attack is to define it as the angle between the zero lift line and the free stream. Finding the zero lift line means taking into account the effect of camber or curvature of the foil, and the relationship between the tip deflection and the angle of attack becomes nonlinear. However if the camber line resulting from the loading is assumed to be fixed in shape, the relationship is linear. If one assumes that the camber line to be $\propto x^2$ and the foil to be cantilevered at 58% of the chord from the leading edge (as in this experiment), then the angle of attack is $\Delta\alpha = 0.25\ \Delta y_{tip}/b$ or $C = 0.25$. The divergence speed in fig.53 may be properly corrected by inserting the constant C in (I).

C-2 Supercavitating Flow

The procedure for finding the divergence speed is the same as before and hence will not be repeated here. Linear theory for calculating the hydrodynamic loads as described in ref.20 is used, and, as in the previous case, the deformation of the foil is calculated by using the load distribution over a flat plate foil.

A note on the linear theory pointing out its assumptions, properties and limitations would be appropriate at this time. For those who are familiar only with airfoil theory, the term "linear" is slightly misleading since the quantities such as lift, drag, and pressure distribution are neither linear in angle of attack nor the cavitation number σ. In our case here, the hydrodynamic load is calculated by fixing the cavity length and letting the cavitation number float. Then the coefficient of pressure is related to angle of attack α by

$$C_p \sim \frac{\alpha}{\frac{\alpha}{s} - 1}$$

where $s^2 = \ell/b - 1$ and ℓ/b is the nondimensionalized cavity length with respect to chord length b. Note that the pressure profiles are different for different cavity lengths. In the interest of avoiding an iterative procedure for solving the divergence speed, we have made a further assumption that $\alpha/s<<1$, which is true for small angles of attack and long cavity lengths.

Figure 54 shows the divergence speed of a cavitating flat plate foil as a function of the location of cantilevered point and cavity length when a value of C=1 is used . The effect of a circular arc camber line has been investigated in ref.21 . If one assumes that the camber of the hydrofoils tested in this experiment (including the rigid part) is a circular arc with an arc angle twice the angle of attack, then the value of C is 0.13.

C-3 Correlation with the Experimental Data

First of all it must be pointed out that none of the foils tested in the FSWT and HSWT were observed to diverge in a cavitating flow. Leading edge flutter occurred before divergence and several foils were destroyed by flutter.

Table 6 shows the theoretical and experimental values of divergence speeds. Foils 1 and 2 diverged in the FSWT with a non-cavitating wake flow. Since a non-cavitating wake flow is similar to a cavitating flow (at least in the steady case), it is expected that the experimental values will be closer to the values from the supercavitating flow theory than to the values from the airfoil theory. In the experiment, the extent of the wake behind these foils was not known.

Comparison with the theoretical values should be made with regard to this fact. The load on a cavitating foil could vary by as much as a factor of 2 between the long and short cavity flows. Therefore the divergence speed could vary by a factor of $\sqrt{2}$.

The experimental value for foil 1 agrees reasonably well with the airfoil and supercavitating theoretical values without camber line. The divergence speed of foil 2 was obtained from a plot of the natural frequency versus velocity as in fig.55 . This value is lower than the airfoil or supercavitating flow prediction. No divergence was observed for foils 3A and 3; only flutter was observed for these foils. From the available experimental data, one may conclude that the theoretical supercavitating values are conservative.

APPENDIX D. ESTIMATION OF THE PRESSURE CREATED BY THE COLLAPSE OF THE BUBBLY CLOUDS

During flutter it was observed that the bubbly region behind the cavity collapsed and rebounded in synchronization with the oscillation of the foil. This bubbly region is actually two-dimensional in shape; however it is well known that 2-D potential solution for the collapse of a "cylindrical bubble" is singular in nature.

Here it will be assumed that the bubbly region is a single spherical bubble with the same projected area as the actual bubbly region when viewed from the side. The consequences of the above assumptions are:

1. Underestimation due to the fact that the actual volume of the bubbly region is larger than the corresponding single sphere.
2. Overestimation due to assuming the bubbly region is a single bubble.
3. Underestimation due to using the 3-D model. It is well known that in 2-d model any pertubation dies off slower than the corresponding 3-D model.

The purpose of this calculation is to obtain the order of magnitude of the pressure pulse and in view of the consequences stated above, this calculation seems to be justified.

The solution for a spherical bubble is well known and will not be repeated here. All relevant parameters are shown below.

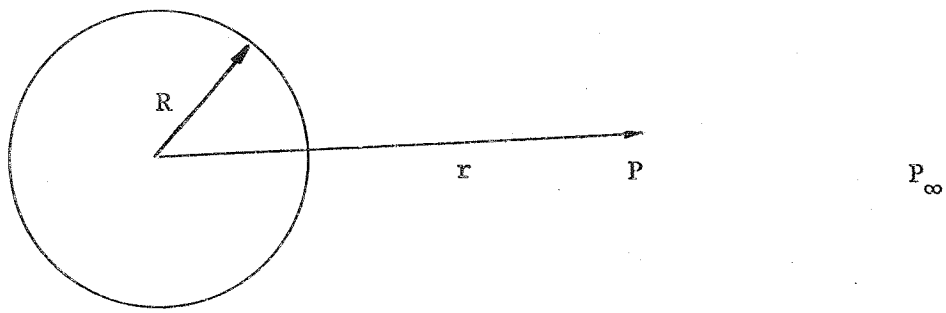

The equation is $\dfrac{P - P_\infty}{\rho} = \dfrac{\ddot{R}\,R^2}{r} + \dfrac{2R\dot{R}^2}{r} - \dfrac{1}{2}\left[\dot{R}\,\dfrac{R^2}{r^2}\right]^2$

Fig 43. shows the typical average radius of a bubbly cloud as a function of time. During the collapse cycle, the rate of change of the bubble size, i.e. $\dot{R}$, is approximately 216 in/sec and $\ddot{R} \simeq 0$. In this particular example the distance from the bubble to the foil, i.e r, is approximately 17 inches. The change in pressure may be calculated from the above equation and its value is maximum at the begining of the collapse cycle. The maximum change in pressure $P - P_\infty$ is 0.87 psi during the collapse cycle and 0.18 psi during the rebound cycle.

APPENDIX E. NONSTEADY HYDRODYNAMICS OF A RIGID FOIL IN PITCHING OSCILLATION AT $\sigma = 0$

In this appendix calculations of the unsteady hydrodynamic moment for pitching oscillation are discussed. Within the context of the linearized theory of unsteady supercavitating flow, the pitching motion about any axis on the foil may be obtained by superposition of pitching motion about the leading edge and heaving motion as shown below.

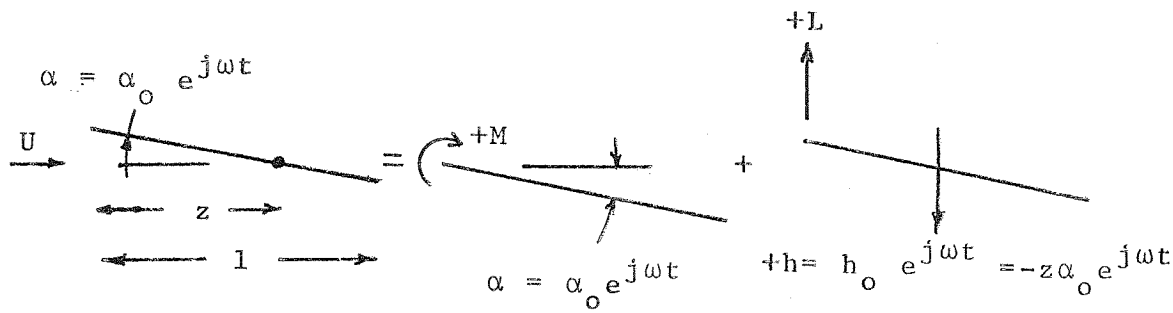

where: α_o = the amplitude of the oscillation α_o is always less than the steady state angle of attack to insure that the instantaneous angle of attack is always positive

α = angle of attack, positive nose up

h = heaving displacement, positive downward

$h_o = -z\alpha_o$

L = lift, positive up

M = Moment at the leading edge, positive nose up

The moment coefficient is given by Parkin (ref. 14) as:

$$C_M = M/\tfrac{1}{2}\rho_w U^2 = \frac{-5\pi}{32}\left\{\left[\Omega(k) + \frac{5}{8}jk - \frac{7}{8}\cdot\frac{35}{64}k^2\right]\alpha_o e^{j\omega t} - z\left[jkW(k) - \frac{7}{8}k^2\right]\alpha_o e^{j\omega t}\right\}$$

The lift due to pitching and heaving may be obtained by combining the lift coefficient due to heaving given by Martin (ref. 13) and the lift coefficient due to pitching from Parkin (ref 14). The result is:

$$C_L = L/\tfrac{1}{2}\rho_w U^2 = \frac{\pi}{2}\alpha_o \left\{ \left[\Omega(k) - \frac{35}{128} k^2 \right] - z \left[jkW(k) - \frac{9}{16} k^2 \right] \right\} e^{j\omega t}$$

where $W(k)$ and $\Omega(k)$ are frequency response functions for heaving and pitching, respectively. They are tabulated in ref. 14.

$k = \omega/U$ the reduced frequency

The coefficient of moment about the axis of pitching is simply given by

$$C_{M\ total} = C_{M\ pitch} + zC_L$$

The polar plot of C_M, α is presented as fig. 48.

REFERENCES

1. JANE'S Surface Skimmers, 1975-76.

2. Waid, R. and Linberg, Z., "Experimental and Theoretical Investigation of a Supercavitating Hydrofoil," CIT Engineering Division Report No. 47-8, April 1957.

3. Spangler, P.K., "Performance and Correlation Studies of the BUSHIPS Parent Hydrofoil at Speeds from 40 to 75 Knots," DTMB Hydromechanics Laboratory Research and Development Report No. 2353, Dec. 1966.

4. Personal communication with Dr. John English of the National Physical Laboratory, England.

5. Ai, D.K. and Harrison, Z.L., "The Wall Effect in Cavity Flow," C.I.T. Hydrodynamic Laboratory Report No. 111.3, April 1965.

6. Murai, H., "Theoretical Study of a Flexible Supercavitating Hydrofoil," Japanese Society of Mechanical Engineering 91st Conference. Paper No. 218 (in Japanese).

7. Song, C.S. and Almo, J., "An Experimental Study of the Hydroelastic Instability of Supercavitating Hydrofoils," University of Minnesota St. Anthony Falls Hydraulic Laboratory. Project Report No. 89, Feb. 1967.

8. Furuya, O. and Acosta, A.J., "An Experimental Study of a Superventilated Finite Aspect Ratio Hydrofoil Near a Free Surface," 11th Symposium on Naval Hydrodynamics, London, England, 1976.

9. Meijer, M.C., "Pressure Measurements in Flapped Hydrofoils in Cavitating Flows and Wake Flows," CIT Hydrodynamics Laboratory Report No. E-133.2, Oct. 1962.

10. Smilg, B., "The Instability of Pitching Oscillation of an Airfoil in Subsonic Incompressible Potential Flow," Journal of Aeronautical Sciences, Nov. 1949, pp. 691-696.

11. Parkin, B.R., "Fully Cavitating Hydrofoils in Nonsteady Motion," CIT Engineering Report No. 85-1, 1957.

12. Wu, T. Yao-Tsu, "Unsteady Supercavitating Flow," CIT Engineering Report No. 85-11, July 1959.

13. Martin, Milton, "Unsteady Lift and Moment on a Fully Cavitating Hydrofoil at Zero Cavitation Number," Journal of Ship Research, June 1962, pp. 15-25.

REFERENCES (continued)

14. Parkin, Blaine R., "Numerical Data on Hydrofoil Response to Nonsteady Motions at Zero Cavitation Number," Journal of Ship Research, December 1962, pp. 40-42.

15. Woods, L.C., "Aerodynamic Forces on an Oscillating Aerofoil Fitted with a Spoiler," Royal Society of London Proceedings, Series A, February-April 1957, pp. 328-337.

16. Klose, G. J. and Acosta, A. J., "Unsteady Force Measurements on Superventilated Hydrofoils in Heaving Motion," Journal of Ship Research, vol. 13, No. 2, pp. 92-102.

17. Personal Communication with S. Shimizu, Institute of High Speed Mechanics, Tohoku University, Sendai, Japan.

18. Stewart, G.W. and Lindsay, R.B., Acoustics; A Text on Theory and Applications, D. Van Nostrand Co., 1930.

19. Gault, Donald E., "An Investigation at Low Speed of the Flow Over a Simulated Flat Plate at Small Angle of Attacks Using the Pitot-Static and Hot Wire Probes," NACA TX13876, March 1957.

20. Wu, T. Yao-Tsu, "A Note on the Linear and Nonlinear Theories for Fully Cavitated Hydrofoils," CIT Hydrodynamics Laboratory Report No. 21-22, August 1956.

21. Wu, T. Yao-Tsu, "A Free Streamline Theory for Two Dimensional Fully Cavitated Hydrofoils," CIT Hydrodynamics Laboratory Report No. 21-17, July 1955.

22. Song, C.S., "Supercavitating Flat Plate With an Oscillating Flap at Zero Cavitation Number," Journal of Ship Research, March 1967, pp. 23-50.

23. Kim, Jong H., "The Wall Effect for Unsteady, Choked Supercavitating Flow," Journal of Ship Research, vol. 16, No. 4, pp. 240-247.